Alma Mater Studiorum - Università di Bologna

SCUOLA DI SCIENZE

Dipartimento di Chimica Industriale "Toso Montanari"

Corso di Laurea Magistrale in

Chimica Industriale

Classe LM-71 - Scienze e Tecnologie della Chimica Industriale

PEDOT:PSS thin films: Applications in Bioelectronics

Tesi di laurea sperimentale

CANDIDATO

Federica Mariani

RELATORE

Chiar.ma Prof.ssa Erika Scavetta

CORELATORI

Prof.ssa Rita Mazzoni

Prof.ssa Róisín M. Owens

Sessione II

Anno Accademico 2015-2016

To my parents,

Daniela and Roberto

Abstract

Owing to their capability of merging the properties of metals and conventional polymers, Conducting Polymers (CPs) are a unique class of carbon-based materials capable of conducting electrical current. A conjugated backbone is the hallmark of CPs, which can readily undergo reversible doping to different extents, thus achieving a wide range of electrical conductivities, while maintaining mechanical flexibility, transparency and high thermal stability. Thanks to these inherent versatility and attracting properties, from their discovery CPs have experienced incessant widespread in a great plethora of research fields, ranging from energy storage to healthcare, also encouraging the spring and growth of new scientific areas with highly innovative content.

Nowadays, Bioelectronics stands out as one of the most promising research fields, dealing with the mutual interplay between biology and electronics. Among CPs, the polyelectrolyte complex poly (3,4-ethylenedioxythiophene) : poly (styrenesulfonate) (PEDOT:PSS), especially in the form of thin films, has been emphasized as ideal platform for bioelectronic applications. Indeed, in the last two decades PEDOT:PSS has played a key role in the sensing of bioanalytes and living cells interfacing and monitoring.

In the present work, development and characterization of two kinds of PEDOT:PSS-based devices for applications in Bioelectronics are discussed in detail. In particular, a low-cost amperometric sensor for the selective detection of Dopamine in a ternary mixture was optimized, taking advantage of the electrocatalytic and antifouling properties that render PEDOT:PSS thin films appealing tools for electrochemical sensing of bioanalytes. Moreover, the potentialities of this material to interact with live cells were explored through the fabrication of a microfluidic trapping device for electrical monitoring of 3D spheroids using an impedance-based approach.

Contents

Introduction

1. Context

In 1977, when a paper entitled "Synthesis of Electrically Conducting Organic Polymers: Halogen Derivatives of Polyacetylene, $(CH)_x$" [1] by Hideki Shirakawa, Alan Heeger and Alan MacDiarmid was published in *Journal of the Chemical Society, Chemical Communications,* nobody could be fully aware that the dawning of a new era for electronics had been marked. Not very surprisingly for scientific research, a kind of serendipity fueled this discovery. Indeed, Shirakawa himself has admitted that he succeeded in synthesizing Polyacetylene directly in the form of a thin film, instead of a black powder, by a fortuitous error: he bubbled acetylene gas into a stirred solution accidentally containing an amount of Ziegler-Natta catalyst nearly a thousand times greater than that normally used. Since no benefit in electrical conductivity was observed in the film form, Shirakawa decided to use the Polyacetylene film as a source of graphite film. He treated the polymeric film with chlorine and subsequently with a basic reagent to eliminate hydrogen chloride, to give a carbon film: the graphitization yield was very low. However, unexpected changes in the IR spectra after the halogenation were noticed, suggesting that the halogen doped material might have unusual electronic properties. Thus, by deepening the halogenation studies, Shirakawa and coworkers obtained highly conducting Polyacetylene bromides and iodides, with a conductivity strongly enhanced from 10^{-6} to 10^{3} $\Omega^{-1}cm^{-1}$, "the largest room temperature conductivity observed for any covalent organic polymer".[2]

The breakthrough of this discovery consisted in finding out a route to obtain highly pure, reproducible and structurally ordered electrically conducting organic polymers, thus finally making them stable and processable through controlled halogen doping. In 2000, the Nobel Prize in Chemistry was jointly awarded to Shirakawa and his colleagues "for the discovery and development of conductive polymers". Thenceforth, Organic Electronics has been standing out as one of the most promising branches of materials science, which deals with a huge variety of applications, such as energy storage and thin film transistors, and involves a broad range of fields, from medicine to communications. Such interdisciplinary and versatile texture seems to remind the different but complementary backgrounds of the three inventors.

Nowadays, the rapid evolution of this technology is fed by an increasing demand for extremely performant, low-cost devices, so as to make electronics more functional, accessible and

sustainable. Taking a glance into the near-future, three main features regarding the huge potential of organic electronics should be enlisted: [3]

i. *Organic materials give electronic devices unique properties impossible to achieve with silicon-based electronic structures*, i.e. sensing, biocompatibility, and flexibility. Thanks to their unique structural and functional variation, organic materials are successfully employed in sensors and biosensors. Together with stretchability and mechanical softness, all these characteristics create, for instance, the potential for innovative electronic skins with tactile sensitivity and other sensing capabilities.

ii. *Organic electronic devices own the concrete likelihood to be more energy-efficient than today's electronics, thus addressing sustainability issues about consumption goods*. This fact relies on the concrete improvements continuously made in this field and regarding, for example, progressively shorter payback times of organic solar cells and lower operating voltages of organic materials-based transistors.

iii. *Organic electronic devices will be manufactured using more resource-friendly and energy-efficient processes than today's methods, further contributing to a more sustainable electronic world.* The main strategies currently dealing with this purpose are: reducing the amount of waste produced (for example, by using printing techniques instead of spin-coating); avoiding toxic materials and solvents as much as possible; looking for alternative raw materials, which can replace the most limited ones.

In particular, thanks to their favourable properties, electrically conducting organic polymers have been emphasized as ideal tools for interfacing with biologic substrates.[4] The advantages include better mechanical compatibility with tissue than traditional "hard" electronic materials and the ability of organic electronic materials to conduct ions, in addition to electrons and holes, which opens up a new communication channel with biology due to the importance of ion fluxes in biological systems.[5] This emerging field is called Organic Bioelectronics and it deals with plenty of healthcare applications, encompassing neuroscience, biosensors and drug delivery.
From an overall point of view, it is clear that such hybrid research fields hold both a high innovative content and demanding challenges, which can be addressed through the synergic interaction of different branches within the scientific community.

2. Conducting Polymers

2.1 Conductivity in CPs

Generally speaking, conductivity is a measure of how readily a material allows the flow of an electric current; it decreases with increasing temperature for metals, while for inorganic semiconductors the trend is opposite, since the hopping of charges is thermally promoted.

As their chemical nature suggests, carbon-based polymers have long been thought as insulators. However, polymers theirselves, as well as common semiconductors, can undergo doping processes to enhance their conductivity. Basically, conductive polymers merge the properties of metals and conventional polymers: they are plastic materials capable of conducting electrical current.

Conductivity ranges for common insulators, semiconductors and conductors with respect to CPs are presented in Fig. 1.

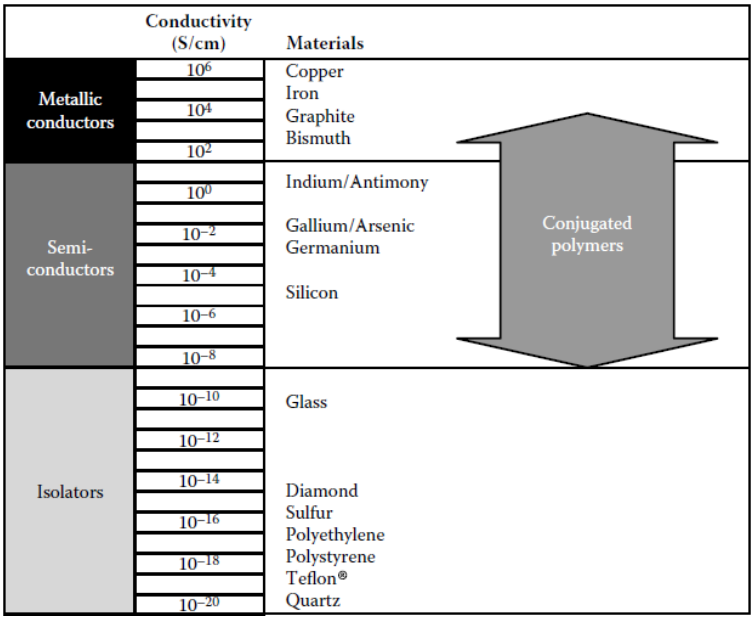

Fig. 1 Overview with widely accepted ranges of conductivity for common insulators, semiconductors and conductors compared to that of conjugated polymers. Adapted from[6].

Two main categories of conducting polymers are known:

- Extrinsically Conducting Polymers (ECPs), i.e. composite materials loaded with a certain percentage of powder or fibers of Cu, Ag, Au or graphite, which act as dopants.
- Intrinsically Conducting Polymers, (ICPs), in which the presence of a conjugated backbone, after a chemical or electrochemical doping, is responsible for conductivity.

Only ICPs' properties and features will be discussed and, in particular, characteristics and recently developed applications of Polythiophenes will be the main topics of this thesis. For this reason, the term "conducting polymers" will always refer to ICPs.

As previously mentioned, a conjugated system is the hallmark of ICPs. In saturated polymers, the Energy Gap (E_G, i.e. the energy difference in eV between the valence band and the conduction one) is huge and the materials show typical insulating properties; for instance, the E_G value reported in literature for linear polyolefins such as Polyethylene (PE) and Polypropylene (PP) is around 7eV. In conjugated polymers, a series of alternating single and double bonds makes the motion of electrons easy to occur, since a delocalized π system is formed along the polymer backbone. The carbon atoms that constitute the polymer backbone form three σ-bonds with neighbouring atoms, while the remaining p_z orbitals engage in the π system. In such a system, π bonding orbitals and π* antibonding orbitals act as valence and conduction bands, respectively.

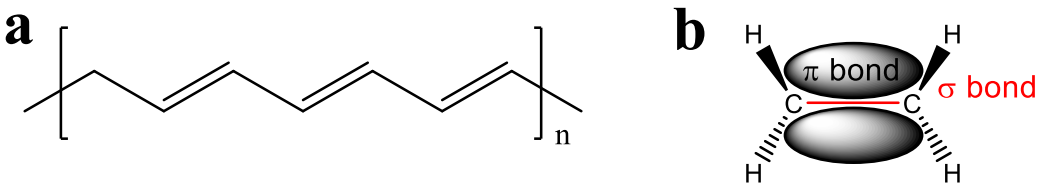

Fig. 2 (**a**) Chemical structure of trans-Polyacetylene. (**b**) Scheme of a π bond.

It is worth pointing out that conjugated polymers in their pristine state typically behave as inorganic semiconductors, since there are no partially filled orbitals at room temperature: all the π bonding orbitals are full of electrons and the π* antibonding ones are empty.[6] This is exactly what Shirakawa noticed for the simplest conjugated polymer, i.e. Polyacetylene, before performing halogenation.

However, plenty of opportunities to enhance the electronic properties of conjugated polymers have been reported in literature.

First of all, it is well-known that, by extending the mean conjugation length, which is related to a lower number of linkage errors during polymerization, a higher intra-chain conductivity occurs (see Fig. 3). In addition, a good stereoregularity leads to an increase in the probability of charge carriers hopping among different chains.[7] On the other hand, as well as conjugation length, rigidity of the polymeric chains consequently grows, owing to the strengthened

intermolecular interactions within the backbone. As a result, drawbacks such as low-solubility and decreased flexibility are observed, negatively affecting the polymer's processability. Alternatively, the formation of charge carriers in neutral conjugated polymers can be locally promoted via thermal- or photo-excitation and the modification of electronic states can be obtained through chemical tailoring (for example, by covalent insertion of functional groups such as alkoxy substituents.[8]

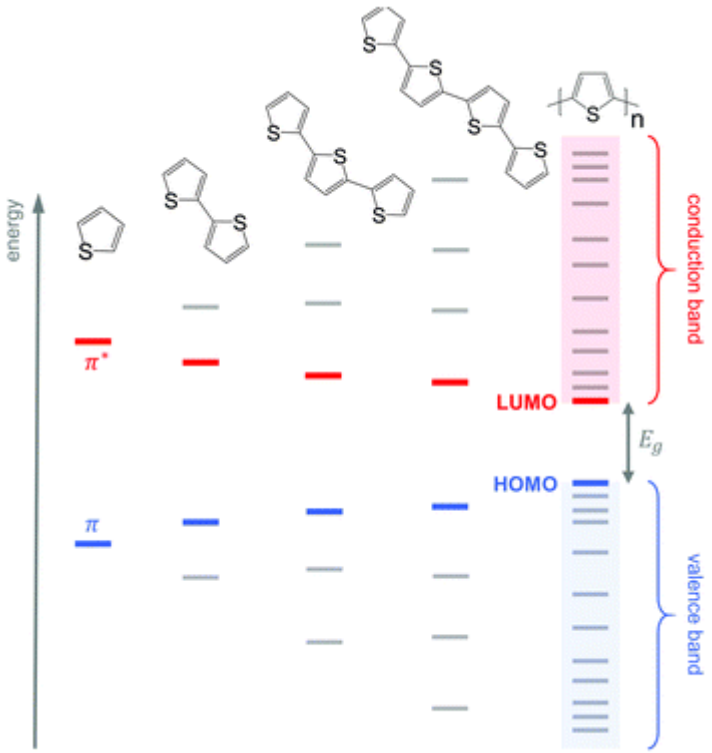

Fig. 3 Evolution of the HOMO and the LUMO levels as well as bandgap E_G with increasing number of thiophene units, resulting for valence and conduction bands for Polythiophene. Adapted from[9].

More interestingly, high conductivities are achieved through chemical or electrochemical doping, which nowadays is most commonly performed during the polymerization itself.

As regards inorganic semiconductors, doping occurs when a foreign neutral atom is embedded into a host lattice, changing the electronic structure in that lattice by introducing electrons or holes. Differently, doping of conducting polymers refers to a chemical reaction, i.e. oxidation or reduction, and it is actually considered a redox reversible process. Both electron donating (n-type) and electron accepting (p-type) dopants, that is, reducing agents and oxidants, have been used to introduce charges into conjugated polymers and make them conductive.

However, the n doping process most commonly requires very strong reducing agents or negative potentials and the strong reducing power of the resulting n-doped polymer makes it unstable.[10]

In case of a p-type doping (Fig. 4), electrons are removed from the π system through the polymer oxidation, which can occur either chemically (i.e. by adding a suitable oxidizing agent) or electrochemically (i.e. by applying a specific oxidative potential). Studies for a clear understanding of doping mechanism are still ongoing, but some hypotheses have been reported.

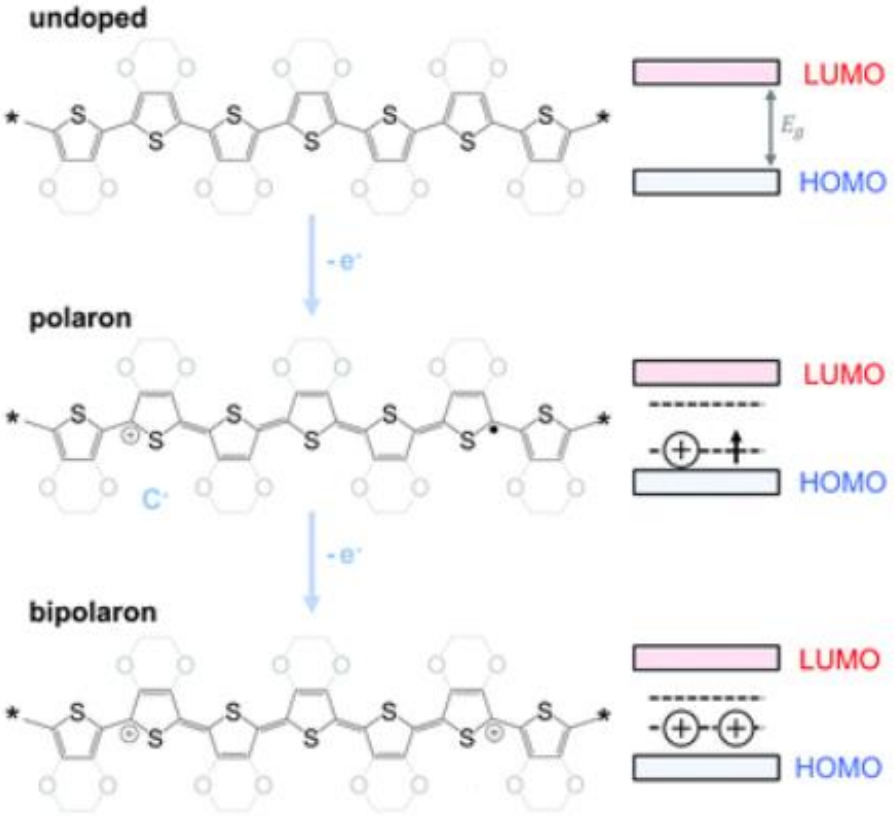

Fig. 4 Polythiophene and PEDOT p-doping process and correspondent evolution of the band structure. Adapted from[9].

First, for each oxidized double bond, a polaron is formed. Polarons are radicalcationic species that, being delocalized along a polymeric fragment, cause a geometric relaxation of the conjugated chain. Once the polymer is charged, the presence of suitable counterions (dopant anions here) to maintain electroneutrality is required.[6] Depending on the doping agent's strength, polarons will have a certain degree of mobility along the chain: the easier the charge transport, the higher the conductivity. Charge delocalization is coupled with structural reorganization into a quinoidal form and a change in fundamental molecular vibrations. UV/vis

and IR/Raman spectra are useful to confirm the appearance of new sub-gap energy states and the formation of a quinoidal structure.[11,12]

Indeed, during the polaron formation, nor the valence band neither the conductive one are involved: the partially occupied levels lie in the band gap and, according to this, no properly metallic character is observed. Doping is reasonably thought to introduce additional electronic states within the band gap of the conjugated polymer without affecting the net probability of a transition to occur among the energy levels. The generated polaron density of state is created by shifting the band density of state upward to band gap.[13]

At a high doping extent, two events may take place: another electron can be removed from the polymeric chain or from the polaron. In the first case, a second polaronic state is generated, while in the other case a bipolaron (i.e. dicationic species) is produced. The formation of a bipolaron, associated with a severe distortion of the lattice, is more likely to occur with respect to the coexistence of two polarons, which would result in a huge electrostatic repulsion. Newly formed bipolaronic states strongly interact with each other and, consequently, the overlap of their electronic wave functions yield a further band of electronic state (usually at a lower energy compared to the polaronic band) within the band gap. Thanks to the formation of an additional, empty band between the valence and the conduction ones, these phenomena lead to an overall decrease of E_G.

It is worth pointing out that E_G and thus conductivity not only change among different ICPs, but are also considerably affected by nature of the dopant, oxidation/reduction level (i.e. doping percentage), synthesis method and temperature. For instance, it is known that a high number of bipolaronic bands, which improves conductivity, is observed at a high doping percentage. As regards the effect of temperature, a semiconductor-fashioned behaviour is observed at low doping level, while an increase in the dopant concentration causes a grow in conductivity when temperature increases.

2.2 Polythiophenes

Although considered as the milestone of ICPs, doped Polyacetylene suffers from its air sensitivity and thus missing processability. With the aim of stabilizing the sensitive π-electron system and reaching higher conductivities, the insertion of heteroatoms in electron-donating substituents or as polymer chain atoms was proven to benefit the conjugated system, especially in the doped, positively charged highly conductive state (bipolaron state). In this scenario, polyheterocycles have emerged as a promising class of conjugated polymers, which exhibit

good thermal stability thanks to their aromaticity, high conductivity and ease of synthesis.[14] In particular, Polypyrrole (PPy), Polyaniline (PANi), Polythiophene (PT) (Fig. 5) and their derivatives stand out as the most scientifically relevant conjugated polymers nowadays.

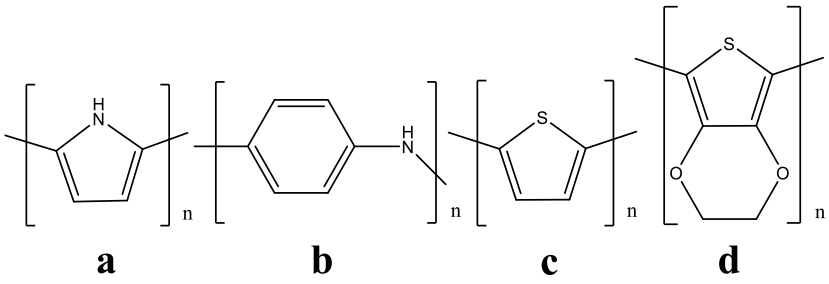

Fig. 5 Chemical structures of PPy (**a**), PANi (**b**), PT (**c**) and PEDOT (**d**).

Since 1967, when it was first mentioned as a potential conducting polymer by A. G. Davies and coworkers[15], Polythiophene has attracted increasing attention, owing to its favourable characteristics in terms of stability, ease of processability and functionalization, reversibility in redox processes and high conductivity (the maximum value reported in literature being 100 S cm^{-1}.[16] In addition, differently from PPy and PANi, PT and its derivatives do not show intense colours, rather enough transparency to be extensively employed in a wide range of thin films applications. Moreover, because of its ease of functionalization, PT has opened up the possibility to fine-tune the electrical properties of a conducting polymer, by optimizing its characteristics for the desired application. In the last decades, an impressive variety of derivatives has been synthesised and intensively examined.[17,18]

Over time, the key points that have been highlighted can be briefly summarised as follows:

- While PT is almost insoluble in the commonly used organic solvents, the introduction of alkyl substituents facilitates the solubilization
- Regioregularity and coplanar arrangement of the aromatic rings, being closely related to interchain contacts and conjugation, are crucial to ensure high conductivity
- Blocking the reactive 3- and 4-position is necessary to inhibits branching, but mono-substituted derivatives suffer from mixed coupling
- Bulky substituents stabilize the polymeric chain, but the steric hindrance sharply lowers conductivity

- Oxygen substituents at the 3- and 4-position in the thiophene moiety further stabilize the doped, bipolaronic state in polythiophenes, thanks to their electron-donating character.

The development of a PT derivative with two heteroaromatic-fused rings, i.e. the introduction of an ethylenedioxy substituent in the 3- and 4- position, addressed all these points. The goals of high conductivity, long-term environmental stability and processability were combined in the unique polymer molecule poly(3,4-ethylenedioxythiophene) (PEDOT, Fig. 5d).

2.3 Synthesis routes of Polythiophenes

Polythiphene and its derivatives can be readily synthesised through chemical or electrochemical oxidative methods. While the chemical routes consist in mixing the monomer solution with an oxidant, such as $FeCl_3$ or $Na_2S_2O_8$, and the doping agent, during the electrochemical polymerization the supporting electrolyte acts as both doping agent and counterion, which progressively diffuses into the growing chain allowing the polymer formation.

Focusing on the electrochemical method, the polymerization is performed through electrodeposition in a three-electrode cell setup, in the presence of a solution containing the monomer, an electrolyte and a suitable solvent. When an opportune potential is applied at the working electrode, the monomer is oxidised and a number of radical-cations is generated. The coupling among these species proceed very fast with respect to the monomer diffusion from the solution, thus it renders the progressive formation of the chain possible nearby the electrode surface, by further radical-radical coupling. The process goes on until an insoluble oligomer is formed and precipitates above the working electrode.

Choosing one method rather than the other will affect from the first steps the nature of the yielding product, its surface and bulk properties and thus the final application.

Chemical synthesis provides a wide variety of routes to obtain different types of CPs: typically, it yields a bulk product, which can be easily modified afterwards. For those reasons, it is particularly suitable for a large-scale production. All CPs can be synthesized chemically, while electrochemical synthesis is limited to those systems in which the monomer can be oxidized by means of an applied potential. However, all standard CPs can be obtained electrochemically, thus electrochemical synthesis is a very common alternative for making CPs. It benefits from a relatively straightforward procedure, high efficiency and, most importantly, it allows the formation of readily tailorable, highly conductive, homogenous thin films.

The importance of addressing the synthetic path towards realisation of specific characteristics of the system is evident.

3. PEDOT:PSS

Poly(3,4-ethylenedioxythiophene) was invented in 1988 at Bayer AG research laboratories, Leverkusen, and it has thenceforth stood out as the gold star of conductive polymers. PEDOT has not only attracted remarkable scientific interest, but also is receiving great attention as technically used material in different products of modern life. Indeed, nowadays it is the only one large-scale produced CP and it finds broad application in plastic electronics, as charge transport material in organic light emitting diodes (OLEDs)[19], organic photovoltaics (OPV)[20], memory storage devices, thin-film transistors, electroactive interface material for bioelectronic applications and so on.

In fact, in addition to the characteristics that make it an excellent CP, PEDOT exhibits attracting properties, such as reversible doping and low-energy band gap (1,6-1,7eV)[21], which render it suitable for electro-optical applications. Moreover, owing to its electrochromism, PEDOT absorbs in the visible region in its blue-colored neutral state, while oxidised PEDOT is very transmissive and its absorption band lies in the NIR region. As previously explained, the presence of an ethylenedioxy group in the thiophene moiety yields a resulting polymer with enhanced regioregularity. Additionally, this substituent is responsible for considerably lowering the oxidation potential of both the monomer and the growing polymer, thus stabilizing its conductive form and facilitating the electrochemical synthesis. A massive drawback of PEDOT is its insolubility: to overcome this problem, water-soluble polyanion poly(styrenesulfonate) (PSS^-) is commonly employed as doping agent and counterion during EDOT polymerization. The result is PEDOT:PSS (Fig. 6), a polyelectrolyte complex that is commercially available as stable dispersion and widely used to obtain thin films through many deposition techniques, such as spin coating and ink-jet printing.

PSS as a counterion for PEDOT is always used in excess, that is, as host polyelectrolyte (HPE). The molar ratio of thiophene groups to sulfonic acid groups in standard PEDOT:PSS dispersions is in the range of 1:1.9 to 1:15.2, which corresponds to a weight ratio range of 1:2.5 up to 1:20. Since only one charge is found for every three to four thiophene rings, the charge excess of PSS is between 6-fold and 46-fold.[6]

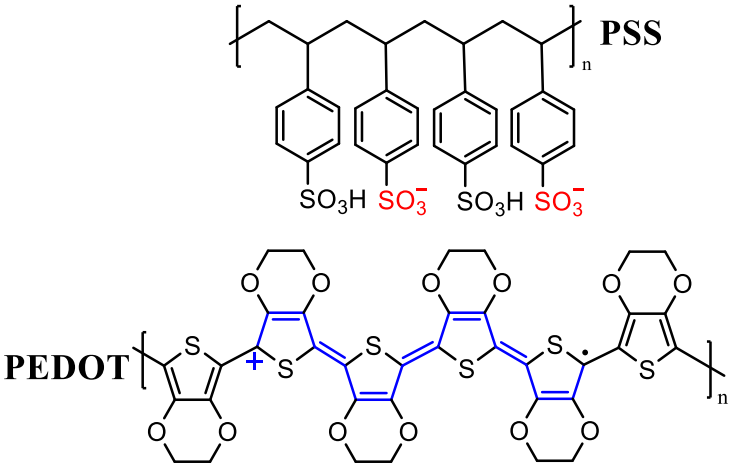

Fig. 6 Chemical structure of PEDOT:PSS.

Due to the electrostatic interactions between PEDOT and the PSS chains, a core–shell structure with a PEDOT core and a PSS shell forms micro-gel particles (10 nm - 1 mm) in water with minimum interactions between PEDOT and water. The non-stoichiometric ratio of PSS to PEDOT also results in a scrambled egg conformation of PEDOT:PSS in water, which remains as colloidal particles at dilute concentrations (<0.1 mg mL^{-1}).[22]

As regards electrical conductivity, the value for both chemically and electrochemically prepared PEDOT:PSS is reported to range from 400 to 600 S/cm while still transmitting around 80% of visible light.[23] It is known that conductivity can be increased of several orders of magnitude by adding some high boiling substances to PEDOT:PSS dispersions, the most common being dimethyl sulfoxide (DMSO), copper(II) chloride, ethylene glycol (EG) and dodecylbenzenesulfonic acid (DBSA).

3.1 PEDOT:PSS thin films properties

It is well known that the properties of materials significantly change when they are in the form of thin films and most of the functional materials are rather applied in thin film form due to their specific electrical, magnetic, optical properties or resistance. Thin film technologies make use of the fact that the properties can particularly be controlled by the thickness parameter.[24]
Thin films deposited from aqueous PEDOT:PSS dispersions have been utilized in a wide range of applications, from integrated circuits to sensors, including photovoltaics, electrochromic devices, displays and memories. Indeed, the processing of materials into thin films allows easy integration into various types of devices.

For organic electronic and electrochemical applications, electrical conductivity of the electroactive film is a crucial parameter to consider. The film thickness, the lattice dimensions and order, the purity and the surface roughness are key aspects in defining the type, mechanism and stability of the electrical transport.

Charge transport in PEDOT:PSS films takes place through a hopping mechanism. The charge is transported between PEDOT-rich conductive regions, separated by insulating, PSS-rich regions, which represent the main obstacle to transport electric current within the material.[25] It is also known that an increase in the order of the PEDOT segments within the film leads to the formation of highly conductive pathways.

This positive effect is observed whether a thermally-promoted rearrangement takes place after the deposition, i.e. if the film is treated with high boiling solvents or undergoes annealing: the blend of polymeric chains rearranges from a ”frozen”, unstable state to a thermodynamic-like form. Moreover, many recent examples dealing with ultra-highly conductive films can be found in literature. For instance, a maximum electrical conductivity of 930 S cm^{-1} has been reached, without losing optical transparency, by treating the film with a solution of 2-Methylimidazole in ethanol[26], while the record-high PEDOT:PSS conductivity of 4600±100 S cm^{-1} (comparable to that of Indium Tin Oxide, ITO) has been obtained by using solution shearing to fabricate highly performant, transparent films for capacitive pressure sensors and ITO-free OPV devices.[27] Optoelectronic properties have been enhanced by doping PEDOT:PSS with different proportions of colloidal Ag nanoprisms, obtaining hybrid thin films for organic solar cells[28] and the influence of different doping agents over PEDOT thin films morphology and performances has been studied.[29]

As already mentioned, additives such as EG and DBSA are commonly employed as stabilizator and surfactant/filmforming promoter, respectively, in PEDOT:PSS dispersions and both of them contribute to increase the film conductivity.[30] Their mechanism of action is still under debate, but some hypotheses propose the occurrence of a screening effect over the polyelectrolyte complex chains, thus enhancing the charge carriers hopping rate[31], a plasticizer effect that improve the reorientation of the PEDOT:PSS chains after annealing[32] or a reorganization of the chains within the lattice.[33] Also, conductivity enhancement has been attributed to the fact that additives may allow the removal of the insulating excess of PSS^-.[34] Among the additives, a particular class includes cross-linkers. These substances are adhesion-promoter, since they boost the formation of covalent bonds between polymer chains, thus changing their physical properties and making the film more stable.

3-glycidoxypropyltrimethoxysilane (GOPS) is the most commonly used cross-linker for PEDOT:PSS dispersions that is capable of preventing film delamination from a substrate. Indeed, due to the high hydrophilicity of PSS, the exposure of PEDOT:PSS to water is usually followed by delamination. Although addressing this issue, increased thickness and lower conductivity of the resulting films are reported as main drawbacks for GOPS use.[30] Several ready-to-use formulations optimized for specific applications and deposition techniques are commercially available, the most commonly used being produced by Heraeus GmbH (Clevios) and Sigma-Aldrich.

3.2 PEDOT:PSS thin films deposition and patterning

Plenty of methods yielding polymeric thin films are currently available and the choice among them should be mainly driven by both the processability of the raw starting material and the specific requirements related to the final application. Generally, the goal is to combine processability, stability and efficiency. The ideal process should involve as few steps as possible, it should be low-cost and free from toxic agents, thus leading to a final product that owns a low environmental impact and that is desirably recyclable.

An overview of the most common film-forming techniques follows.[6,35]

First of all, it is useful to distinguish between coating and printing techniques: roughly, while coating is used to describe a process by which a layer of ink is transferred to the substrate by essentially pouring, painting, spraying, casting or smearing it over the surface, printing often implies that a complex pattern is impressed. However, the boundary line is far from being well-defined: ink-jet printing, for instance, is essentially a coating technique that gives the possibility to reproduce a complex pattern.

Being spin coating, doctor blading and casting the most widespread techniques, from a processing point of view more desirable film-forming features can be found in slot-die coating, gravure coating, knife-over-edge coating, off-set coating, spray coating and printing techniques such as ink jet printing, pad printing and screen printing. Afterwards, electrochemical oxidative polymerization will be treated and photolithography as a route to perform structured depositions will be considered.

- Casting

Probably the simplest film-forming technique available, no equipment is needed apart from a very horizontal work surface. The procedure is to simply cast a solution onto a substrate

followed by drying. While it is possible to prepare films of good quality and also thick films, the technique obviously suffers from a lack of control.

- Spin coating

Typically, this technique involves the application of a liquid (for example, a PEDOT:PSS dispersion) onto a substrate and, after that, the substrate is accelerated to a chosen rotational speed through a suitable equipment. Alternatively the liquid solution may be applied while the substrate is spinning. The resulting thickness, morphology and surface topography of the film are closely related to rotational speed, viscosity, volatility, diffusivity, molecular weight and concentration of the solutes. The deposition of PEDOT:PSS dispersions by spin coating, with respect to the other techniques, has proven to be an easily accessible technique to obtain uniform, highly reproducible films in a thickness range from 10 to 1000 nm. It has several advantages over other coating techniques and allows the formation of very homogenous films over a large area (the diameter of the substrate can be as high as 30cm). The technique is also used in the microelectronics industry during application of polymeric photoresists to silicon wafers. The main drawbacks are that spin coating does not allow for patterning and it produces a considerable amount of waste, since during the spinning the majority of the solution is lost.

- Doctor blading

If a well defined film thickness is required, using a doctor blade is a valid alternative to spin coating. The deposition procedure consists in placing a sharp blade at a fixed distance from the substrate surface that is to be coated; then, the coating solution is placed in front of the blade, which is moved linearly across the substrate leaving a thin wet film after the blade. In contrast to spin coating, the technique avoids excessive waste formation, but it also shows the inconveniences of being time-consuming and easily obstructed by aggregates formation.

- Ink jet printing

Ink jet printing is a relatively novel process with respect to the other deposition technologies. The ink jet printing process has the advantage of quite high resolution, ranging from 300 up to 1200 dpi (dots per inch). In contrast to most other printing relevant techniques, such as screen printing, it does not require a complex master, as the source image to be printed is digitally impressed. The printing technique is based on the formation of a small droplet of ink that is then deposited on the substrate. The formation of the droplet may be by mechanical compression of the ink through a nozzle (piezoelectric) or by heating the ink (and thus creating a pressure increase). The droplet is then electrostatically charged and accelerated towards the substrate by an electric field. This all puts some constraints on the ink formulation. Generally the inks are required to be of low viscosity and require to be electrostatically charged. The

advantages include the possibility of creating complex patterns, but the printing speed is highly affected by the ink composition and viscosity.

- Electrochemical oxidative polymerization

In the electrochemical oxidative polymerization, the monomer EDOT undergoes polymerization at an electrode,which is the substrate that is to be coated. During the polymerization, anionic dopant PSS from the electrolyte diffuse into the growing chains of PEDOT. Electrodeposition can be carried out in a three-electrodes setup cell using three different techniques: the galvanostatic, the potentiostatic and potentiodynamic methods. Among them, the most suitable for filmforming is the potentiodynamic deposition, during which the potential of the working electrode is ramped linearly versus time at fixed scan rate. By tuning deposition parameters, such as monomer concentration, scan rate and applied potential, a fine control of the film quality is possible. The electropolymerization of PEDOT:PSS has been proven to produce films and micro-structured systems[36] with facile electrochemistry, high-ionic conductivities, good electrochemical stability and high capacitance. Moreover, this technique enables the efficient functionalization of electroactive PEDOT:PSS films.[37] A major limitation is, obviously, that the substrate must be conductive for the polymeric film, thus the range of shapes and quantities that can be synthesized will be restricted by the geometry and surface area of the electrode. On the other hand, electrochemical oxidative polymerization provides a high efficiency of material usage and the formation of a homogeneous outer polymer layer, which show excellent edge and corner coverage. Other advantages include a wide variety of available counter ions, the possibility of patterning and control over thickness as well as the oxidation state and morphology of the polymer layer.

- Spray coating

Mostly employed in organic photovoltaics, this technique is based on forcing the printing ink through a nozzle, whereby a fine aerosol is formed. A carrier gas and electrostatic charging may be involved to aid in directing the aerosol at the surface that is to be coated. The nozzle is moved at a constant rate over the temperature-controlled substrate and the solution coalesces and spreads over the entire substrate. Once the solvent evaporates, the electrically-conducting film is formed. Critical deposition parameters that govern the properties of the cast films are: the substrate temperature, solvent composition and additives, volumetric spray rate, lateral nozzle speed, and nozzle-to-substrate distance. Spray coating requires a precise temperature control and patterning can be performed with a millimetric-scale resolution. It does not need high quantities of chemicals and the process is scalable to mass production. As an example, highly

conductive, transparent PEDOT:PSS thin films have recently been achieved by spray coating for solar cells applications.[38]

- Photolithography

Recent developments in the fabrication of OLED and OTFT have dug out the need for high-resolution and chemically compatible patterning techniques for organic semiconductors. Nowadays, shadow masks patterning and ink-jet printed structured depositions are mostly considered inadequate to achieve micrometer resolutions, large area stencils are hard to fabricate and maintain, while ink jet methods require specially formulated inks and non standard equipment. In this scenario, photolithography, which is the technique of choice for the patterning of inorganic electronic materials, remains the most attractive thin film patterning technique to date. This is due to the host of advantages photolithography offers, which include straightforward scaling to large area substrates, availability of a broad basis of equipment and expertise, and the high throughput fabrication.[39] Basically, this technique uses light to transfer a geometric pattern from a photomask to a light-sensitive chemical, called photoresist, on the substrate. Features and possible approaches will be deeply discussed in the next chapters.

4. Emerging applications of PEDOT:PSS in Bioelectronics

4.1 OECTs: working principles

Originally developed by White et al.[40], an organic electrochemical transistor is basically a three terminal device in a transistor configuration, where a conductive channel (i. e. a thin film of a CP in its doped, conducting state) is deposited onto a supporting substrate, source (S), drain (D) and gate (G) contacts are usually metallic and an electrolyte medium in direct contact with the channel and the gate is an integral part of the device structure.

These devices exploit the reversible doping/dedoping effect induced on the CP-based channel by the application of a gate voltage, V_g, through an electrolyte solution. Thanks to the high difference in conductivity between doped and dedoped states of conjugated polymers, the effect of the gate voltage is to induce a pronounced switch between an "on" (i.e. conductive) and an "off" (i.e. non conductive) state of the polymer.

This change in conductivity can be observed by measuring the modulation of the current flowing between source (grounded) and drain electrodes, I_d, generated by an applied source-drain voltage V_d, upon the application of the gate voltage.

OECTs can work in accumulation or depletion mode, the latter meaning that the conducting polymer is used in its pristine doped state, and is then switched to de-doped by the application

of V_g during the operation. Since PEDOT:PSS-based OECTs are used in depletion mode for the applications described in this thesis, only this operation mode will be analysed. Moreover, dealing with a degenerately p-doped CP, the nomenclature will be referred to p-type doping, with negligible contribution to electrical conductivity from electrons and anions. This implies that the application of a positive V_g (relative to ground, i.e. the source electrode), by causing the injection of cations from the electrolyte into the PEDOT:PSS film, leads to a de-doping of the CP itself and thus decreases the source-drain current I_d.

The behaviour of an OECT can be understood by considering a model based on the interaction of two electrical circuits: the electric one, accounting for the hole transport within the channel, i.e. between source and drain, and the ionic one, in which ions are transported through the electrolyte and across the electrolyte/semiconductor interface.

- The electronic circuit is approximated by a resistive element following Ohm's law:

$$J(x) = q\mu p(x)\frac{dV(x)}{dx}$$

where J is the current flux, q is the elementary charge, μ is the hole mobility, p is the hole density and dV(x)/dx is the electric field through the semiconductor. By applying a positive V_g, cations are repelled from the gate electrode into the organic semiconductor, and to maintain charge neutrality, for each ion entering the film a hole extracted from the source is not replaced from injection at the drain electrode. Generally, μ is taken as a constant with respect to electrical field and carrier density, while the total charge density is assumed to be uniform within the whole film thickness.

- The ionic circuit, accounting for the motion of ions through the electrolyte and the charge

transfer and accumulation at the gate electrode/electrolyte and channel/electrolyte interfaces, can be modeled as a resistor (R_s) and a capacitor (C_d) in series. The resistor stands for the conductivity of the electrolyte and depends on its ionic strength, while the capacitor is the sum of two capacitors in series, which correspond to the polarization occurring at the interfaces just mentioned.

In the presence of a reactive species in the electrolyte solution, the Faradaic regime of operation should be considered. Such species induce a shift in the electrochemical potential of the solution, thus leading to a shift in the gate voltage: $V_g^{eff} = V_g + V^{offset}$, where the resulting V_g^{eff}

is the effective gate voltage acting on the channel, while V^{offset} is an offset voltage that depends on the analyte concentration.
If the non-Faradaic regime of operation is considered, the application of a gate voltage is followed by the charging of the capacitor C_d, which refers to the amount of ions that can be stored in the bulk of the CP. Indeed, rather than capacitance per unit area, volumetric capacitance has been pointed out as a suitable parameter for describing OECTs operation.

Two distinct behaviours for OECTs have been extensively studied[41] and the systematic dissertation will be omitted in this thesis. The steady-state behaviour concerns the study of I_d as a function of V_d, while V_g is maintained at a fixed value. On the other hand, when V_d is kept at a constant value and V_g follows a square waveform, the observation of I_d as a function of time is related to the OECT transient behaviour.

OECTs have recently been employed in sensing and interfaced with cells for both in vitro and in vivo applications. In most of the cases, the device convert a modulation in the gate voltage, ΔV_g, to a modulation in the drain current, ΔI_d. The figure of merit that determines this conversion is transconductance, g_m, a key parameter that governs signal amplification:

$$g_m = \frac{\Delta I_d}{\Delta V_g}$$

A high transconductance value, for instance in sensing, leads to an increase in the S/N ratio and a lower detection limit, which in turn result in a higher sensitivity, since a small input signal yelds a large response in the output.

The transistor performances, which are affected by the interplay between ionic and electronic currents, can be tuned by varying some parameters, such as the material/size of the gate, the resistance of the electrolyte and the size/geometry of the channel. For instance, micrometer scale transistors exhibit fast responses that are stable for higher frequencies, thus making these devices suitable for monitoring biological events. Indeed, a thinner channel undergoes de-doping more easily if compared to a thicker film. At the same time, the drain current decreases, leading to a lower transconductance.
Otherwise, the employment of CPs with higher volumetric capacitance would lead to devices with a higher transconductance.

Obviously, further improvements can be achieved through chemical functionalization or synthesis of new materials. [42,43]

4.2 Sensing with PEDOT:PSS

Since 1980s, when R. W. Murray claimed that "chemical modification yields a new degree of freedom in electrochemical science" in his review "Chemically Modified Electrodes"[44], electrochemistry at chemically modified electrodes (CMEs) has revolutionized the field of electroanalysis. In particular, the evolution of amperometric sensing from the bare to the modified electrode systems has been triggered by the development of three main electrode modifiers, namely conducting polymers (CPs), SAMs and nanostructures[45], all of them providing an electrocatalytic effect that springs from their inner nature of electron transfer mediators.[46] Commercial availability of precursors, ease of synthesis and feasibility of further functionalizations have strongly facilitated the wide diffusion of these materials. Among them, CPs and especially polytiophenes are nowadays considered as flagship surface modifiers for electrode systems devoted to amperometric sensing. Their popularity relies on the fact that polytiophenes supply antifouling properties and impart a certain electrocatalytic activity to the electrode, both of these features being added values sought in the realization of an effective amperometric sensor.

An amperometric sensor is a device that provides quantitative information about a redox-susceptible species, i.e. the analyte. By applying a suitable potential waveform, in which the potential can be either steady or transient and is accurately controlled with respect to a reference electrode, the electroactive analyte undergoes reduction and/or oxidation and the current resulting from the faradaic process is recorded. The quantitative detection of the target molecule depends on the proportionality existing between the intensity of the current signal and the analyte's concentration. A critical point concerning the development of an amperometric sensor is the choice of the sensing material.

As polytiophene derivative, PEDOT shows desirable features,[10,47] such as antifouling properties, that is, it prevents poisoning, insulating layers to form or adsorb onto the electrode surface. This is a key point in order to record reliable and repeatable measurements, thus expanding the linear response range of the sensor towards the target molecule. Moreover, a major advantage in the use of PEDOT as sensing material is its electrocatalytic activity. The capability to activate catalytic charge transfers, which belongs to redox mediators, implies two significant benefits for sensing: first, it boosts the redox process by allowing it to take place at

lower potentials with respect to those required for bare electrodes, sometimes even avoiding them to occur beyond the solvent discharge; furthermore, catalysis is also responsible for enhancing resolution whether interfering species are present. Thanks to the improved reversibility degree of the electrochemical process induced by electrocatalysis, the resulting currents are generally higher, thus leading to a lower limit of detection (LoD). Additionally, owing to the low oxidative potential at which EDOT polymerizes, PEDOT shows a wide anodic potential window and, since the polymerization is easily run in aqueous media leading to electrochemically stable films, PEDOT:PSS based sensors results noteworthy tools for many electroanalytical applications. Nevertheless, being PEDOT readily functionalizable, selectivity towards the target molecule can be driven up by using the PEDOT:PSS coated electrode as a matrix to covalently bind the desired functional groups.

For all the aforementioned reasons, PEDOT:PSS and its composites have been extensively employed as appealing sensing element in amperometric sensors, electronic tongues and noses, organic electrochemical transistors and smart textiles not only for the detection of a broad spectrum of biomolecules, gases, metal ions, but also for monitoring environmental parameters such as humidity, temperature, pressure and so on.

4.2.1 Dopamine detection

3,4-dihydroxyphenyl ethylamine, commonly known as dopamine (DA), is an important neurotransmitter in the mammalian central nervous system, where is involved in motor control, hormonal release and emotional responses. It is well documented that dopamine deficiency is related to the onset of Parkinson's disease[48] and other neurological disorders. Therefore, rapid and accurate determination of DA is a topic objective for diagnostics and healthcare. For this purpose, a substantial variety of studies in the electroanalytical research field has been devoted to DA detection, but, to date, performances satisfying analytical requirements for relevant applications in real matrices have still to be attained.

Traditional methods of DA detection in biological fluids include chromatographic, colorimetric and spectroscopic techniques. However, these methods require non-standard, expensive equipment or reagents, as well as long sample processing times, which hinder their use in clinical applications and make exploratory research slow and costly. In this scenario, electrochemical methods that take advantage of the redox activity of DA have received considerable interest, since they enable a facile, rapid analysis of biological samples using low-cost electrodes as sensors. After all, current electrochemical sensors suffer from serious shortcomings, namely poor sensitivity and specificity towards DA. With respect to DA

electrochemical detection, plenty challenging circumstances have been stressed in literature and all of them should be borne in mind while approaching this topic.

Firstly, physiological levels of DA vary within the nanomolar range (10-20 nM in brain, < 1 nM in plasma and urine), thus demanding highly sensitive devices with very low detection limits. Furthermore, the ubiquitous presence of electroactive species, such as ascorbic acid (AA) and uric acid (UA), which usually coexist with DA in real samples and hence act as interfering molecules in DA detection, highlights the problem of selectivity. Besides that, AA and UA show similar redox behaviour compared to DA and their levels are generally 100-1000 times higher than that of DA in physiological samples. In particular, oxidation potentials of DA and AA are so close at conventional bare electrodes, such as Au, Pt and GCE, that the two signals appear completely overlapped. Moreover, the oxidation product of DA can catalyse the oxidation of AA, which may lead to the electrode fouling with poor selectivity and reproducibility.

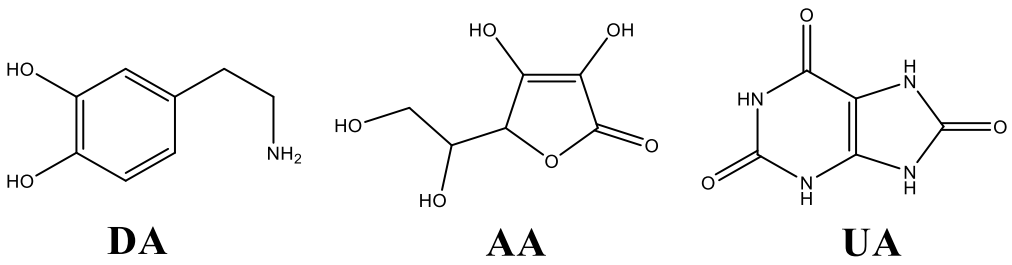

Fig. 7 Chemical structures of DA, AA and UA.

4.2.2 Dopamine detection: state of the art

To address all these issues, a variety of CMEs showing different performances and involving a broad spectrum of materials has been proposed recently. Some relevant examples are reported below.

In 2014, our group developed a ferrocene clicked PEDOT:PSS coated electrode for dopamine amperometric detection, in the absence of interfering agents.[37] Simultaneous determination of DA, AA and UA has been carried out by using a poly-2,6-diaminopyridine/MWCNTs modified GC electrode[49], a carbon ionic liquid electrode (CILE)[50], a HGNs (hollow gold nanospheres) modified pencil graphite electrode (PGE)[51] and a PEDOT-modified integrated microelectrode[52] for differential pulse voltammetry (DPV) experiments in ternary mixtures. Among these references, the first one reports the lowest detection limit towards dopamine (i.e. 0,0416 μM).

Moreover, G. Fabregat et al. designed a PEDOT coated GC electrode for the selective detection of DA by performing cyclic voltammetry (CV); they also pointed out the inefficacy of

embedding AuNPs within the polymeric film and found out that better resolution and sensitivity towards dopamine are achievable by replacing PEDOT with hydroxymethylPEDOT, in which the hydroxy group facilitates the formation of intermolecular hydrogen bonds between the sensing material and the oxidized form of DA.[53]

It is worth pointing out that recent advancements in organic electrochemical transistors (OECTs) technology have opened up new possibilities for getting higher performances towards biomolecules sensing. An OECT belongs to the wide family of organic thin film transistors (OTFTs) and it basically consists in a stripe of conductive polymer that works as a channel and by another electrode, namely the gate, which is usually metallic. This device can work as chemical sensor, as long as the redox-active analyte affects the electrochemical processes that control the doping of the CP, thus changing the current that flows in the channel. In addition to its ease of fabrication, an OECT does not require any reference electrode and the signal can be rapidly collected with a very simple and low cost readout electronics. The reason why OECTs are considered promising tools for tricky sensing purposes relies on the inherent signal amplification provided by the transistor configuration. Indeed, since small potential changes due to the analyte presence are followed by a large variation of the channel current, high sensitivity and a very low limit of detection are achievable. An all-PEDOT:PSS OECT was proposed last year as low cost and enzyme-free sensor for the determination of ascorbic acid.[54] Among the latest developed PEDOT:PSS-based OECTs for dopamine detection, remarkable interest has been attracted by the work of H. Tang et al., who have developed a highly sensitive device employing a Pt gate[55], C. Liao et al., with a gate modified with Nafion-graphene[56] and K. Tybrandt et al., who performed dopamine detection in fast scan cyclic voltammetry with a OECT-gold microelectrode integrated system[57], the first two devices obtaining the best performances in terms of sensitivity and lowering the LoD down to 5 nM.

It clearly stands out from literature that, in order to pursue a selective and sensitive determination of dopamine, a deeper understanding of the cross-talking effect occurring over DA is essential in multi-analyte samples. It implies avoiding reckless generalizations, since every electrochemical system has its own peculiarities and should be coherently considered with respect to its specific reference context. However, it has been proven that, by simply tuning experimental parameters and choosing an appropriate technique for the measurements, discrimination among the signals and electrochemical detection of the target molecule in a ternary mixture of DA, AA and UA can be achieved by using an amperometric sensor. PEDOT:PSS thin films as sensing coatings are suitable to be exploited for this purpose, thanks

to their favourable antifouling and electrocatalytic properties. On the other hand, whether amperometric sensing poses too many constraints in terms of detection limits, OECT technology can be evaluated for real applications.

4.3 PEDOT:PSS for cells monitoring

Despite the demanding research for materials allowing the communication with the biologic world has slightly held back the emphasis in developing new applications, the novel field of organic bioelectronics has grown rapidly over the last decade.[58,59]

The employment of CPs, and especially PEDOT:PSS, at the interface with life sciences has disclosed many opportunities and is fuelled by some unique features of these materials.[4] First of all, owing to their soft nature (if compared to the hard silicon-based electronics), conducting polymers show good mechanical compatibility with both biological tissues and flexible mechanical substrates. Moreover, this peculiarity echoes in their capability of transporting not only electrons and holes, but also ions, thus allowing the transduction of biological events. Indeed, thanks to the van der Waals interactions among the chains and the water-induced swelling, there is enough space for ions to move within the film lattice. As well as the majority of CPs, PEDOT:PSS is fully biocompatible and its high transmittance renders its films perfect substrates for microscopy-assisted analysis and optical transmission imaging. Additionally, CPs allow for oxide-free interfaces with aqueous electrolytes, thus they can be in direct contact with the biological milieu. In conclusion, their facile processability and functionalization renders CPs a tunable, versatile platform for a great deal of applications. Among the most appealing organic electronic devices used in bioelectronics, PEDOT:PSS-based organic electrochemical transistors (OECTs) play a key role in the development of novel biomedical devices for therapeutics and diagnostics.

4.3.1 Cell Culture Biology towards the 3rd dimension

In 2015 Biopharmaceutical R&D report, Pharmaceutical Research and Manufacturers of America (PhRMA) group stated that “from drug discovery through FDA approval, developing a new medicine on average takes at least 10 years and costs $2.6 billion. Less than 12% of the candidate medicines that make it into phase I clinical trials will be approved by the FDA”.

Reliable in vitro models are urgently required, in order to reduce costs and time in the assessment of new drugs and to handle toxicological profiling of more than 30000 chemicals imported in Europe, according to the REACh’s guidelines, which also insist on the reduction of animal-based testing methods.

So far, the most commonly used approach to study tissues in vitro has relied on 2D monolayer tissue cultures, however they have the major disadvantage of not reproducing the communication network that maintains the specificity and homeostasis of tissue in organs. Recent advancements in the field of biology have demonstrated that, by allowing cells to grow and interact with their surroundings, thus in 3D, it is possible to achieve more physiologically relevant in vitro cell models. Indeed, 3D cell cultures closely retain tissue-specific architecture based on cell-cell and cell-extracellular matrix interactions, thus accurately mimic both in vivo mechanical and biochemical characteristics. [60,61] By improving the quantitative and physiological accuracy of in vitro systems, 3D models can have a profound impact on the screening of newly formulated drugs.[62]

In this scenario, mono and multicellular spheroids have stood out as a promising technology for the development of 3D in vitro culture models. A spheroid culture consists in a non-substrate-adherent, aggregated, mutually adherent population of cells adopting a spherical-like shape and a major advantage of cell spheroids is their ease of fabrication protocols, as it is not required the use of any external scaffolds to form. [60]

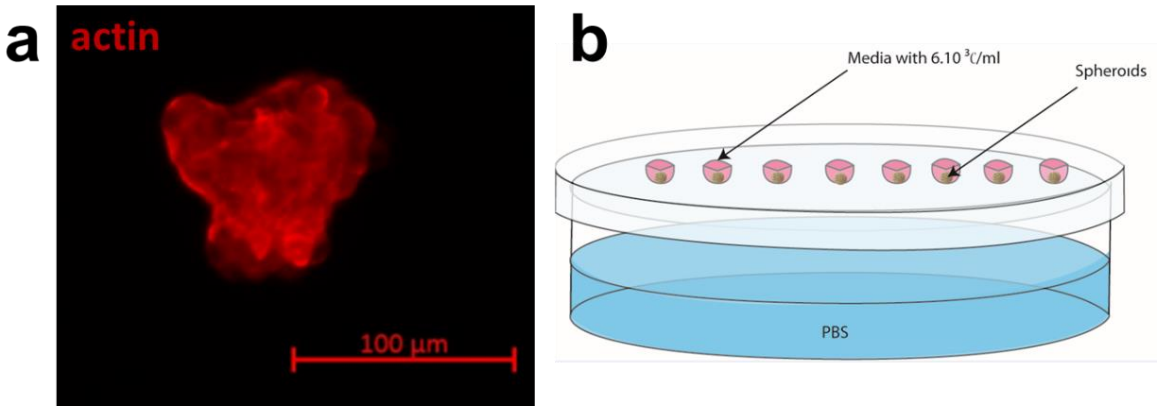

Fig. 8 (**a)** Picture of an MDCKII spheroid obtained at BEL (Department of Bioelectronics, Ecole Nationale Supérieure des Mines de Saint-Etienne) using the Hanging Droplet Culture Plate (HDCP) technique (**b**).

On the other hand, isolation, manipulation and efficient characterization of spheroids and cysts pose some challenges for existing technologies. Among the currently available techniques, only few systems are suitable to monitor spheroids' electrical properties effectively.

4.3.2 OECTs as impedance sensors for cells monitoring

It is known from literature that, within epithelial as well as endothelial cell layers, the preservation of intercellular junctions resulting in a tight cellular barrier is crucial for the physiological activities of the corresponding tissue.[63] To assess and quantify the barrier integrity, permeability assays based radioactively labelled substances or fluorescent dyes are available. Alternatively, a straight-forward method is the measurement of biologically relevant parameters such as TEER (trans-epithelial/endothelial electric resistance) and capacitance of the membrane. Electrochemical impedance spectroscopy (EIS) has long been used to investigate the phenomena occurring at electrode/electrolyte interfaces. A typical EIS experiment consists in the application of a small AC bias across the system of interest and the subsequent recording of the output current response over a fixed frequencies range. Electrical impedance sensing is a particularly promising approach that allows high-throughput, label-free testing for in vitro toxicology and drug screening. Impedance can be expressed as the sum of two contributions, i.e. a real part and an imaginary part:

$$Z = R + jX$$

In biological samples, resistance (R, the real part) is affected by factors that block the ions flow when an electric field is applied (i.e. insulating cell membranes or cell junctions), while reactance (X, the imaginary part) is related to the presence of insulating cell membranes acting as capacitors.

As previously mentioned, in a OECT the drain current depends on the number of ions that enter the channel and the ionic flux determines the speed at which the transistor reaches the steady state. Thus, the OECT acts as a transducer of ionic signal to electronic current. This feature, combined with the inherent amplification exhibited by this device, can be exploited to detect changes in the ionic flux into the channel induced by the presence of a biological membrane. Additionally, as long as low level gate currents can be transduced and the device exhibits a fast response time, also high frequency data are accessible. Both the gate and the drain currents of an OECT can be utilized to perform frequency-dependent measurements, an impedance spectrum over a broad range of frequency can be obtained. Thus, it allows the accurate sense of both highly resistant cell barrier as well as low resistant and adherence cells (coverage).

Afterwards, the collected data can be applied to an equivalent circuit models to extract biologically relevant parameters. This impedance-based approach for cells sensing through the

use of OECTs has been recently employed for studying MDCK I (Madin-Darby canine kidney) epithelial cells monolayers seeded onto the OECT channel[64], for monitoring the barrier tissue integrity within a Caco-2 cell line, seeded in a transwell filter in proximity of the channel[65] and to assess the barrier integrity of cyst-like 3D cultures, after being isolated by capillarity.[66]

4.3.3 Manipulation of 3D cell cultures: Microfluidics

Microfluidics is the multidisciplinar technology of systems that process or manipulate small amounts of fluids (from 10^{-6} down to 10^{-15} L), using channels with dimensions ranging from tens to hundreds of micrometers.

Exciting applications of microfluidics currently deals with DNA chips, Lab-on-a-chip and the newborn Organ-on-a-chip technologies. Moreover, even the scaling-up of chemical processes can take advantage of microreactors, which facilitate the safe and easy handling of hazardous or instable materials and highly exothermic reactions, allow a scale-independent synthesis and provide energy-savings through control over reaction temperature, improved mixing quality, instant removal of the material from the reaction zone, offering several upgrades relative to traditional batch procedures.

Focusing on cell culture biology, this micro-domain technology has opened up new opportunities for interacting with life science and mimicking the in vivo environment. First, thanks to their micro-scale dimensions, microfluidic systems can easily imitate the dynamic phenomena that dominate a bio microenvironment. As well as in a living tissue, in a microchannel device the fluid flow is laminar and the mass transport is possible only by diffusion. Furthermore, plenty of biocompatible materials have been reported (above all, PDMS) for the fabrication of easily feasible and tunable micro-networks. For all these reasons, microfluidic platforms can be very useful for in vitro drug testing where 3D cell cultures are involved: these systems allow for the growth of spheroids of homogeneous sizes and for the subsequent exposure to the desired treatments.[67,68]

Aim of the work

The purpose of this thesis is twofold. By taking advantage of the well-known versatility and favourable characteristics of poly (3,4-ethylenedioxythiophene) : poly (styrenesulfonate) (PEDOT:PSS) as a key figure in organic electronics, its applications in the form of thin film have been explored in two main research fields, namely electrochemical sensing and cells monitoring. A multidisciplinary approach turned out to be the *conditio sine qua non* for attending all the results presented in this work.

1. *Optimization of a low-cost, PEDOT:PSS-based amperometric sensor for the selective detection of Dopamine in a ternary mixture.*

The accurate determination of 3,4-dihydroxyphenethylamine, also known as dopamine (DA), is crucial in the diagnosis of several neurological disorders. However, owing to ubiquitous interferants, such as ascorbic acid (AA) and uric acid (UA), which are abundantly present in real matrices, and nanomolar DA physiological concentration, the sensing of dopamine raises demanding issues in terms of selectivity and detection limit. A systematic study has been carried out in order to investigate the occurrence of the cross-talking effect in a ternary mixture containing DA, AA and UA and to find out the optimum sensing conditions to enhance selectivity towards dopamine.

First, the well documented electrocatalytic and antifouling properties of its films have been fundamental criteria for choosing PEDOT:PSS as sensing material. Additionally, differential pulse voltammetry (DPV) has been selected among the available electrochemical techniques, as the differential recording of the redox process allows for an accurate monitoring of the faradic current, thus leading to higher sensitivity and resolution. Furthermore, the adopted strategy to improve the sensor's performances towards dopamine detection consisted in tuning some experimental parameters which are known to affect the ternary system, i.e. scan rate, pH of the solution and nature of the polymer (via chemical functionalization of PEDOT). All the experiments have been carried out at the Analytical Chemistry and Organometallic Chemistry labs, Department of Industrial Chemistry T. Montanari (University of Bologna).

2. *Fabrication of a microfluidic trapping device for electronic monitoring of 3D speroids.*

During a visit at the Department of Bioelectronics (BEL) - Centre Microélectronique de Provence (Ecole Nationale Supérieure des Mines de Saint-Etienne) promoted by the Erasmus+ Mobility for Traineeship program, the research has been focused on the design and calibration of an integrated platform for electrical monitoring of 3D cell cultures.

Mono and multicellular spheroids have recently stood out as a promising technology for bridging the gap between scarcely predictive 2D cell cultures and complex in vivo models in clinical testing. However, only few systems are suitable for monitoring spheroids' electrical properties, such as TEER (trans-epithelial/endothelial electric resistance), effectively.

In the last years, the BEL group has intensively worked on a new generation of PEDOT:PSS-based organic electrochemical transistor (OECTs) that can accurately sense both highly resistant cell barrier as well as low resistant and adherence cells (coverage). The interplay between microfluidics and OECTs technology have been exploited for the fabrication of an easy-to-use platform for this purpose. The microfluidic device consists of a single microchannel in which a 'bottleneck' structure is used to trap the spheroid at the desired location. The trapped spheroid affects the ionic flux of the OECT, thus the transistor output current response. Then, by using an impedance-based approach, the collected data are fitted with a simple equivalent circuit to model the system and TEER (*Trans* Endothelial/Epithelial Electric Resistance) and capacitance values can be extracted.

The microfabrication of both the OECT and the microfluidic cell has been carried out by photolithography in the class 100/1000 clean rooms at Centre Microélectronique de Provence, following optimized protocols. The fully assembled platform has been calibrated through the use of polystyrene microbeads with different diameters, i.e. 60 and 160 μm, to simulate controlled blockage of the microchannel.

Optimization of a low-cost, PEDOT:PSS-based amperometric sensor for the selective detection of Dopamine in a ternary mixture

The behaviour of the employed electrode, in which the sensing material is a PEDOT:PSS film deposited by spin coating onto a glass slide from a commercial dispersion (Clevios PH1000), had been already characterized and preliminary studies for dopamine, ascorbic acid and uric acid detection were carried out by cyclic voltammetry in aqueous solutions.

Owing to the purpose of the present work, differential pulse voltammetry (DPV) was the technique of choice to perform dopamine selective determination in ternary mixtures, in which interferences form other redox species might occur. Indeed, taking advantage of a complex potential waveform and a differential recording of the current, DPV allows for achieving better resolutions through the suppression of the capacitive contribution, deriving from the polymer charging, in favour of the faradic current due to the analytes' redox processes.

1. Results and discussion

A plethora of studies coming from literature reports that, when oxidative amperometry experiments are carried out, a cross-talking effect over DA takes place whether AA and UA coexist in the sample. In order to build up a selective sensor for dopamine detection in ternary mixtures, a PEDOT:PSS coated glass slide was employed as the working electrode within a three electrodes cell setup. PBS acted as electrolyte and the measurements were carried out by differential pulse voltammetry (DPV). First of all, the response of the sensor was assessed. After that, the effect of the variation of two experimental parameters, namely pH of the system and scan rate, on the whole system was evaluated. Finally, the chemical functionalization of the sensing material was considered as a route to achieve a better selectivity towards dopamine.

1.1 Electrode response

Accordingly with literature, the interference results in an overlapping voltammetric response, which lowers the peak-to-peak resolution and may lead to a broad signal made up of indistinguishable contributions. This overlap is generally due to (1) the close potential values at which AA, DA and UA undergo oxidation and (2) the poor electrochemical reversibility of AA oxidation, which produces a non-symmetric, wide peak that also tends to increase the background current, thus lowering both selectivity and sensitivity towards the target molecule. Furthermore, an homogeneous catalytic effect of DA oxidation over AA oxidation has been reported to massively contribute in making the signal convoluted and enhancing the peak intensity, which may give raise to overestimations.[69] Finally, owing to the fouling effect of the oxidation products occurring at the electrode surface, the measurements are scarcely reproducible.

Preliminary DPV experiments performed in the presence of the three analytes are shown in Fig 1.

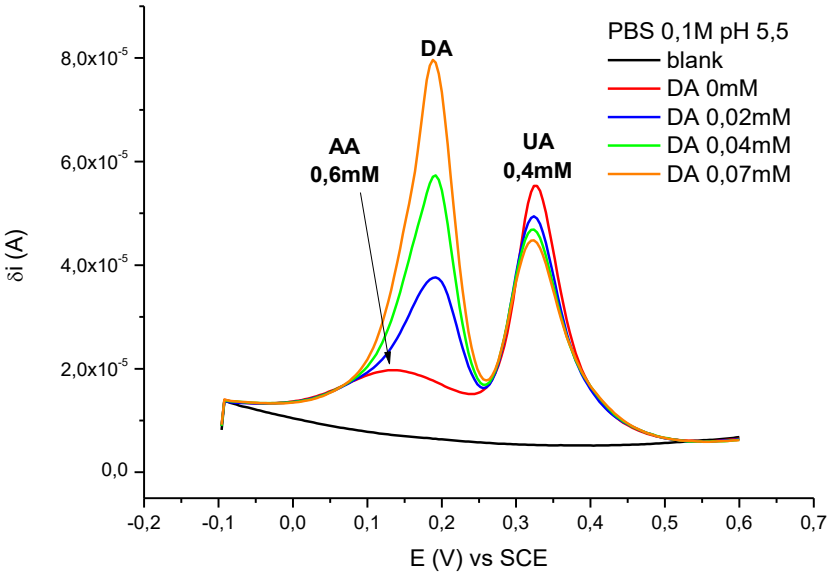

Fig. 1 Voltammetric response obtained with slow DPV parameters in PBS 0,1M only (black line), after the addition of 0,6mM AA and 0,4mM UA (red line) and for increasing concentrations of DA (from 0,02 to 0,07mM,).

Looking at the current intensities in Fig. 1, it clearly stands out that PEDOT:PSS exhibits higher sensitivity towards dopamine, with respect to AA and UA.

The aspect of the curves is in conformity with the data available from literature: AA electro oxidation is the easiest to occur (i.e. it takes place at the lowest potential) and results in a broad signal that enhances the background current in the potential range of interest, which may negatively affect any quantitative analysis. Ep_A values for AA, DA and UA are 136, 188 and 324 mV, respectively, with a very poor peak-to-peak resolution between AA and DA.

Aiming to clarify the evolution of the system in case of subsequent additions of AA, another DPV experiment was carried out and is reported in Fig. 2.

By increasing the concentration of AA, the electrode's sensitivity towards DA results negatively affected. Moreover, each AA addition is followed by a higher background current and Ep_A for DA and UA are progressively shifted towards more positive values, meaning that a growing amount of ascorbic acid obstructs the electro oxidation of the other two analytes.

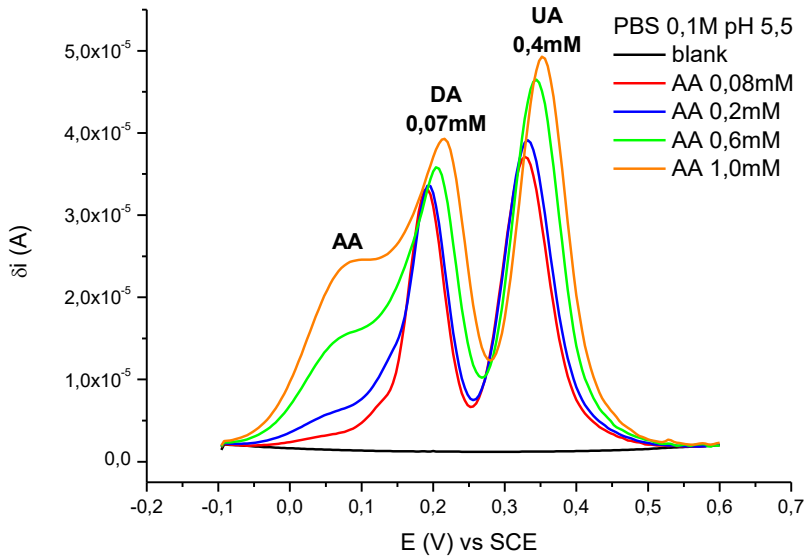

Fig. 2 Voltammetric response obtained with slow DPV parameters in PBS 0,1M only (black line), in presence of AA 0,08mM, DA 0,07mM and UA 0,4mM (red line) and for increasing concentrations of AA (until 1,0mM).

1.2 pH variation

Aiming at finding out the best working conditions to improve the peaks resolution, the system's behaviour was investigated by screening various pH values for the electrolytic solution.

The same DPV experiment depicted in Fig 1 was carried out at pH 3,5, 5,5 and 7,0 for increasing DA concentrations and it is reported in Fig. 3.

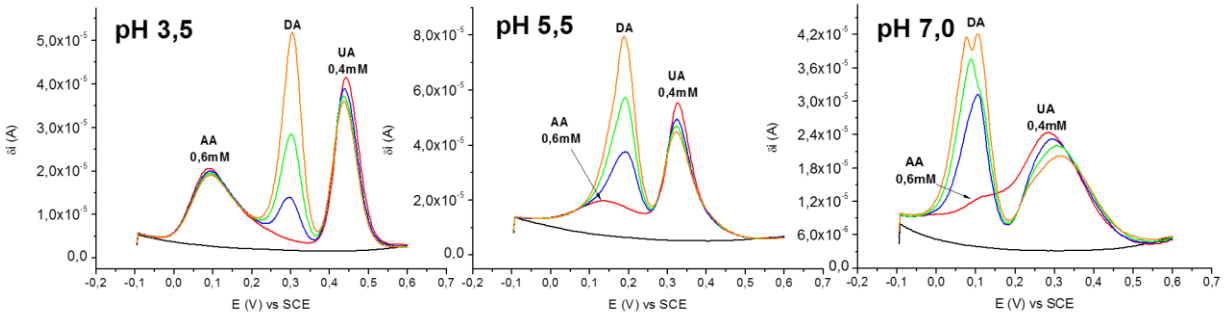

Fig. 3 Voltammetric responses obtained with slow DPV parameters for different pH solutions. In each graph: blank (black line), AA 0,6mM and UA 0,4mM (red line) and increasing DA concentrations (0,02mM blue line, 0,04mM green line, 0,07mM orange line).

A strongly pH-dependent electrochemical behaviour of this system is evident and the interpretation of the collected data required further experiments. Each analyte was independently studied in the same experimental conditions and the resulting curves recorded at different pH values were coherently plotted (Fig. 4).

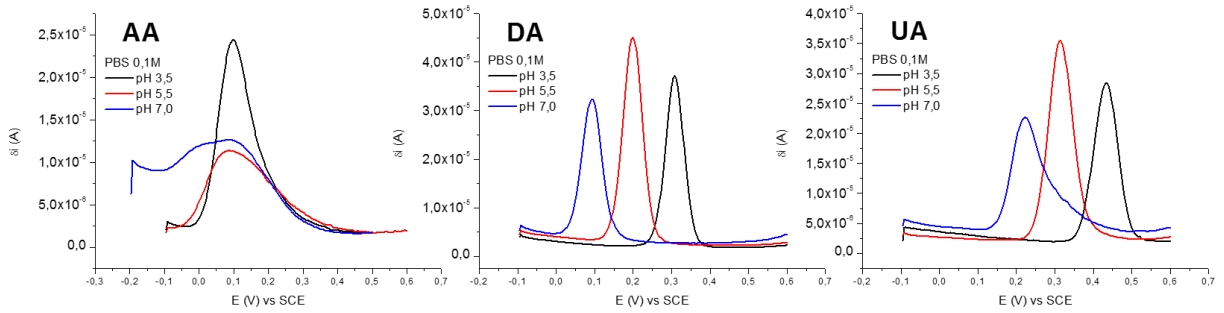

Fig. 4 Independent DPV curves recorded for the three analytes at different pH values. [AA] = 0,6mM; [DA] = 0,07mM; [UA] = 0,4mM.

From the graphs shown above, the pH-dependency of Ep_A can be extracted for each species (all the EpA values are reported in Table 1): while the AA peak position does not significantly changes, by increasing the pH value of the electrolytic solution from 3,5 up to 7,0, a shift in the potential at which DA and UA undergo oxidation was observed towards less anodic values. This means that an higher pH facilitates dopamine and uric acid oxidation at the PEDOT:PSS electrode, but, on the other hand, a decrease in sharpness and symmetry of the correspondent peaks is observed at pH 7,0, which is ascribable to a less reversible redox process occurring at the electrode. This effect is more evident in UA than DA. Owing to the independency of the experiments plotted within the same graph (i.e. different electrodes were employed and thus

different blank curves were associated to each peak), making considerations about the pH-dependency of the current intensities may lead to risky approximations.

pH	AA Ep_A (V vs SCE)	DA Ep_A (V vs SCE)	UA Ep_A (V vs SCE)
3,5	+0,10	+0,31	+0,44
5,5	+0,09	+0,20	+0,31
7,0	+0,10	+0,09	+0,22

Table 1 Ep_A values collected at different pH values of the electrolytic solution.

Afterwards, DPV curves recorded for AA, DA and UA at the same pH value were superimposed to assess the cross interference among the different analytes and visualize the peak-to-peak resolution (Fig. 5).

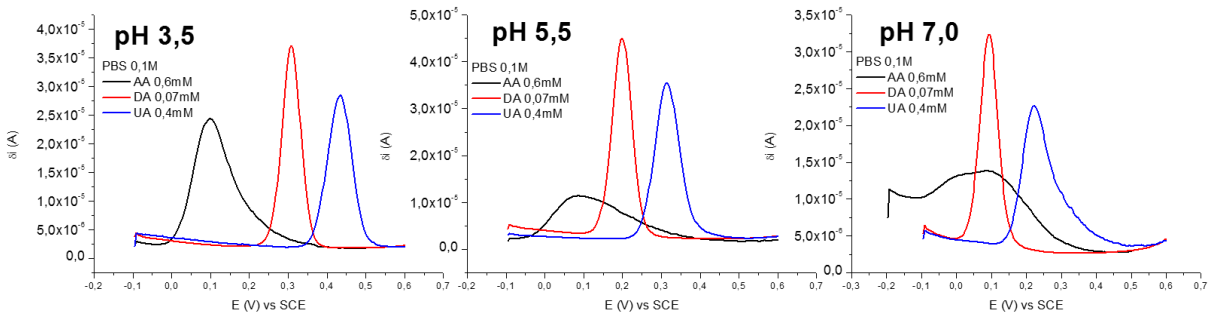

Fig. 5 Independent DPV curves recorded for the three analytes and superimposed for each pH value.

Looking at the graphs and in accordance with the DPV responses shown in Fig. 3 for ternary mixtures, it clearly stands out that the better peak-to-peak resolution was obtained at pH 3,5, which allows for well separated signals and thus, quantitatively speaking, for the most accurate evaluation of DA peak intensity. On the other hand, the worst resolution was achieved at pH 7,0, as AA and DA signals are completely overlapped.

The susceptibility to pH variations relies on the different pK_A values belonging to AA, DA and UA in aqueous solutions; UA is a monoprotic acid whose pK_A is 5,7, while AA and DA are diprotic acids whose pK_{A1} are 4,1 and 8,9 and pK_{A2} are 11,8 and 10,6, respectively.[51,70] The proton transfer involved in the acid-base equilibrium of each species, occurring in conjunction with the electro oxidation processes, is thought to affect the interaction between the analytes and the electroactive PEDOT:PSS film. In particular, it is worth noting that, in a 3,5 pH solution, ascorbic acid, dopamine and uric acid mainly exist in their protonated forms. Differently, at pH 5,5, ascorbic acid is mainly present in its deprotonated, monoanionic form. Finally, at physiological pH (i.e. 7,0), only DA retains its protons form, whereas all ascorbic

acid exists in the form $A^{=}$ and most of uric acid is in the form A^{-}. As regards the system of interest, less sharp signals, which stand for poorly reversible processes, are obtained for AA and UA at pH that are higher than their pK_A values, or, in other words, when they are mainly present in solution in their anionic forms. The more plausible hypothesis is that the electrostatic repulsion between the polyanionic PSS^{-} and a negatively charged species prevents the latter from undergoing facile electro oxidation, thus hindering the electrode neighbourhood. Otherwise, an enhanced interplay among anionic species in solution and positively charged PEDOT regions has been proposed,[52,71] but it is not in agreement with the present results.

1.3 Scan rate variation

DPV parameters were changed in order to perform experiments at different scan rate. Two experimental speeds were found out to significantly minimize the AA contribution to the recorded signal. The proposed DPV settings led to faster recordings compared with the default parameters usually employed. Halfway scan rates did not lead to significant differences. Voltammetric DPV curves obtained for ternary mixtures at different scan rates, with increasing AA concentration, are shown in Fig. 6. The curves obtained in the slowest conditions are presented for comparison (6A).

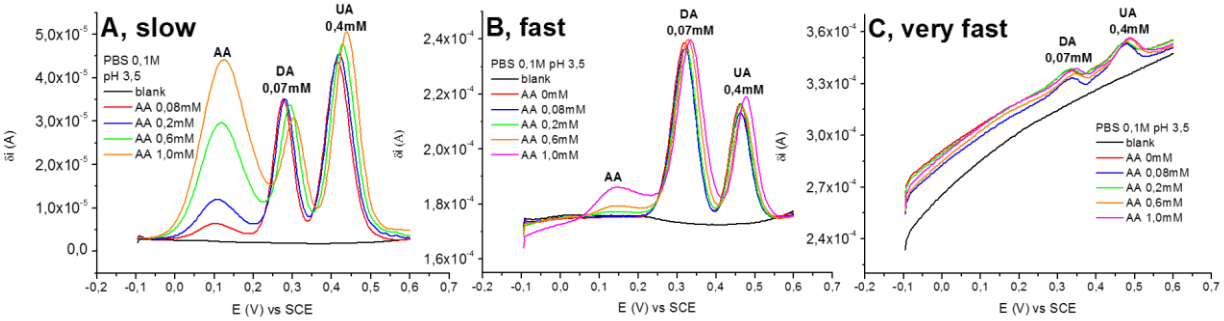

Fig. 6 Voltammetric DPV responses obtained for ternary mixtures by varying the scan rate: (**A)** slow condition, 33' duration; (**B**) fast condition, 170" duration; (**C**) very fast condition, 34" duration.

First, it is worth underlining that higher scan rates in electrochemical measurements reduce the time consumption, but, on the other hand, they enhance the capacitive contribution to the recorded current with respect to the faradic one and worsen the S/N ratio, thus lowering the quality of the resulting measurement. However, it is also evident from the comparison among the graphs in Fig. 6 that, by scanning the applied potential more rapidly (i.e. from A to C), the

peak ascribable to AA progressively disappears. This means that ascorbic acid electro oxidation is under kinetic control and a slow charge-transfer mechanism takes place at the PEDOT sites, which is in accordance with literature[72]. Therefore, scan rate can be fruitfully tuned in order to inhibit AA detection and avoid the cross-talking effect over the other two analytes. For the aforementioned consequences of scan rate on the quality of the recordings, a compromise is needed depending upon the desired performances.

In order to evaluate the optimum experimental condition in terms of peak-to-peak resolution and sensitivity towards dopamine, a first selection among the investigated parameters led pH 7,0 and very fast scan rate conditions to be screened out. Thus, in Table 2 are reported the sensitivity values associated to dopamine detection in the presence of 0,6mM AA and 0,4mM UA, for the best sensing conditions. Calibration curves were obtained from DPV recordings for increasing DA concentration and are shown as inset.

Sample label	Scan rate	pH	DA Ep_A (V vs SCE)	DA Sensitivity ($\mu A\ mM^{-1}\ cm^{-2}$)
A	Slow	3,5	0,30	461 ± 31
B	Slow	5,5	0,19	591 ± 32
C	Fast	3,5	0,32	787 ± 60
D	Fast	5,5	0,20	297 ± 34

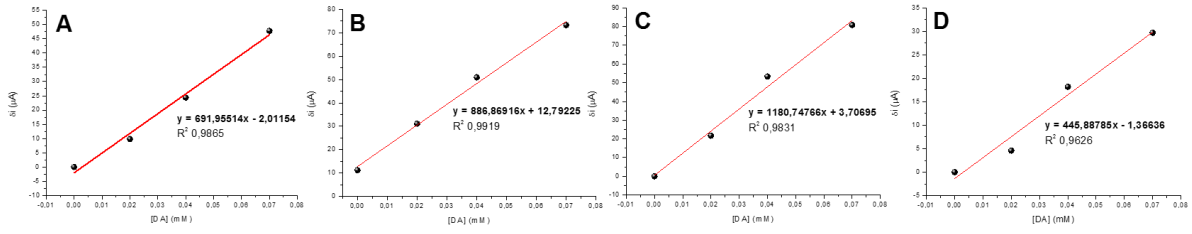

Table 2 DA sensors performances in the presence of 0,6mM AA and 0,4mM UA, in selected experimental conditions. Inset: calibration curves.

As previously noted, the highest peak-to-peak resolution was achieved at pH 3,5, but such a low pH value is too far from the physiological condition. Therefore, being the present work devoted to the optimization of a selective sensor for real applications, the pH value set for further experiments was 5,5. Moreover, since the best sensitivity at this pH condition was achieved for the slower measurements, the "slow" scan rate was fixed as optimized parameter.

1.4 Functionalization of PEDOT:PSS

The functionalization route, i.e. the introduction of chemical functional groups in the polymer chain, was considered with the purpose of improving both sensitivity and selectivity of the sensor towards dopamine.

In particular, a Poly(hydroxymethyl-3,4-ethylenedioxythiophene):PSS (PHMeDOT:PSS) film and two Ferrocene-modified films were tested ad sensing materials, all of them having the electrodeposition onto a standard PH1000 electrode as a common starting point.

1.4.1 PHMeDOT:PSS

PHMeDOT:PSS-coated sensors were obtained by potentiodynamic electrodeposition onto standard PH1000 electrodes, following the procedure described in the Experimental part. Figure 7 illustrates deposition (7A) and characterization (7B) curves obtained for the sensor in question.

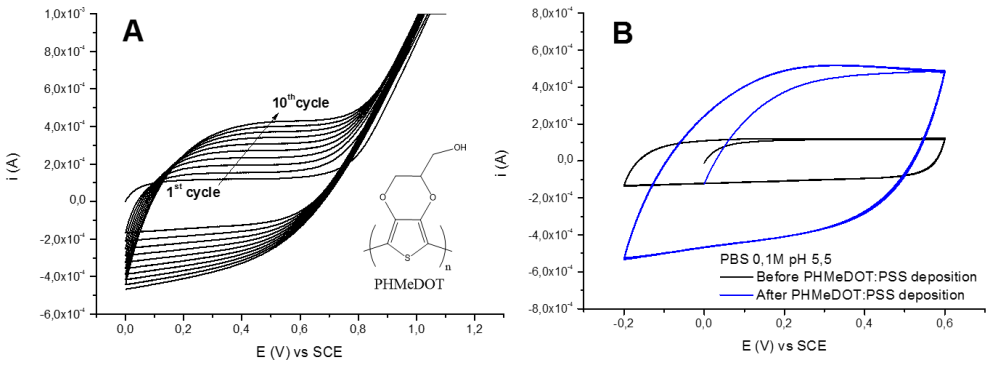

Fig. 7 PHMeDOT:PSS electrodeposition curve (**A**) and voltammetric characterization before and after the deposition (**B**). (**A)** Inset: chemical structure of PHMeDOT. The polymerization was carried out potentiodynamically from an aqueous dispersion of monomer HMeDOT and PSS^-, with a PH1000-coated glass slide acting as the working electrode and the substrate. The voltammetric characterization of the sensor before and after the deposition was performed in PBS 0,1M pH 5,5.

As shown in Fig. 7A, the oxidation of the monomer HMeDOT occurs at ≈ +0,8V vs SCE and the effective growth of the PHMeDOT:PSS film onto the substrate is proven by the increasing capacitive current recorded from the 1st up to the 10th deposition cycle within the potential range 0<E<+0,8V vs SCE. The voltammograms in Fig. 7B demonstrate the successful modification of the electrodic surface: the black line accounting for the PH1000-coated glass slide before PHMeDOT:PSS deposition and the blue one obtained for the same sample, after the deposition. The additional electroactive film deposited onto the electrode is responsible for the enhanced capacitive contribution to the recorded current and assesses the good status of the underlying PH1000 film (i.e. no over oxidation of the polymeric substrate occurred). Furthermore, it is

worth pointing out that the signal stability over potential cycles is indicative of the sensor's electrochemical stability.

As following step, the sensor performances were tested in ternary mixtures containing AA, DA and UA. DPV responses are shown in Fig. 8; curves recorded for a standard PH1000 sensor in the same experimental conditions are reported for comparison.

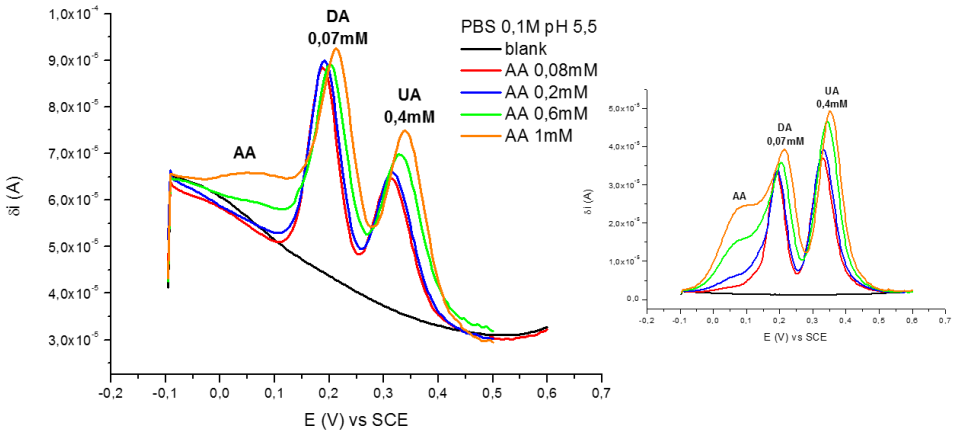

Fig. 8 Voltammetric responses obtained in slow DPV condition for a PHMeDOT:PSS modified sensor (main graph on the left) in a ternary mixture with increasing AA concentrations. Inset: PH1000 performances for the same experiment.

In their in-depth study dealing with selective dopamine detection,[53] G. Fabregat et al. have proposed the rational design of a PHMeDOT-coated ITO or GC electrode, taking inspiration from quantum mechanical calculations regarding the C--H--O interactions between oxidised DA and PEDOT. Indeed, while retaining the electronic characteristics of PEDOT that are mainly defined by the π-conjugated system and the oxygen atoms of the dioxane ring, PHMeDOT should more easily form intermolecular hydrogen bonds with oxidised forms of DA, AA and UA, thanks to the exocyclic hydroxymethyl group. In the present work, no significant enhancements deriving from the use of PHMeDOT:PSS were observed with respect to PH1000-coated sensors in terms of sensitivity towards dopamine. Rather, in accordance with the results presented in Fig. 8, a slightly better peak-to-peak resolution was observed and the modified electrode was found out to be a worse sensor for ascorbic acid and uric acid, if compared to PH1000. In particular, calculated PHMeDOT:PSS sensitivity towards AA came out to be less than half the value obtained for PH1000. Sensitivity values associated to ascorbic acid detection in presence of 0,07mM DA and 0,4mM UA are reported in Table 3. Calibration curves were obtained from DPV recordings for increasing AA concentration and are shown as

inset. This result is important in view of the development of a sensor for DA: looking at the data, it is evident that using a PHMeDOT:PSS coated electrode is possible to avoid AA interference up to a concentration of 0,6 mM.

Sample	Scan rate	pH	AA Ep_A (V vs SCE)	AA Sensitivity ($\mu A\ mM^{-1}\ cm^{-2}$)
PH1000	Slow	5,5	0,068	14,2 ± 0,2
PHMeDOT	Slow	5,5	0,056	7,3 ± 1,1

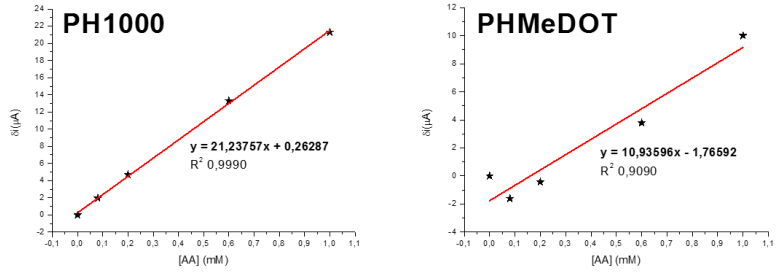

Table 3 Sensors performances in AA detection detection in the presence of 0,07mM DA and 0,4mM UA in selected experimental conditions. Inset: calibration curves.

1.4.2 Long-chain Ferrocene functionalized sensors

In our previous work, electrodeposited PEDOT:PSS ferrocene-modified sensors for dopamine detection had been obtained through a multi-step procedure involving a click reaction.[37] In this paper, we assessed the electrocatalytic properties of the covalently bonded ferrocene with respect to DA electro oxidation, finally obtaining an enzyme-free sensor for dopamine detection whose mean sensitivity was 196 $\mu A\ mM^{-1}\ cm^{-2}$.

Following this approach for applications in ternary mixtures, two types of newly developed modified electrodes were prepared, as explained in the Experimental section, and tested as selective sensors. Briefly, PEDOT/Poly(chloromethyl-3,4-ethylenedioxythiophene):PSS (**1**) and PEDOT/Poly(hydroxymethyl-3,4-ethylenedioxythiophene):PSS (**2**) films were electrodeposited onto PH1000-coated glass slides. After that, the modified electrodes were functionalized through covalent anchorage of (**1**) -O–$(CH_2)_{11}$–triazole–ferrocene and (**2**) -CO_3–$(CH_2)_{11}$–triazole–ferrocene.

The resulting structures are schematically shown in Figure 9.

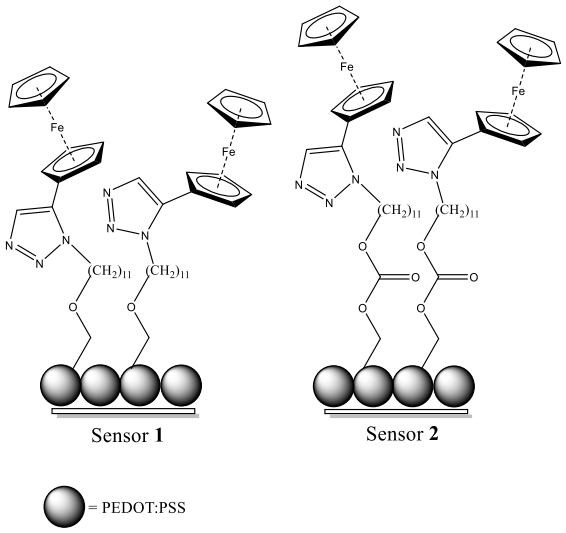

Fig. 9 Schematic representation of the two long-chain Ferrocene functionalized sensors.

First of all, both sensor **1** and **2** were characterized by cyclic voltammetry (Fig. 10) in order to assess the success of the functionalization procedure.

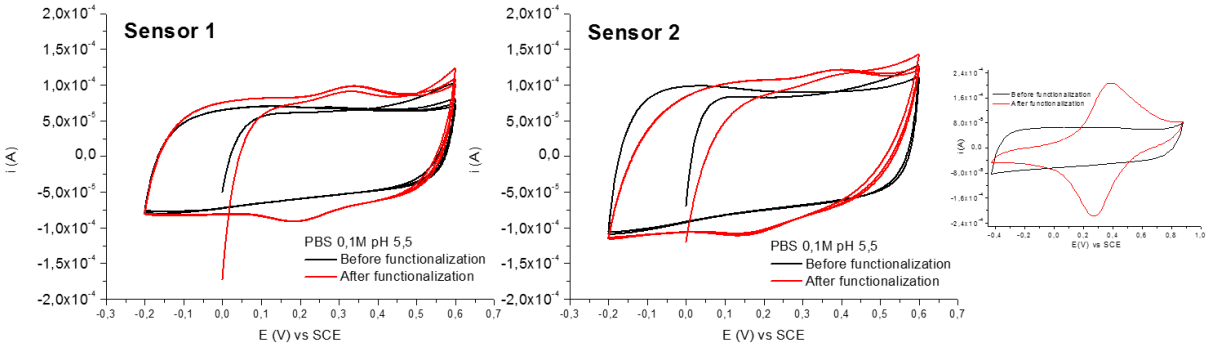

Fig. 10 Voltammetric curves obtained for the long-chain Ferrocene modified electrodes. Each sensor was characterized by cyclic voltammetry after the electrodeposition step (black line) and after the covalent anchorage of ferrocene (red line). Inset on the right: characterization curves of a previously developed short-chain ferrocene electrode (reported for comparison).

As regards the voltammetric curves recorded before the ferrocene functionalization step, the capacitive character of the electroactive film clearly dominates the current signal in the potential range of interest. Nevertheless, once ferrocene has been immobilized onto the electroactive film, a change in the voltammogram shape is observed as two redox peaks, due to the faradic contribution given by the redox process that involves the species Fe^{III}/Fe^{II}, appear for both the sensors.

The couple ferrocene/ferrocenium (Fc/Fc^{+}) is a well-known redox mediator here employed with the aim of enhancing the sensitivity towards dopamine, taking advantage from its

electrocatalytic properties. Obviously, as long as $E°_{Fc/Fc^+}$ is higher than the standard redox potential of other redox-active species present in solution, not only dopamine may benefit from the electrocatalysis provided by the redox mediator. This is the reason why a long alkyl chain was embedded within the modifying group. Indeed, this additional feature was hypothesized to discourage hydrophilic and/or bulky analytes to approach the surface of the sensors.

Comparing these results with the ones previously obtained for short-chain ferrocene modified electrodes (see inset in Fig. 10), it is evident that the persistence of a capacitive shape after the functionalization step is due to the presence of a long alkyl chain between the polymeric film and ferrocene. Consequently, higher values for ferrocene ΔE_p (i.e. farther from the ideal 59mV of a monolayer film) are observed, being 158 and 245mV for sensor **1** and **2** respectively, while the short-chain counterpart shown a ferrocene ΔE_p of 110mV in the voltammogram reported as inset.

After the characterization, the sensors were then tested in ternary mixtures for increasing concentrations of AA and DA. The resulting DPV curves are presented in Fig. 11A for sensor **1** and 11B for sensor **2**.

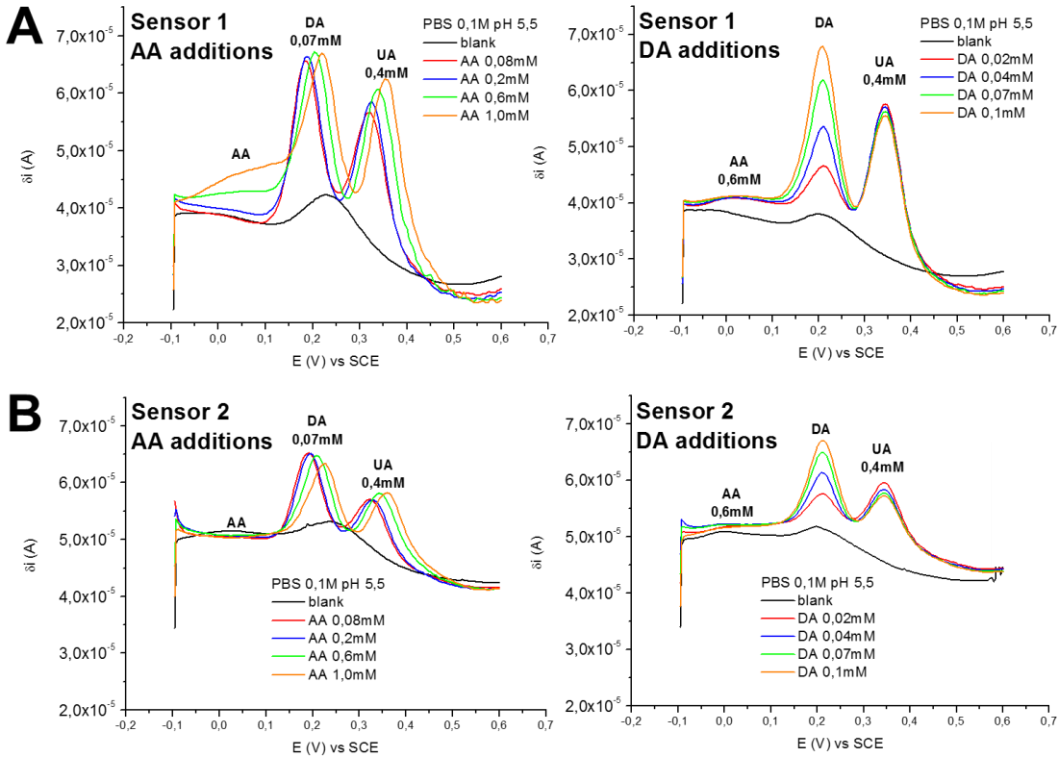

Fig. 11 Voltammetric responses obtained in slow DPV condition for sensor **1** (**A**) and sensor **2** (**B**) in ternary mixtures with increasing AA (left) or DA (right) concentrations.

Looking at the DPV curves recorded for increasing concentrations of ascorbic acid, in the case of sensor **1** it is not possible to ascribe a proper peak to AA, but rather a broad, smoothed background of growing intensity as ascorbic acid concentration rises. As regards sensor **2**, for the same experiment no peak accounting for AA electro oxidation is observed. For both sensors, the main effect of AA additions consists in shifting DA and UA Ep_A towards more anodic values, meaning that their electro oxidation at the working electrode becomes progressively harder. The effect is particularly pronounced when AA concentration in the ternary solution is equal to and higher than 0,6mM.

When DA is added to the ternary solution, a well-defined, sharp peak grows together with dopamine concentration. A good peak-to-peak resolution is observed for both sensor **1** and **2**. The potential region of interest for AA electro oxidation is flat, especially for sensor **2**.

Therefore, the presence of a long alkyl chain embedded within the modifying groups seemed to affect negatively AA electro oxidation.

Sensitivity values associated to dopamine detection in the presence of 0,6mM AA and 0,4mM UA are reported in Table 4. Calibration curves were obtained from DPV recordings for increasing DA concentration and are shown as inset.

Sample	Scan rate	pH	DA Ep_A (V vs SCE)	DA Sensitivity ($\mu A\ mM^{-1}\ cm^{-2}$)
Sensor 1	Slow	5,5	0,21	197 ± 17
Sensor 2	Slow	5,5	0,21	100 ± 16

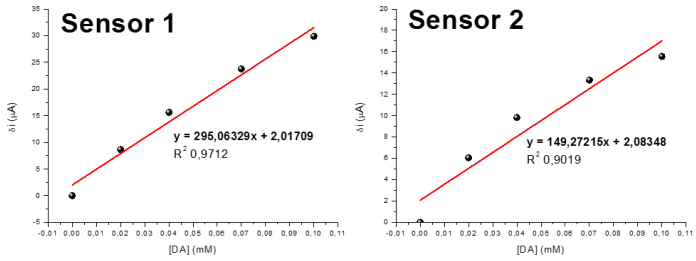

Table 4 DA sensors performances in the presence of 0,6mM AA and 0,4mM UA, in selected experimental conditions. Inset: calibration curves.

1.5 Further improvements

Although interesting results have been obtained in terms of peak-to-peak resolution and selectivity by combining a sensitive technique such as DPV and optimized experimental conditions, detection limits calculated for dopamine in ternary mixtures lie within the micromolar range. Consequently, whilst being consistent with the data reported in literature for

dopamine amperometric detection in the presence of AA and UA,[49–53] the performances exhibited by the proposed sensors are not adequate for physiological applications.

Thereafter, the collected data about optimized parameters and interference study presented in this work were fruitfully exploited for the development of a low cost, all PEDOT:PSS OECT for dopamine selective detection. Indeed, the inherent amplification provided by an OECT configuration embodies a concrete opportunity in order to achieve higher sensitivities and lower detection limits.

Size and geometry of the amperometric sensor are compared to those of the developed OECT in the picture above (Fig. 12).

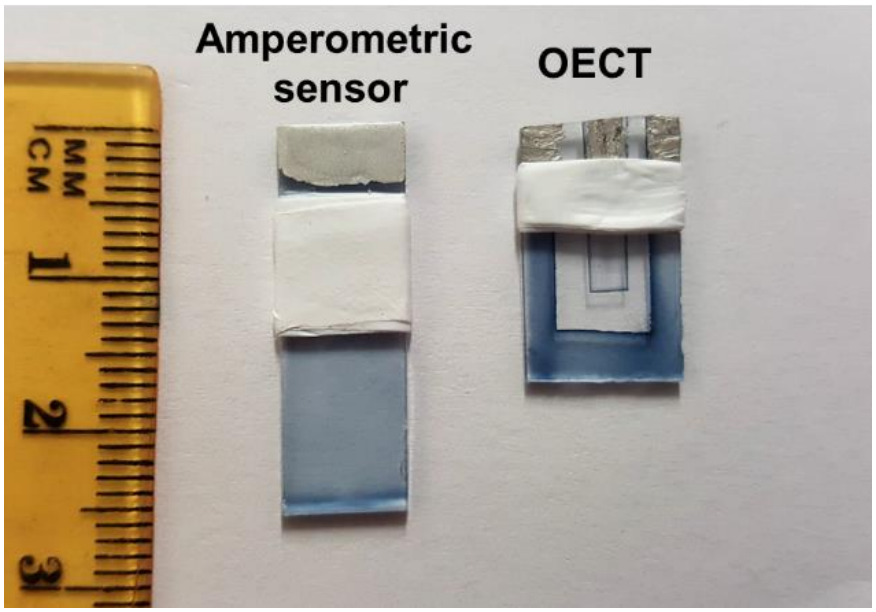

Fig. 12 Top view of all-PEDOT:PSS amperometric sensor and OECT.

2. Experimental

2.1 Reagents and materials

Reagents were purchased from Sigma-Aldrich, if not otherwise specified, with the best available degree of purity. Class A glassware has been employed when a good accuracy in the measurement of volumes was required. Bidistilled water was used for electrochemical solutions preparation. All solvents used for synthesis were dried and distilled under nitrogen prior to use.

- glass slides;
- PEDOT:PSS Clevios PH1000 (Heraeus);
- 3,4-ethylenedioxythiophene, EDOT;
- Poly(sodium 4-styrenesulfonate) average Mw ≈ 70,000, NaPSS;
- Hydroxymethyl EDOT, HMeDOT;
- Potassium dihydrogen phosphate, KH_2PO_4;
- L(+)Ascorbic acid (Carlo Erba Analyticals), AA;
- Dopamine hydrochloride (Fluka), DA;
- Uric acid (Fluka), UA;
- 11-Bromo-1-undecanol;
- sodium azide;
- copper(II) sulfate pentahydrate;
- sodium ascorbate;
- ethynylferrocene;
- 3,4-dimethoxythiophene;
- 3-chloro-1,2-propanediol;
- 2,6-di-tert-butyl-4-methylphenol;
-1,1’-carbonyldiimidazole;
- p-Toluenesulfonic acid;
- Conductive silver paste (Elettrò 340);
- Teflon tape;
- Parafilm.

2.2 Equipment

- single compartment three electrodes electrochemical cell;

- aqueous saturated calomel electrode (SCE);
- Pt wire;
- CH INSTRUMENTS Electrochemical WorkStation 660C;
- pHmeter AMEL INSTRUMENTS 338 and pH combination electrode 211/SGG/12 AMEL;
- spincoater.

2.3 Methods

Supporting electrolytes and polymerization solutions were bubbled with N_2 prior to each measurement or electrodeposition, both of them carried out in an electrochemical cell under N_2 atmosphere with no magnetic stirring. All electrochemical experiments were performed in a three electrodes configuration (see Fig. 13), where a PEDOT:PSS-based film deposited onto a glass slide was the working electrode and a Pt wire acted as counter electrode, while potentials were measured with respect to an aqueous saturated calomel electrode (SCE) (i.e. the reference electrode). 0,1 M PBS as supporting electrolyte was prepared from KH_2PO_4, while 1M NaOH or 1M HCl were added in order to adjust the pH at the desired value.

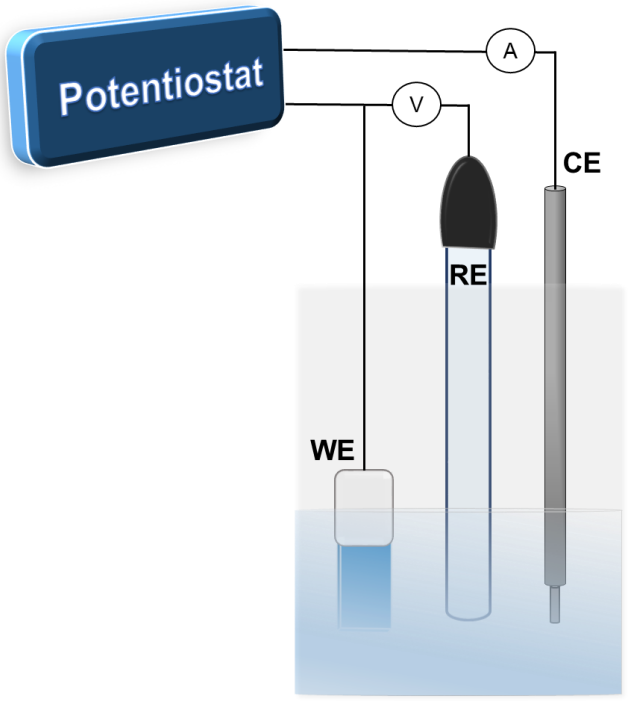

Fig. 13 Scheme of the three electrodes setup.

2.3.1 Sensors preparation

Performances of four kind of sensors (acting as working electrodes in the three electrode configuration) were investigated, each of them characterized by a different sensing material as

electroactive film covering a glass slide. Among them, two newly synthesised, ferrocene-based structures were employed as modifiers. Contacts were realized with a brush of conductive silver paste at the glass slide extremity. Electroactive area was fixed at 1,5 cm^2 and defined with Teflon tape and parafilm, which also insulated the contact.

- PH1000 electrode

Clevios PH 1000 suspension (PEDOT:PSS) was prepared by spincoating on a glass slide at 500 rpm per 3 s at the Department of Physics Astronomy (University of Bologna).

- PHMeDOT electrode

A PHMeDOT:PSS film was electrodeposited on a PH1000 electrode using cyclic voltammetry (i.e. potentiodynamic polymerization) from an aqueous solution containing 10mM HMeDOT and 0,1mM PSS. The applied potential range was 0<E<+1,1V vs SCE for 10 deposition cycles at 0,1 V s^{-1}.

- Long-chain Ferrocene functionalized electrodes

Synthesis and electrodeposition steps required in the preparation of the modified films are described in this section for sensor 1 and 2 (see schemes 1 and 2, respectively). Products purification was carried out using column chromatography on silica gel and assessed by ^1H and ^{13}C-NMR spectrometry.

Sensor 1

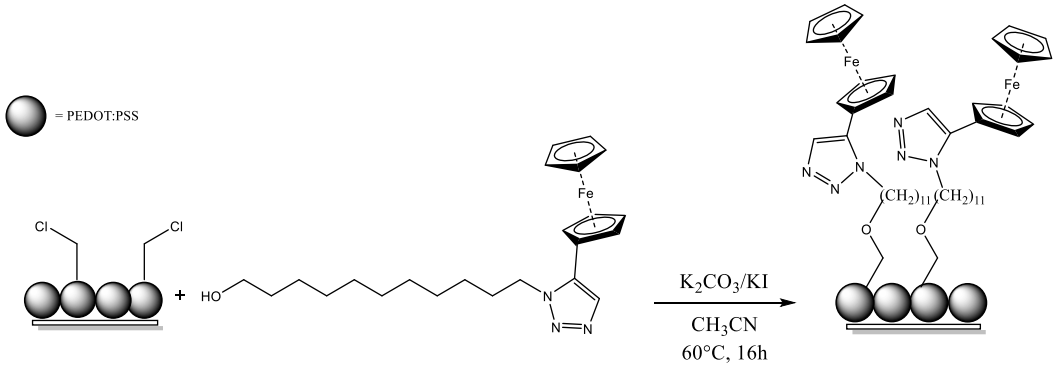

Scheme 1 Sensor **1** preparation from a PEDOT/PClMeDOT:PSS electrodeposited film and ferrocene-triazole-1-undecanol.

1) *Synthesis of chloromethylEDOT*. Chloromethyl EDOT (ClMeDOT) was synthesised by reacting, under N_2 using standard Schlenk techniques, 0.50 g (3.47 mmol, 1 eq.) of 3,4-dimethoxythiophene dissolved in anhydrous toluene (12mL) with 0.87 mL (10.4mmol,

3 eq.) of 3-chloro-1,2-propanediol, in the presence of 0.762 mg (3.47 mmol, 1 eq.) of 2,6-di-tert-butyl-4-methylphenol and 0.060 g (0.347 mmol, 0,1 eq.) of p-toluenesulfonic acid (p-TSA) at 90°C. After 24 h, 0.87mL of 3-chloro-1,2-propanediol were added to the reaction mixture, which was stirred at 90°C for further 3 h. The solvent was removed under vacuum. Then, 40mL of a solution of Na_2CO_3 (10% in water) were added to the crude and the product was extracted three times with CH_2Cl_2 (20mL x 3). The organic phases were combined, washed with water (40 mL) and dried on $MgSO_4$. The solvent was removed under vacuum and the product 2-chloromethyl-2,3-dihydrothieno[3,4-b][1,4]dioxine obtained with a 34% yield by flash column chromatography on silica gel (eluent: 1 : 1 CH_2Cl_2–petroleum ether).

2) *PEDOT/PClMeDOT:PSS film electrodeposition*. A PEDOT/PClMeDOT:PSS film was electrodeposited on a PH1000 electrode using cyclic voltammetry (i.e. potentiodynamic polymerization) from an aqueous solution containing 5mM EDOT, 5mM ClMeDOT and 0,1mM PSS. The applied potential range was 0<E<+1,1V vs SCE for 10 deposition cycles at 0,1 V s^{-1}.

3) *Synthesis of Ferrocene-triazole-1-undecanol*. 0,221g (0,879mmol) of 11-bromo-1-undecanol and 0,125g (1,930mmol) of sodium azide were dissolved in 15mL of DMSO and put in a 100mL round-bottom flask under inert atmosphere. The reaction mixture was stirred overnight at R.T.. Afterwards, 15 mL of water were added and the organic phase was extracted three times with ethyl acetate. The organic phases were then collected and dried under vacuum. The resulting product was 11-azido-1-undecanol (yellow oil), which was further functionalized with ferrocene by click chemistry.
0,179g (0,840mmol) of 11-azido-1-undecanol, 0,021g of $CuSO_4$ (10%mol, 0,084mmol), 0,066g of sodium ascorbate (40%mol, 0,340 mmol) and 0,176g of ethynylferrocene (0,840mmol) were mixed in a 100mL round-bottom flask in the presence of 5mL of water and 5mL of ^tBuOH. The mixture was stirred at R.T. for 24h under N_2. After that, 50mL of an aqueous solution of NH_3 10% were added and the organic phase was extracted three times with CH_2Cl_2. The collected organic phases were washed with water and brine and dried over $MgSO_4$, thus the solvent was removed under vacuum. The resulting brown oil was washed with hexane and further dried to afford Ferrocene-triazole-1-undecanol as an orange powder (yield = 79%).

Characterization of Ferrocene-triazole-1-undecanol: ^{1}H-NMR (599.7 MHz, $CDCl_3$) δ (ppm): 7.43 (s, 1H, CH_{trz}), 4.73 (t, 2H, -NCH_2-), 4.36-4.32 (4H, Cp), 4.12-4.10 (5H, Cp), 3.63 (t, 2H, -CH_2OH), 1.92 (m, 2H, -CH_2-), 1.53-1.27 (m, 16H, -CH_2-). ^{13}C-NMR (150.8 MHz, $CDCl_3$) δ (ppm): 146.62 (C_{trz}), 118.56 (CH_{trz}), 69.45, 69.54, 68.59, 66.59 (Cp), 63.04 (-CH_2OH), 50.25 (-NCH_2-), 32.76-25.67 (-CH_2-). ESI-MS (m/z) (+) = 423 $[M+H]^+$; 446 $[M+Na]^+$.

4) *Electrodic surface functionalization*. In a 10mL vial, 0,021g of ferrocene-triazole-1-undecanol (5mM), 0,014g of K_2CO_3 (0,1mmol, 1eq.) and 0,008g of KI (0,05mmol, 1eq.) were dissolved in 10mL of dry CH_3CN. The previously prepared PEDOT/PClMeDOT:PSS film was immersed and maintained in the solution for 16h at 60°C under stirring. Once the reaction time was complete, the modified electrode was abundantly rinsed with CH_3CN and water.

Sensor 2

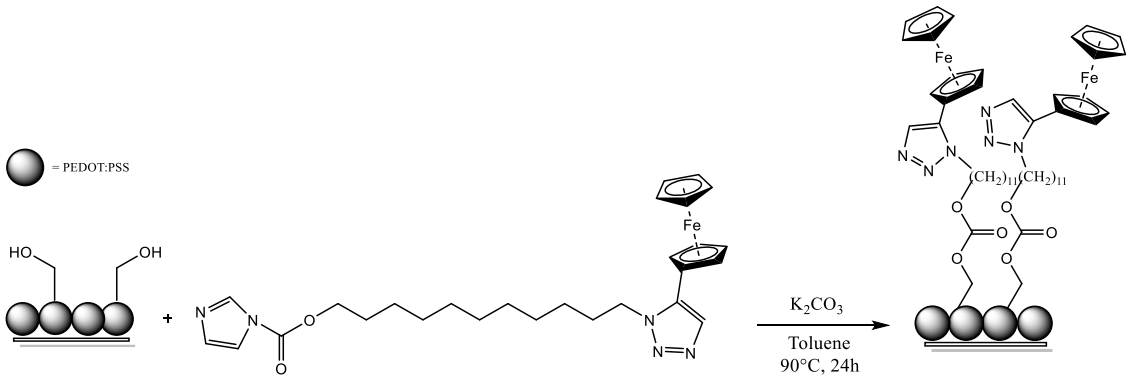

Scheme 2 Sensor **2** preparation from a PEDOT/PHMeDOT:PSS electrodeposited film and ferrocene-triazole-carbonylimidazole-undecane.

1) *PEDOT/PHMeDOT:PSS film electrodeposition*. A PEDOT/PHMeDOT:PSS film was electrodeposited on a PH1000 electrode using cyclic voltammetry (i.e. potentiodynamic polymerization) from an aqueous solution containing 5mM EDOT, 5mM HMeDOT and 0,1mM PSS. The applied potential range was 0<E<+1,1V vs SCE for 10 deposition cycles at 0,1 V s^{-1}.

2) *Synthesis of Ferrocene-triazole-1-carbonylimidazole-undecane*. In a 50mL round-bottom flask 0.045g (0.282mmol) of 1,1'-carbonyldiimidazole were added to a solution

of ferrocene-triazole-1-undecanol (0.040g, 0.094mmol) in 10mL dry CH_2Cl_2 and stirred at room temperature for 2h. At the end of the reaction, the mixture was washed with water (2x20mL) and extracted with CH_2Cl_2. The resulting orange solid obtained in quantitative yield was identified as ferrocene-triazole-1-carbonylimidazole-undecane. Characterization of ferrocene-triazole-1-carbonylimidazole-undecane: ^{1}H-NMR (599.7 MHz, $CDCl_3$) δ (ppm): 8.13 (s, 1H, NCHN), 7.43 (s, 2H, CH_{trz} + CH_{im}), 7.07 (s, 1H, CH_{im}), 4.73 (t, 2H, -NCH_2-), 4.40 (t, 2H, -CH_2O), 4.36-4.32 (4H, Cp), 4.08 (5H, Cp), 1.92 (m, 2H, -CH_2-), 1.74 (m, 2H, -CH_2-), 1.40-1.28 (m, 14H, -CH_2-). ^{13}C-NMR (150.8 MHz, $CDCl_3$) δ (ppm): 148.76 (-OC(O)N-), 146.61 (C_{trz}), 137.06 (CH_{im}), 130.61 (CH_{im}), 118.54 (CH_{trz}), 117.09 (CH_{im}), 69.50, 68.56, 68.47, 66.56 (Cp), 50.23 (-NCH_2-), 30.28-25.66 (-CH_2-). IR (CH_2Cl_2, cm^{-1}): (ν C=O) 1762. ESI-MS (m/z) (+) = 517 $[M+H]^+$; 540 $[M+Na]^+$.

3) *Electrodic surface functionalization*. In a 10mL vial, 0,025g of Ferrocene-triazole-1-carbonylimidazole-undecane (5mM) and 0,014g of K_2CO_3 (10mM) were dissolved in 10mL of dry toluene. The previously prepared PEDOT/PHMeDOT:PSS film was immersed and maintained in the resulting solution for 24h at 90°C under stirring. Once the reaction time was complete, the modified electrode was abundantly rinsed with toluene and water.

2.3.2 CV measurements

Cyclic voltammetry experiments were carried out in order to characterize the desired sensor prior to each DPV experiment and as a proof of surface functionalization for the modified electrodes. All the measurements were performed using 0,1M PBS at pH 5,5 as supporting electrolyte by scanning the potential from -0,2 up to +0,6V vs SCE for 10 cycles at 0,05 V s^{-1}.

2.3.3 DPV measurements

All sensors were tested using differential pulse voltammetry in 0,1M PBS as supporting electrolyte at various pH values (3,5, 5,5 or 7,0), as specified for each experiment. The measurements consisted in a blank recording before any bioanalyte was added, thus the response of the sensor was assessed by increasing the bioanalyte concentration, with or without the concurrent presence of a fixed amount of interfering agents. The applied potential ranged

from -0,1 to +0,6V vs SCE and instrumental variables were studied in order to perform experiments at different scan rates. Three main experimental conditions were investigated, here called “slow”, “fast” and “very fast”. DPV parameters and overall scanning duration are reported in Table 1.

Condition label	**Slow**	**Fast**	**Very fast**
Increment (V)	0,004	0,004	0,004
Pulse amplitude (V)	0,05	0,05	0,05
Pulse width (s)	5	0,2	0,06
Sample width (s)	4	0,06	0,02
Pulse period (s)	10	1	0,2
Sensitivity (A)	1×10^{-4}	1×10^{-4}	1×10^{-4}
Duration	33 min	170 s	34 s

Table 4 DPV parameters and resulting duration for different scan rate conditions.

Fabrication of a microfluidic trapping device for electronic monitoring of 3D spheroids

Over the last decade, organic electrochemical transistors (OECTs) technology has turned out to be a versatile, efficient approach to interface with life sciences, as it has fruitfully been employed for the detection of bio-signals and the real-time monitoring of biological processes. In particular, electrical monitoring of 3D cell cultures for therapeutics and diagnostics has stood out as an innovative application of these devices, which can act as transducer of ionic signal to electronic current. For instance, by using an impedance-based approach, an OECT can work as impedance sensor for cells in order to extract biologically relevant parameters, such as TEER (trans-epithelial/endothelial electric resistance) and capacitance of the membrane. However, the design of an OECT-integrated platform suitable for manipulation and control of 3D cell cultures is a demanding point, which might be addressed by taking advantage of microfluidics.

The purpose of the present work has been the development of an easy-to-use platform for electrical monitoring of 3D spheroids. The architecture of the proposed device is shown in Fig. 1.

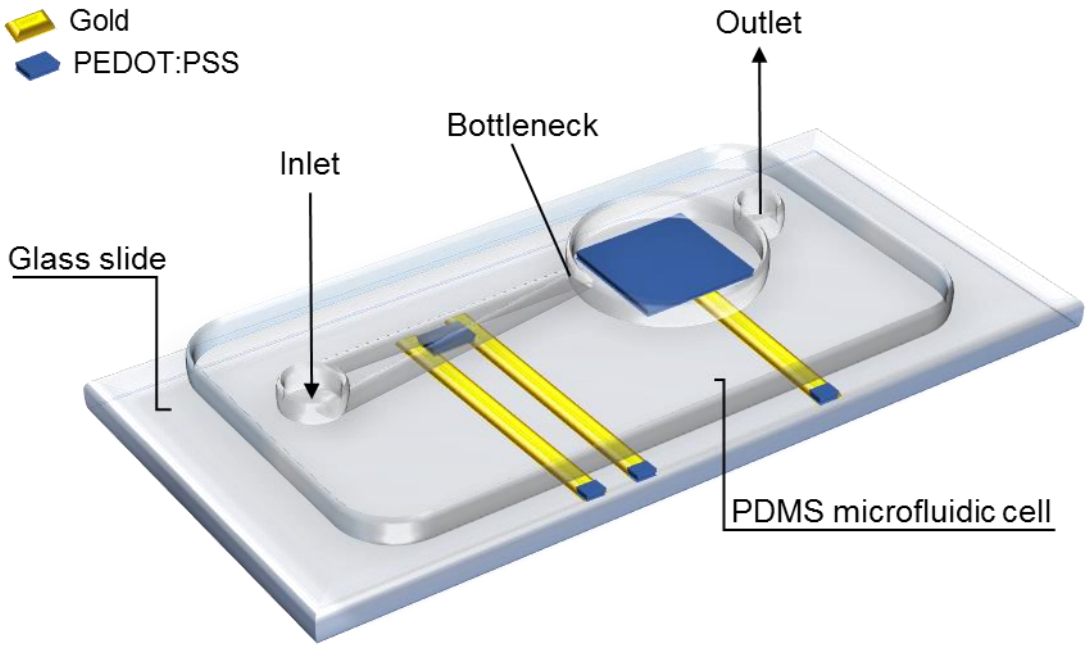

Fig. 1 Schematic representation of the proposed platform for electrical monitoring of 3D spheroids.

In the OECT, both the channel (10×10, 25×25 or 50×50μm^2) and the gate (0,4mm^2) consist of a of PEDOT:PSS thin film, deposited by spincoating from a commercial aqueous dispersion and patterned using photolithography. Gold source, drain and gate contacts are also patterned by photolithography onto the glass slide, which acts as support. Source and drain contacts define the channel length.

The PDMS microfluidic cell, well-positioned above the OECT so that to fit with its geometry, is fulfilled by injecting the electrolyte from the inlet. The liquid flows through the microchannel in which a bottleneck structure (50 or 100μm diameter) is used to trap the spheroid at the desired location, i.e. between the channel and the gate of the OECT.

The trapped spheroid affects the ionic flux of the OECT, thus the transistor output current response. By performing frequency-dependent measurements and employing a simple equivalent circuit to model the system, the desired data about the spheroid can be extracted (i.e. TEER and capacitance of the membrane).

The development of the integrated device is discussed below step by step.

1. Results and discussion

1.1 Development of an alternative fabrication protocol for ParyleneC-free OECTs

As starting point, OECTs have been fabricated following the optimized procedure for additive patterning described in the experimental section. In those devices resulting from the standard fabrication protocol, here abbreviated "2PaC", a superficial layer of ParyleneC covers the whole area, except for PEDOT:PSS patterned regions. Being its films highly insulating, chemically resistant, flexible and transparent, ParyleneC is widely exploited in microelectronics because of its barrier properties.[73]

For the development of a sensing platform suitable for long term operation, a key aspect that needs to be considered is also the affinity of the employed materials, in this case the PaC layer which insulates the OECT and the PDMS of the microfluidic cell. However, scarce adhesion between the hydrophobic ParyleneC layer covering the devices and the PDMS-based microfluidic cell was observed. This in turn led to electrolyte leaks during the recordings, as shown in Fig. 2.

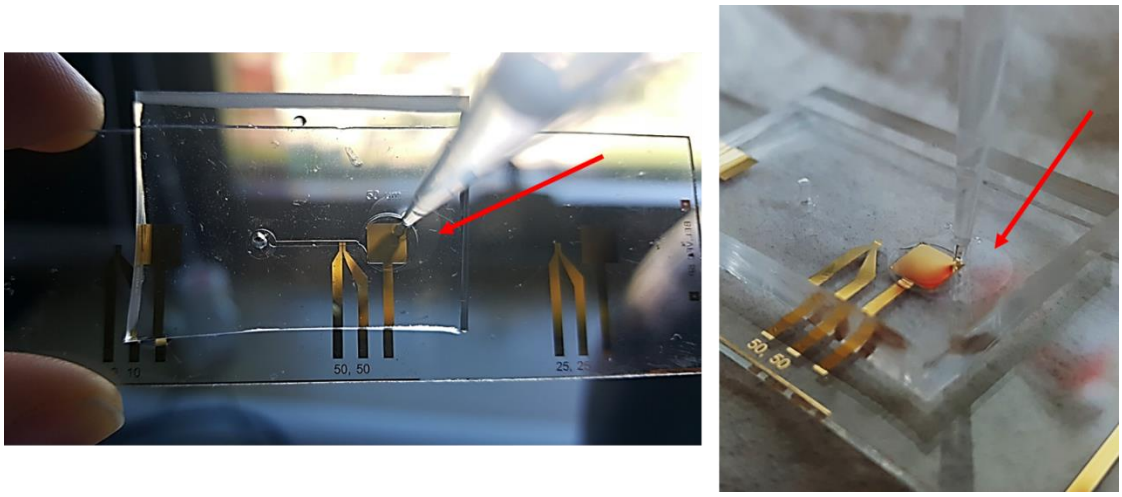

Fig. 2 Electrolyte leaking out of the integrated device because of ParyleneC-PDMS bad adhesion.

The electrolyte containment is essential to maintain not only the trapped spheroid in the right position, but also a correct communication between gate and channel through the passage of the ionic current, as previously explained in paragraph 4.1 of Introduction section. Consequently, an alternative strategy was evaluated to overcome this issue and ensure a good adhesion between the OECT device and the microfluidic cell.

In order to obtain a better surface affinity between the OECT and microfluidic cell, a modification of the existing fabrication protocol was needed, so as to avoid the ParyleneC coverage and leave the glass exposed on the OECT surface. The new procedure (here abbreviated "1PaC") consists in only one deposition of ParyleneC, namely the sacrificial layer, instead of the two depositions performed in the standard protocol. Thus, being the sacrificial layer peeled off in the final step, the resulting device surface is ParyleneC-free. On the other hand, the reduction of the overall ParyleneC thickness caused PEDOT:PSS film to be less protected from the mechanical stress deriving from the peel off step and delamination of PEDOT:PSS was finally observed. In particular, the regions in which the delamination took place were exclusively those one where PEDOT:PSS covered gold contacts, while, for example, the channel area did not show any delamination since GOPS as adhesion promoter ensured strong siloxane linkages between the polymeric film and glass.

Therefore, the 1PaC fabrication protocol was implemented through an additional step, involving the formation of an alkanethiol self assembled monolayer (SAM), here (3-mercaptopropyl)trimethoxysilane (MPTMS), on the patterned gold, focused on the improvement of the PEDOT:PSS-gold linkage. Indeed, while the thiol head group of MPTMS is anchored to Au, the methoxy tail groups are available to bond with GOPS, which is, in turn,

commonly added to PH1000 dispersion for spincoating as cross-linking agent. The structural formulas for MPTMS and GOPS are shown in Fig. 3.

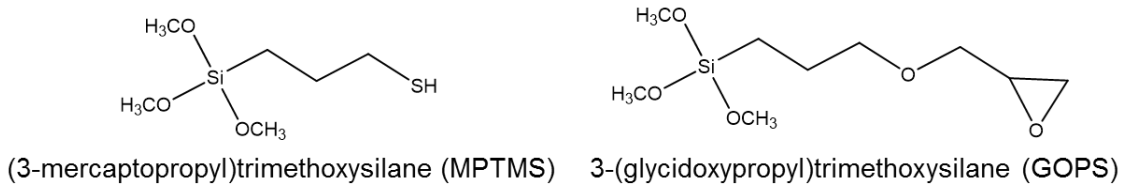

Fig. 3 Structural formulas of MPTMS, the alkanethiol chosen to form the SAM, and GOPS, the cross-linking agent and adhesion promoter commonly added to PH1000 commercial dispersions.

The role of SAMs as modifying agents in electroanalysis has been mentioned in the Introduction and their applications cover a great variety of fields, ranging from the fabrication of novel molecular microstructures to biological sensing, studies of wettability and adhesion. The most appealing feature of those systems is their ease of synthesis, which generally includes the immersion of the gold sample that is meant to be modified into the alkanethiol solution; plenty of protocols are available in literature[74–76].

The proposed mechanism for the grafting process provided by MPTMS is schematically illustrated in Fig. 4.

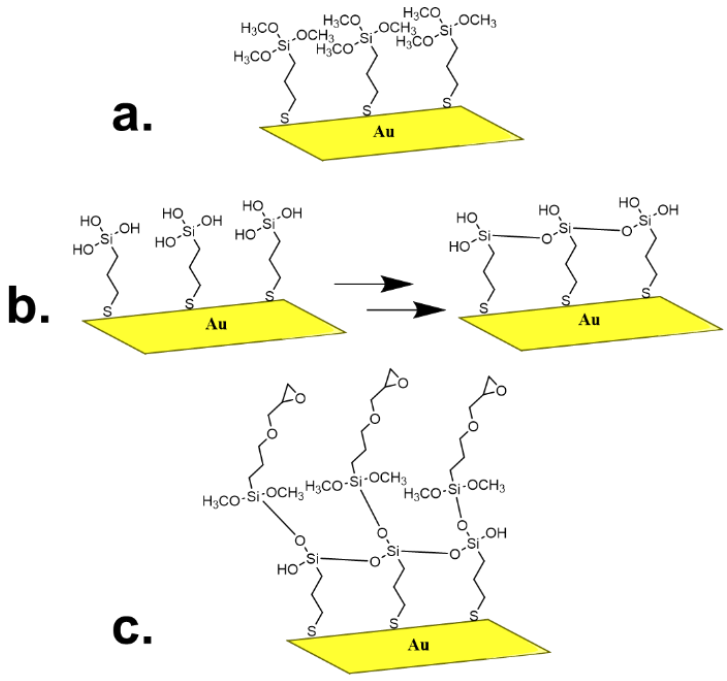

Fig. 4 Proposed mechanism for SAM formation and bonding to GOPS, where **a**) chemisorption step, **b**) hydrolysis and condensation of the MPTMS tail groups, **c**) siloxane bonds formation with GOPS methoxy groups.

First, the sample with patterned gold is cleaned in an oxygen plasma chamber to remove organic contaminants; after that, the sample is immersed in a DI water / IPA solution of MPTMS. During this operation, the fast chemisorption process (Fig. 4a) takes place: head groups of MPTMS molecules approach the gold surface and the strong Au-S interaction readily anchors the alkylthiol chains. Afterwards, the sample is rinsed and dried under N_2, thus put into the plasma chamber to undergo surface activation. This step is thought to promote hydrolysis of the methoxy tail groups of MPTMS, which then undergo self reorganization through spontaneous condensation to give siloxane bonds (Fig. 4b). Finally, PH1000 dispersion containing appropriate additives is spincoated onto the sample. Here and during the further annealing steps, the residual hydroxyl groups of MPTMS are available to bond with the methoxy moieties of GOPS (in the same way that activated, hydrophilic glass surface interacts with GOPS) and a linkage between the gold surface and the polymeric film is established (Fig. 4c). For clarity, it is worth pointing out that GOPS chains are thought to interplay within each other through the epoxy groups in a tangled arrangement, differently from what is represented in the simplified figure above.

A screening study has been done in order to determine the best values for MPTMS concentration and dipping time. A channel resistance below 500Ω and no observed delamination of the polymeric film were fixed as selection criteria.

1, 10 and 100mM MPTMS concentration values in DI water/IPA 1:3 solutions were tested for 1, 5 and 10 minutes dipping time. In general, the combination of low concentrations and short dipping time did not lead to adhesion improvements, while matching high concentrations with long dipping time was found to completely prevent the delamination of the polymeric film from the gold contacts in the peel off step. On the other hand, a long time immersion was always observed to produce highly resistant films, which is probably related to the organization of a dense layer of MPTMS between gold an PEDOT:PSS.

The parameters that gave the best results in terms of film quality and adhesion were 10mM MPTMS concentration and 1 minute dipping time. Pictures of 1PaC devices with and without the optimized MPTMS treatment were taken using an Optical Microscope and are presented in Figure 5.

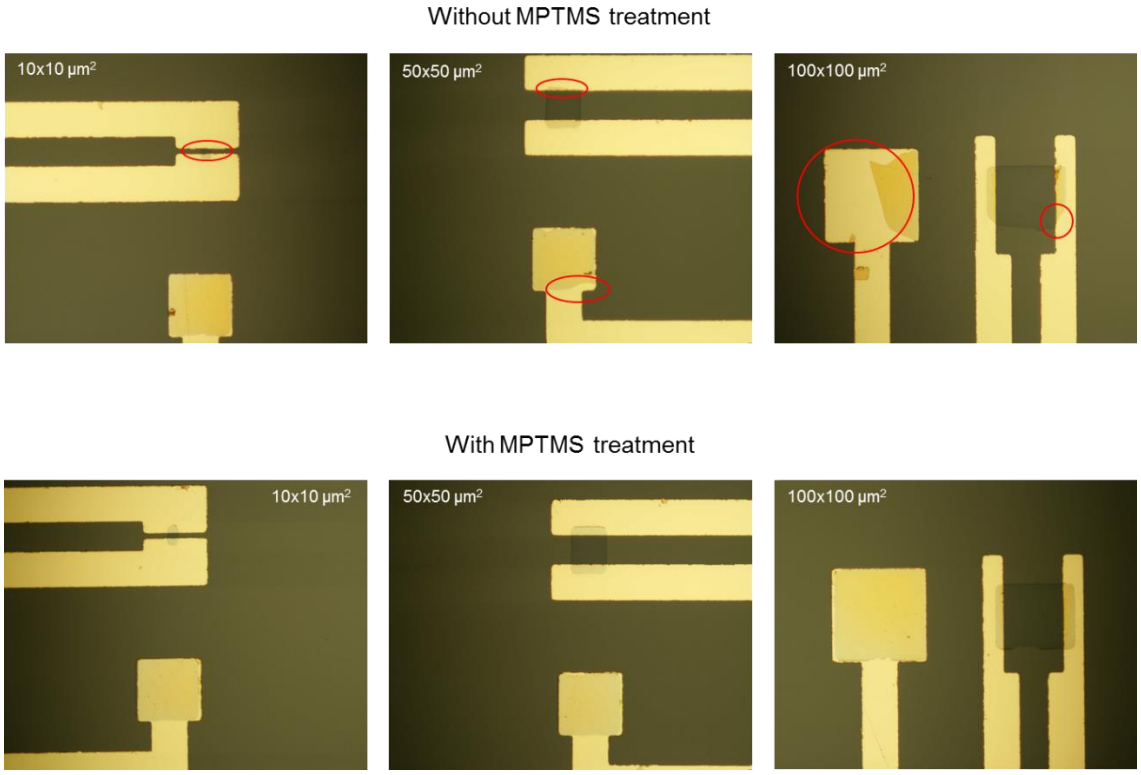

Fig. 5 Pictures of a 1PaC test device without (top) and with (bottom) optimized MPTMS treatment. Red circles in the top pictures highlight the regions where delamination of PEDOT:PSS from gold contacts occurred. For every pictures, the size of the channel is reported in white. Magnification 10x.

1.2 OECTs characterization

Owing to the surface modification performed on the 1PaC devices, further characterizations have been carried out in order to compare the performances of the PEDOT:PSS films obtained with the two fabrication protocols, where standard 2PaC OECTs accounted for reference devices.

1.2.1 Electrochemical behaviour

Electrochemical characterization was carried out for both the protocols at different fabrication steps, by varying electrolyte and scan rate in CV experiments (Fig. 6 and 7). Analogous responses were obtained in PBS and NaCl 0,1M as electrolytes, thus only the ones recorded in 0,1M NaCl are reported here. In Figure 6, the evolution of the two systems during fabrication is presented: for the 2PaC protocol (left), voltammograms of patterned gold and complete device (i.e. after PEDOT:PSS spincoating) are shown, while for 1PaC protocol (right), voltammograms of patterned gold, functionalized gold (i.e. after MPTMS treatment) and complete device are superimposed. As regards voltammetric curves recorded for patterned, bare gold in both the protocols, a system of sharp peaks appears, which should be ascribed to the presence of adsorbed impurities. This hypothesis was confirmed by a further CV experiment

performed in the same conditions using a polished gold working electrode, which clearly showed, as expected, the absence of redox peaks in the potential range of interest. The red voltammogram, accounting for a 1PaC device after MPTMS treatment, is a proof of the accomplished modification of the gold surface: the newly formed SAM covers the gold contacts and produces a change in the shape of the voltammetric response, with respect to the black curve. Finally, after PEDOT:PSS spincoating, the well-known capacitive character of the correspondent blue lines dominates both 2PaC and 1PaC devices responses.

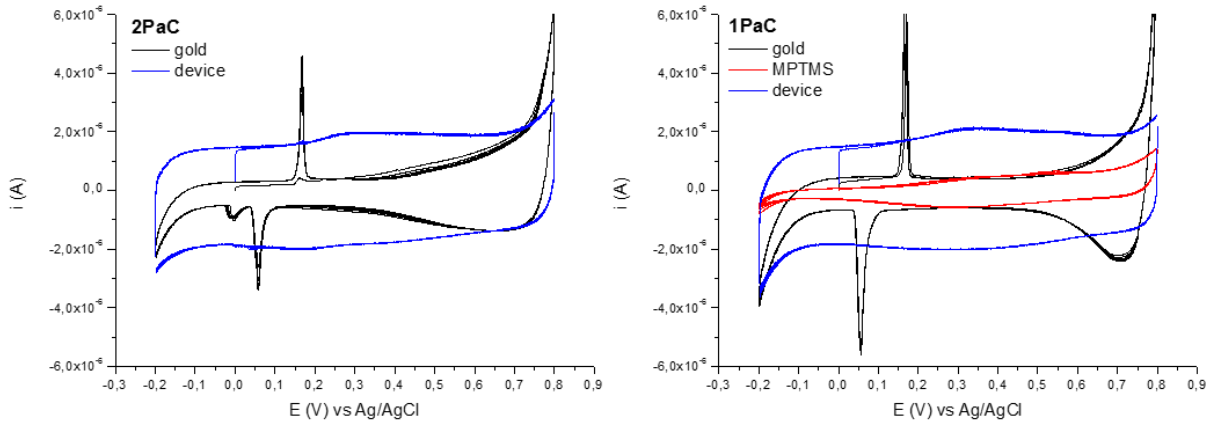

Fig. 6 CV experiments carried out in NaCl 0,1M using the gate as working electrode showing the evolution of the systems deriving from the two protocols for subsequent fabrication steps; scan rate 0,05 V s^{-1}.

In order to assess the electrochemical feature of the resulting films, CV experiments at different scan rates were carried out (Fig. 7a) and the current values recorded for each experiment were normalized to the correspondent scan rate (Fig. 7b). Finally, the devices' voltammetric responses were superimposed (Fig. 7c).

In particular, looking at the voltammetric traces shown in fig.7b, a capacitive behaviour is observed, since the curves resulting from the normalization of the recorded current to the correspondent scan rate are superimposable. This behaviour is typical of PEDOT:PSS and is evident for both 2PaC and 1PaC devices. Moreover, the voltammograms plotted in fig. 7c highlight the fact that the capacitive content of the films resulting from the two fabrication protocols is comparable.

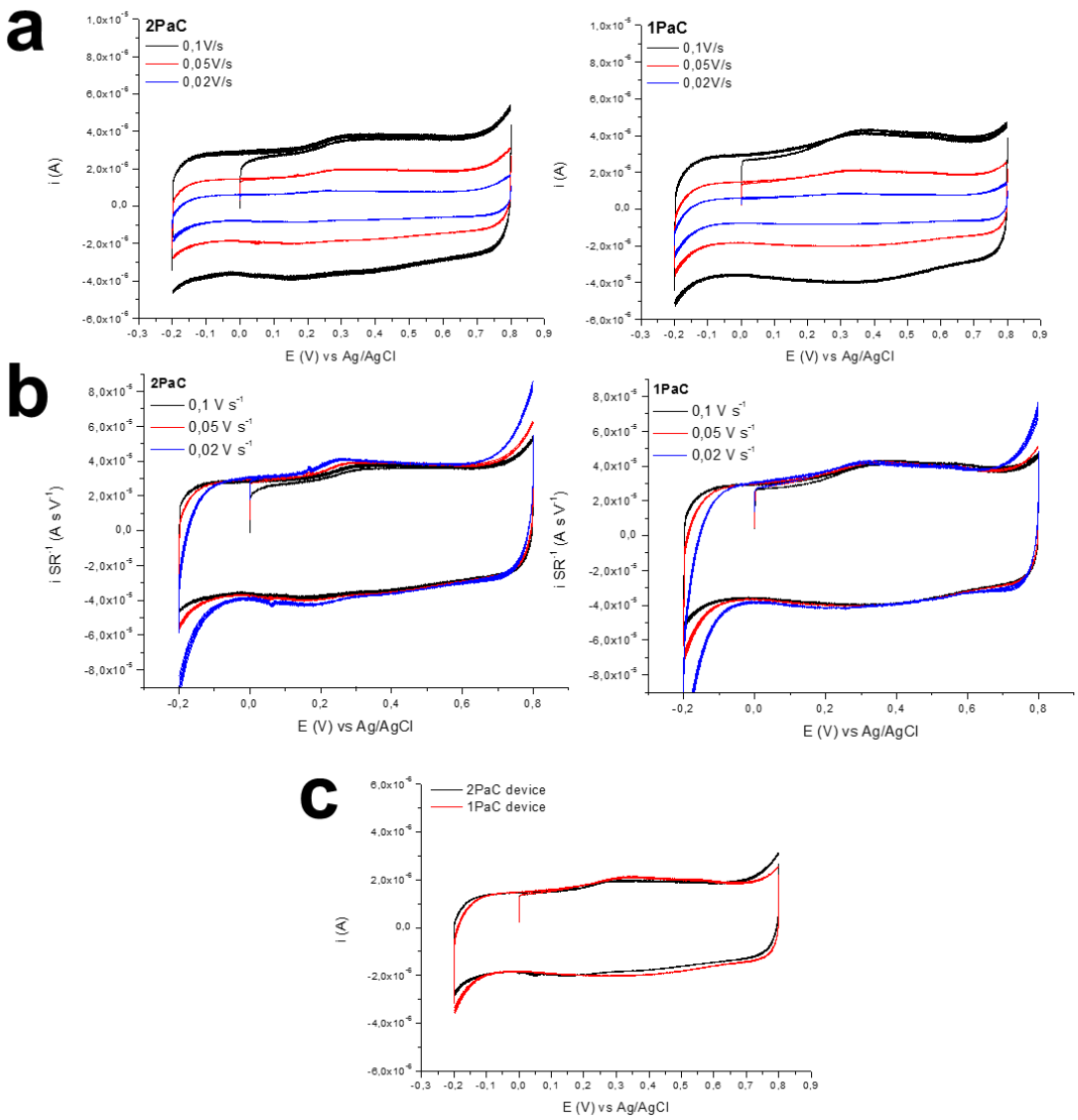

Fig. 7 CV experiments of the final devices carried out in NaCl 0,1M using the gate as working electrode at different scan rates (**a**). (**b**) Graphs obtained through current normalization to the correspondent scan rate. (**c**) Superimposition of the voltammograms recorded at 0,05 V s^{-1} for 1PaC and 2PaC devices.

1.2.2 EIS measurements

The channel-electrolyte interface was investigated by Electrochemical Impedance Spectroscopy (EIS). The Bode plots obtained for 50x50 μm^2 channel devices resulting from the two fabrication protocols are shown in Fig. 8. It was possible to fit the impedance spectra with the same equivalent circuit, consisting of a resistor (Rs, accounting for the electrolyte resistance) in series with a capacitor ad a resistor in parallel (Cp and Rp, i.e. capacitance and resistance of the polymer, respectively).

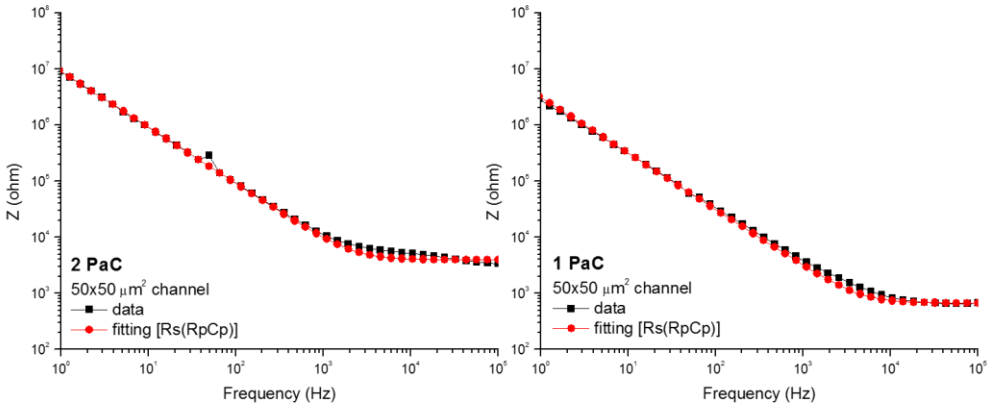

Fig. 8 Bode plots obtained by EIS experiments where NaCl 0,1M was the electrolyte and 2PaC or 1PaC 50x50 µm^2 channel acted as working electrode.

Correspondent channel sizes, output data provided by the fitting procedure and calculated capacitance and resistance values normalized on volume or area are presented in the tables below (Fig. 9).

a

Device label	W µm	L island µm	L channel µm	Thickness µm	Volume µm^3	Area µm^2
2PaC	56,9	77,5	44,4	0,177	780	4410
1PaC	55,4	72,7	45,2	0,061	246	4028

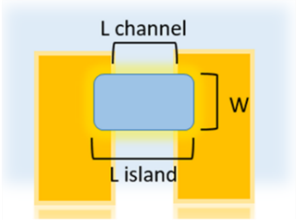

b

Device label	C polymer (Cp) F	R polymer (Rp) Ω	R electrolyte (Rs) Ω	Volumetric Cp (C*) F cm^{-3}	Volumetric Rp (R*) Ω cm^{-3}	Surface Rp Ω cm^{-2}
2PaC	1,76 10^{-8}	1,66 10^{8}	3958	22,53	2,13 10^{17}	8,97 10^{7}
1PaC	5,12 10^{-8}	6,03 10^{7}	670	208,32	2,45 10^{17}	1,66 10^{7}

Fig. 9 The tables report (**a**) measured values for the characteristic channel dimensions referred to the scheme on the right and (**b**) output data (Cp, Rp and Rs) and calculated data (C*, R* and Surface Rp) for the channels.

Furthermore, by plotting the capacitance values (Cp) obtained for 1PaC channels of different geometries versus the channels volume (Fig. 10), it was possible to estimate the mean volumetric capacitance of the channels (C*) for the newly developed protocol. Rivnay et al.[77] reported that the dependence of capacitance on volume stands for direct evidence for ion penetration in the channel of OECTs, thus the value of C* is the appropriate parameter to predict the ionic charge that is injected in the channel of an OECT.

The value of C* for 1PaC channels was found to be 97,8 ± 6,8 F cm^{-3}, i.e. higher than expected if compared to that reported in literature for 2PaC devices (C* = 39.3 ± 1.3 F cm^{-3}). Further studies are required in order to give an exhaustive explanation for these results.

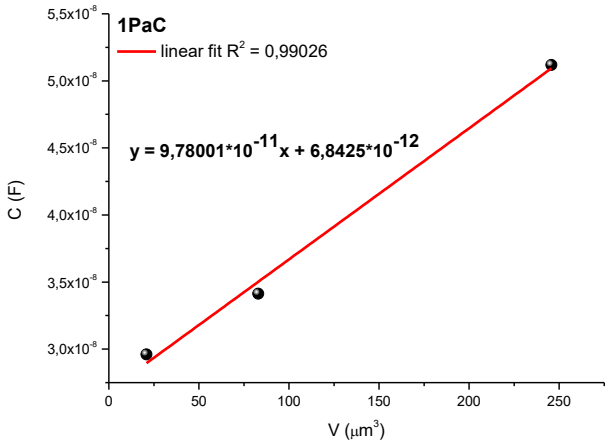

Fig. 10 1PaC PEDOT:PSS channels capacitance (determined from EIS measurements) vs channels volume. The linear fit to the capacitance data (red line) yields a C* = 97,8 ± 6,8 F cm^{-3}.

1.2.3 Steady-state behaviour

Output characteristics were recorded for the three channel sizes (10x10, 25x25 and 50x50µm^2) in both 2PaC and 1PaC OECTs. These measurements are useful to assess the gate voltage control over the channel current by promoting the doping and de-doping processes of PEDOT. When a positive bias is applied at the gate, oxidation of PEDOT takes place at this electrode. Then, cations from the electrolyte are injected into the channel and compensate the polyanionic charge of PSS. This causes the polymer reduction to occur at the channel, resulting in a decrease of the drain current. Figure 11 shows I_d-V_d curves recorded by varying the gate bias for 25x25µm^2 channel 2PaC and 1PaC devices, which are representative for all the channel sizes.

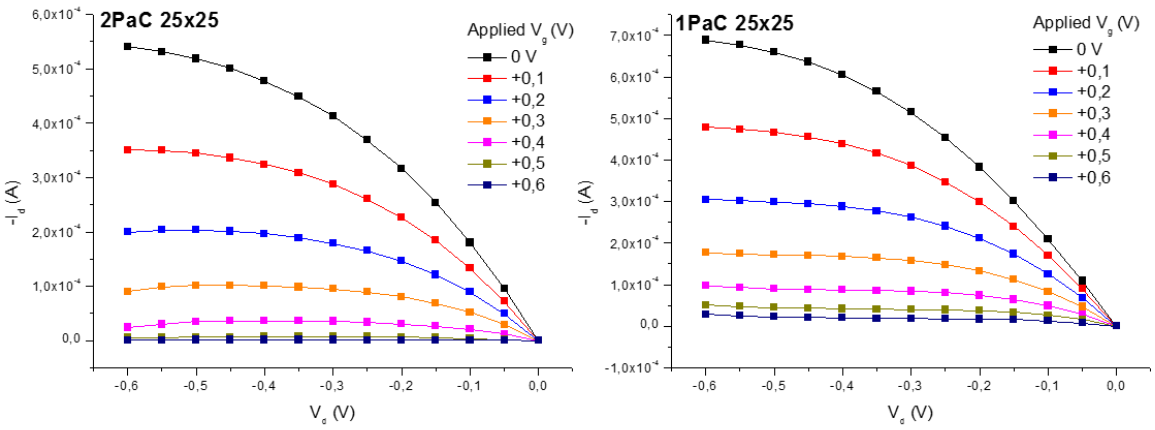

Fig. 11 I_d-V_d curves recorded for 25x25µm^2 channel 2PaC and 1PaC devices in PBS 0,1M. I_d was measured as a function of V_d by varying V_g from 0 to +0,6V (potential step 0,1).

As stands out from the graphs, in both cases the ionic current induced by the applied V_g readily modulates the transistors response and the recordings are consistent with operation in the depletion regime.

1.3 Platform assembly and calibration

Once the OECTs fabrication had been optimized, microfluidic cells with various geometries were obtained by soft lithography via SU8 moulding and the integrated platform was assembled. An easy-to-use pumping system for injecting the electrolyte into the cell consisted in two micropipette tips, with different filling levels, inserted into the inlet and outlet holes (Fig. 12). The higher hydrostatic pressure at the inlet given by a greater liquid height makes the electrolyte to flow through the microchannel, towards the outlet, until an equal filling level of media is achieved inside the exit tip and, in the meantime, the microfluidic cell is filled up with electrolyte.

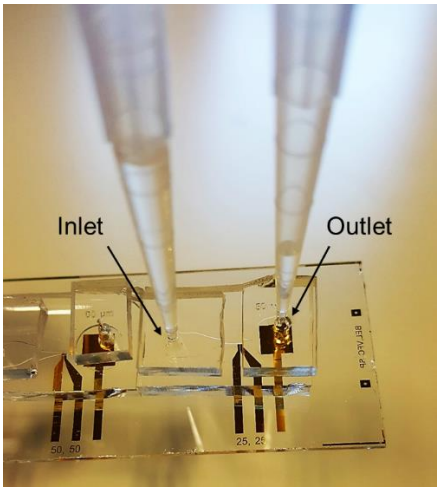

Fig. 12 Fully assembled platform with working pumping system.

As expected, no electrolyte leakage occurred using 1PaC devices: exposed glass on the surface ensured complete adhesion with the PDMS microfluidic cell. As further step, the platform was calibrated by using polystyrene beads of 60 or 160 µm diameter to simulate controlled blockage of the microchannel. Microbeads were isolated at the microscope using a micropipette (see Figure 13a). Once caught, the microbead is pushed inside the inlet and, following the fluid flow, it rolls through the microchannel until being trapped in correspondence of the microfluidic bottleneck. Pictures of trapped microbeads are shown in Fig. 13b.

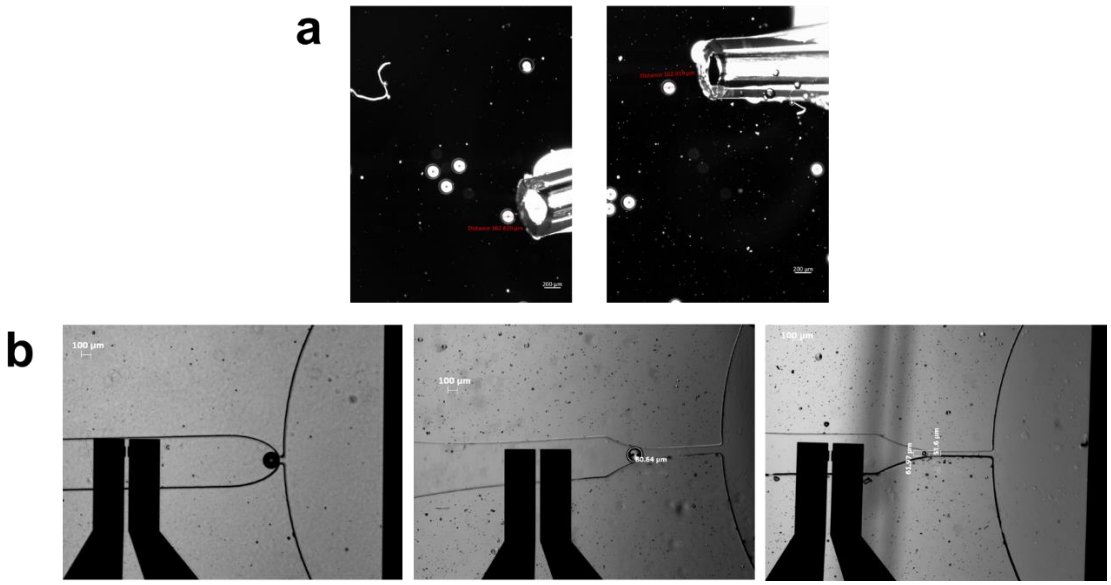

Fig. 13 Polystyrene microbeads isolation and trapping. **a**) pictures of an attempt to catch a 160 µm diameter microbead with a mictropipette. **b**) from left to right: 160 µm diameter microbead trapped in a 50 µm bottleneck; 160 µm diameter microbead trapped in a 100 µm bottleneck; 60 µm diameter microbead trapped in a 50 µm bottleneck.

The electrical measurements were performed using the OECT as impedance sensor, as explained in the experimental section. In Figure 14a is reported the frequency dependent normalized transconductance of a 10x10 μm^2 channel device with and without the microfluidic cell and after microbead trapping.

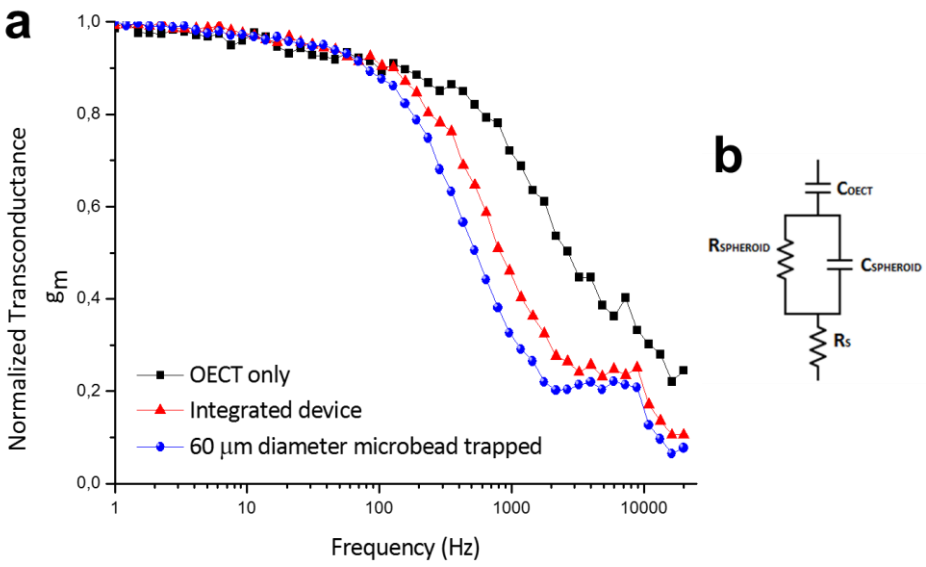

Fig. 14 (**a**) Frequency-dependent normalized transconductance recorded for OECT alone, fully assembled platform and after microbead trapping, as indicated. (**b**) Equivalent circuit modelled to fit the recorded data and measure TEER and capacitance of the spheroid.

For OECT alone, the cut-off frequency, defined at −3 dB of the transconductance at DC bias, is 1061 Hz. In the presence of the microfluidic cell, the additional resistance due to the electrolyte confinement in the 50 µm width microchannel trap produces a decrease in the cut-off frequency (402 Hz). Once the 60 µm diameter microbead is trapped, the cut-off frequency is further reduced to 261 Hz, indicating observable impedance to ion flow. The equivalent circuit modelled to fit the collected data and extract TEER and capacitance of a trapped spheroid is reported in Fig. 14b.

The proposed platform was compared to the work previously published by Huerta et al.,[66] who performed electrical monitoring of cysts using organic electrochemical transistors. Similarly, an impedance-based approach was employed in order to extract physiologically relevant data about 3D cell cultures. However, the setup described by Huerta et al. had two major limitations: first, the capillary glass tube containing the microbead provided massive contribution to electrolyte resistance; then, no impedance to ion flow caused by the 60 µm bead was observable, since the bead's diameter did not block completely the capillary tube.

The graph reported in figure 14a proofs that complete blockage of the microchannel is not necessary to affect the measurement, thus the developed platform is suitable for monitoring a wider spectrum of samples dimensions. Moreover, the sensor response can be modelled by easily tuning the microchannel architecture, i.e. bottleneck width, cell thickness and microchannel length.

2. Experimental

2.1 Reagents and materials

- glass slides;
- PEDOT:PSS Clevios PH1000 (Heraeus);
- Ethylene glycol, EG (Sigma-Aldrich);
- p-dodecylbenzenesulfonic acid, DBSA (Sigma-Aldrich);
- 3-glycidoxypropyltrimethoxysilane, GOPS (Sigma-Aldrich);
- (3-mercaptopropyl)trimethoxysilane, MPTMS (Sigma-Aldrich);
- Silicon wafers;
- trichloro(1H,1H,2H,2H-perfluorooctyl)silane, FDTS (Sigma-Aldrich);
- Silicone elastomer and curing agent kit (Dow Corning Sylgard);
- ParyleneC;
- 3-*(*trimethoxysilyl*)*propyl methacrylate, A-174;
- S1813 positive photoresist and MF-26 developer;
- AZ9260 positive photoresist and developer;
- SU-8 negative photoresist and developer.

2.2 Equipment

- Spincoater;
- BOC Edwards Auto 500 electron-beam evaporator;
- Oxford Plasma RIE;
- Plasma Etch System PE100;
- SUSS MBJ4 mask aligner;

- photomasks;

- SCS Labcoater 2;

- Nanonex nanoimprintor;

- Optical Microscope;

- Autolab PGSTAT 128N;

- CH INSTRUMENTS Electrochemical WorkStation 660C;

- National Instruments (NI) PXI system and customized LabView software.

2.3 Methods

2.3.1 OECT fabrication

OECT fabrication was carried out in 100/1000 class cleanrooms following ParyleneC optimized protocol (here abbreviated "2PaC"). In parallel, a new fabrication method (here abbreviated "1PaC") was developed and optimized by modifying the *PEDOT:PSS patterning* step of the standard 2PaC protocol. In this section, the two methods are presented by comparing the fabrication steps (Figure 15).

Gold patterning. A glass slide was accurately cleaned with DI water and soap, then sonicated and rinsed with acetone, DI water and IPA and finally dried under N_2. Gold source, drain and gate contacts were patterned via lift-off lithography and then thermally evaporated. First, positive photoresist S1813 was spincoated onto the glass substrate, baked and exposed to UV light through a photomask in the mask aligner, thus undergoing photo-bleaching. The photoresist was then developed and the glass slide was rinsed, dried and activated in the plasma etcher. 10 nm of chromium and 150nm of gold were deposited using the metal evaporator. After that, metal lift-off was performed using acetone.

2PaC protocol PEDOT:PSS patterning. Following the 2PaC protocol, a first deposition of ParyleneC with 3-(trimethoxysilyl)propyl methacrylate as adhesion promoter was carried out in the SCS Labcoater. After that, 2% soap solution was spincoated on the glass slide and an

additional layer of ParyleneC, i.e. the sacrificial layer, was deposited on the previous one. ParyleneC film was patterned using positive photoresist AZ9260, which was spincoated, baked, exposed to UV light and finally developed. Then, reactive ion etching with Oxford Plasma RIE was performed and the surface was activated in the plasma etcher. PEDOT:PSS formulation for spincoating consisted in Clevios PH1000 containing 1% GOPS, 5% EG and 0,25% DBSA: the blue dispersion was mixed and sonicated, than spincoated and soft-baked. After that, the second layer of ParyleneC was peeled-off and the final device was hard-baked for 1h.

The surface of the resulting OECT is entirely covered by an insulating, fixed layer of ParyleneC, except for PEDOT:PSS channel, gate and far end of the gold contacts. The thickness of the ParyleneC layer was measured using a profilometer and was found to be 1,6 μm, while the thickness of the polymeric film in the channel was calculated and the estimated mean value was 170 nm.

1PaC protocol PEDOT:PSS patterning. In this case, the first ParyleneC deposition with adhesion promoter was avoided and only the sacrificial layer, with spincoated soap underneath, was deposited onto the glass slide. ParyleneC was the patterned following the procedure described for the 2PaC protocol, i.e. using photolithography and reactive ion etching. Then, the MPTMS treatment was performed in order to promote the adhesion between PEDOT:PSS and gold. After surface activation, the device was soaked in 10mM MPTMS solution DI water/IPA 1:3 for 1minute, then rinsed with DI water, IPA and dried. A second activation was carried out and PEDOT:PSS formulation (as prepared for 2PaC protocol) was spincoated onto the glass slide. After that, soft-baking, peel-off and subsequent hard-baking were performed as final steps, as explained for the 2PaC method.

The resulting OECT is ParyleneC-free, i.e. the glass surface is exposed and no insulating layer covers the device, since the only one ParyleneC layer deposited (the sacrificial layer) was removed through peel-off. In this case, it was possible to measure directly the polymeric film thickness in the channel using the profilometer and the mean value was found to be 58 nm.

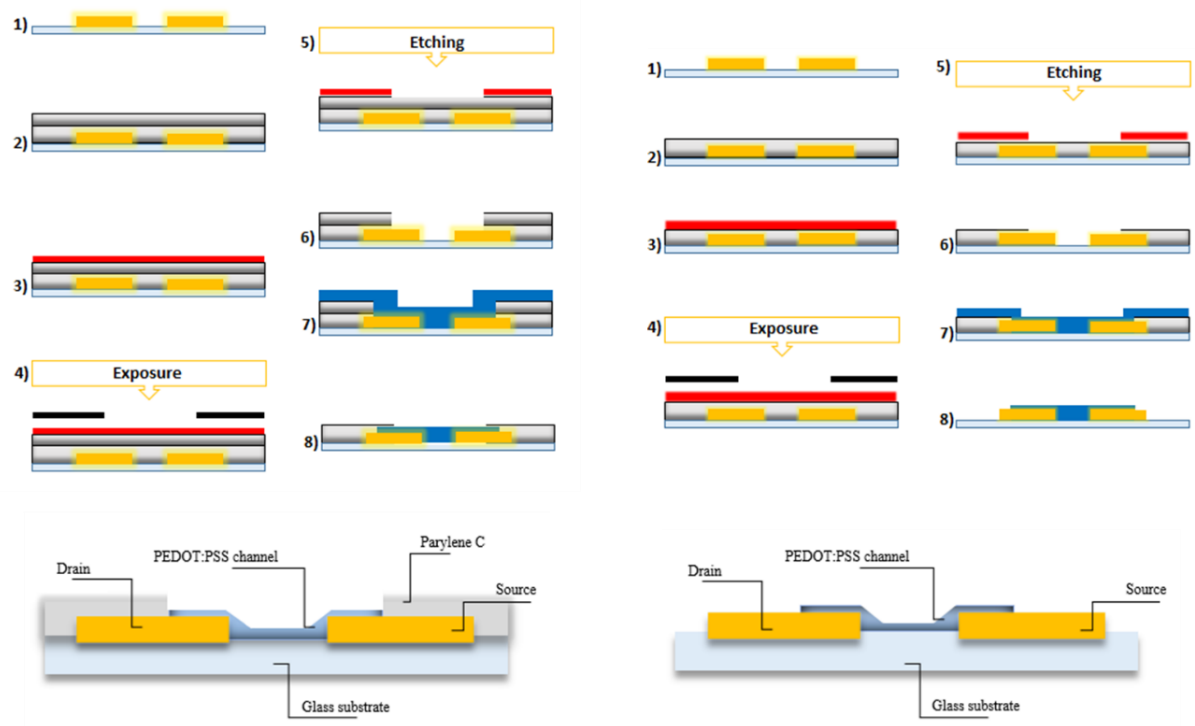

Fig. 15 Schemes of the 2PaC (left) and 1PaC (right) protocols with cross-sections of the resulting OECTs below. For each protocol: **1**) patterned gold; **2**) ParyleneC deposition (2 layers for the 2PaC protocol, only 1 layer for the 1PaC method); **3**) AZ photoresist deposition; **4**) Photo-bleaching; **5**) ParyleneC etching; **6**) patterned ParyleneC; in case of 1PaC protocol, MPTMS treatment follows this step; **7**) spincoated PEDOT:PSS formulation; **8**) device after peel-off.

2.3.2 Microfluidic cell fabrication

PDMS microfluidic cells were fabricated by soft lithography via SU-8 moulding (Fig. 16). In order to prepare the master mould, a silicon wafer was rinsed with acetone, IPA and DI water, thus dried under N_2 and put in an oven at 150°C under vacuum (4mbar) for 3 hours to remove any water trace. After that, negative photoresist SU-8 was spincoated on the wafer and a double step pre-exposure baking was performed. Then, UV-photo bleaching of the substrate through a suitable photomask followed and a double step post-exposure baking was carried out. The photoresist was developed and the master mould was rinsed with IPA, new developer and DI water. Once dried, the master mould was covered with an antiadhesive layer of FDTS using a Nanonex nanoimprintor, which is a fundamental step to allow for the final easy release of cured PDMS. Therefore, silicone elastomer and curing agent were mixed in 10:1 ratio in a centrifuge and poured above the master mould, which had been previously fixed in a petri dish. The mixture was repeatedly degassed under vacuum and then cured at 65°C, 1atm for one day. Finally, the cured PDMS was demoulded and cleaned under N_2; inlet and outlet holes were

made using a microfluidic PDMS puncher. To obtain the microchannel height, patterned SU-8 thickness was measured using a profilometer directly on the master mould, before FDTS deposition. By varying the working parameters during SU-8 pattering, the thickness of the final mould can be tuned as desired. For this work, two sets of microfluidic cells with different microchannel height were prepared: the first set having a mean microchannel height of 120 µm, while the second one's height was not possible to determine since SU-8 thickness exceeded the upper limit of the profilometer.

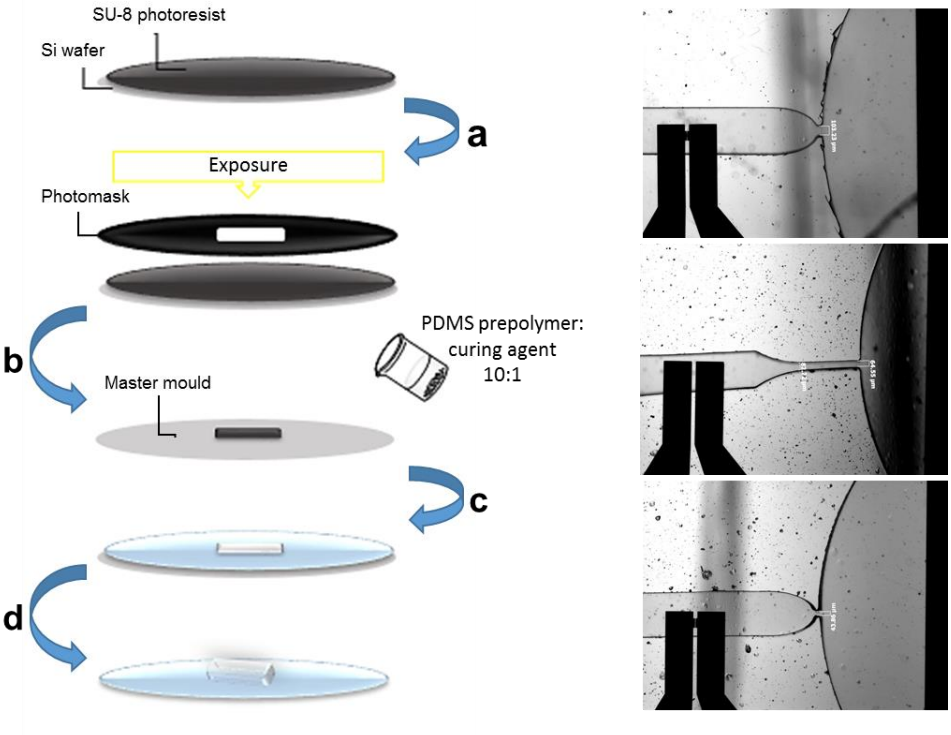

Fig. 16 Scheme of the soft-lithography fabrication protocol for microfluidic cells (right) and pictures of resulting bottleneck structures having different architectures. In the scheme: **a**) SU-8 photoresist patterning through photo-bleaching; **b**) after SU-8 development, the silicone elastomer mixture is poured onto the master mould; **c**) cured PDMS on the master mould; d) PDMS cell after demoulding.

2.3.3 OECT characterization

CV experiments were carried out in the Analytical Chemistry lab. of the department of Industrial Chemistry (University of Bologna) using a CHi 660C electrochemical workstation and adopting a three-electrode configuration. The gate was employed as working electrode, a Pt wire was the counter electrode and an Ag/AgCl electrode acted as reference. All the measurements were performed in PBS 0,1M and NaCl 0,1M by scanning the potential from -0,2 up to +0,8 V at different scan rates (0,02, 0,05 and 0,1 V s^{-1}).

EIS experiments were carried out using the FRA module of an Autolab potentiostat. The electrolyte was NaCl 0,1M and the channel acted as working electrode (source and drain shorted together), while Ag/AgCl electrode and Pt foil were used as reference and counter electrode, respectively. The device OCP was set as working potential. Signal type was 1 sine and AC amplitude was fixed at 10mV. The frequency range was 0,1 – 100000 Hz. The collected data were fitted with an equivalent circuit consisting of a resistor in series with a capacitor and a resistor in parallel.

Steady-state measurements were performed using a National Instruments (NI) PXI system with 2DMMs and a common source configuration, interfaced with a customized LabView software. In particular, I_d-V_d curves were obtained in depletion mode by recording I_d while biasing the drain from 0 to -0,6 V and varying V_g from 0 to +0,6 V (0,1 V potential step). PBS 0,1M was the electrolyte.

2.3.4 Frequency dependent measurements of transconductance

In order to carry out the frequency dependent measurements of transconductance, the drain was biased at -0,5 V and a sinusoidal waveform with 20 mV amplitude and frequency ranging from 1 to 20000 Hz was applied at the gate. The gate and drain currents, I_g and I_d, were simultaneously acquired and synced with the measured gate voltage, V_g.

In general, the information from I_d yields the small signal transconductance, $\Delta I_d/\Delta V_g$, while the information associated with I_g comprises the impedance of the system, $|Z| = \Delta V_g/\Delta I_g$. Therefore, by using a customized LabView software and a Matlab script, it is possible to combine transconductance and impedance frequency-dependent data to obtaining a broad-band impedance spectrum while keeping low applied bias. Furthermore, the collected data can be fitted with a suitable equivalent circuit to model the system.

Conclusions and future outlook

Over the last two decades, Organic Electronics and Bioelectronics have experienced incessant growth and widespread, rapidly pervading most aspects of life science. Owing to their interdisciplinary focus, the increasing availability of flexible, organic conducting materials and versatile technologies that allows for their facile synthesis, processing and manipulation has fueled the development of these research fields and the spring of new applications. In particular, PEDOT:PSS thin films have played a key role in the sensing of bioanalytes and living cells interfacing and monitoring. This thesis focuses on the development and characterization of two kind of PEDOT:PSS-based devices, i.e. a low-cost, PEDOT:PSS-based amperometric sensor for the selective detection of dopamine in ternary mixtures and a microfluidic trapping device for electronic monitoring of 3D spheroids.

Generally, amperometric sensors for 3,4-dihydroxyphenethylamine (dopamine, DA) detection suffer from the cross-talking effect occurring in real matrices because of the abundant amount of interfering agents, such as ascorbic acid (AA) and uric acid (UA), which compromise both selectivity and sensitivity of the measurements. First, thanks to the electrocatalytic and antifouling properties of PEDOT:PSS and employing a sensitive technique such as Differential Pulse Voltammetry, it was possible to discriminate three current peaks in the voltammetric trace, each of them ascribed to AA, DA and UA electro oxidation at a PH1000 spincoated film, in the potential range 0<E<+0,5V vs SCE. Therefore, a systematic study has been carried out in order to optimize the sensor performances, in terms of selectivity and sensitivity towards DA, in ternary mixtures. In particular, the adopted strategy consisted in the identification of the optimum experimental conditions by assessing the system's dependency on pH and scan rate, i.e. different pH values of the investigated ternary solution were tested and recordings at different scan rate, by varying DPV parameters, were performed; after that, modification of the electrodic surface was evaluated as a chance to improve the quality of the detection. For a PH1000 film as sensing material, the best peak-to-peak resolution was observed at pH 3,5, which, in turns, resulted an unfeasible condition for physiological application; as regards the scan rate, it came out to dynamically affect the ternary system by masking the AA electro oxidation peak in case of a fast potential scan. However, by matching the screening results, a "slow" recording at pH 5,5 was set as the best experimental condition, affording a DA

sensitivity of 591 µA mM^{-1} cm^{-2}. Furthermore, the modification of the previously mentioned sensor has been successfully carried out through electrodeposition of PHMeDOT:PSS and covalent anchoring of two newly synthesised long chain ferrocene derivatives, which were then tested as sensing materials. PHMeDOT:PSS-based sensor was found out to hide AA contribution to the recorded voltammetric trace for AA concentration values up to 0,6mM, while the presence of a ferrocene-functionalized long alkyl chain showed a "masking effect" against AA until 1,0mM (sensor 2). On the other hand, ferrocene-modified sensor 1 and 2 afforded DA sensitivities of 197 and 100 µA mM^{-1} cm^{-2}, respectively. For a PH1000 film, calculated detection limits for DA lain in the micromolar range, which is in accordance with the LoD values reported in literature for most of amperometric sensor operating in the presence of AA and UA as interferents. As further improvement of sensor performances, this group has recently fabricated an all-PEDOT:PSS OECT, built up following the same procedure described for the PH1000-based sensor: thanks to the inherent amplification provided by the OECT configuration and taking advantage of the experimental conditions optimized in this work, a better sensitivity towards dopamine can be obtained. Moreover, additional studies are currently in progress to assess the influence of different counterions for PEDOT on the sensors' performances and to synthesise new modifying agents capable of retaining the desirable "masking effect" provided by the long chain ferrocene derivatives and, at the same time, showing enhanced sensitivities towards DA.

A different kind of sensor for 3D cell cultures electrical monitoring was developed at Department of Bioelectronics (BEL) - Centre Microélectronique de Provence. The device consisted in an integrated platform, resulting from the assembly of a PEDOT:PSS-based OECT and a PDMS microfluidic structure, both fabricated using photolithographic techniques. A new fabrication protocol for PEDOT:PSS patterning ("1PaC") was implemented in order to render the OECT surface compatible with PDMS and ensure good adhesion between the two components, which is required for the electrolyte containment. The proposed procedure involves the formation of a mercapto silane (MPTMS)-based self assembled monolayer between the gold contacts and the spincoated polymeric film, thus preventing PEDOT:PSS to undergo delamination during the peel-off step. OECTs resulting from the newly developed protocol showed a channel resistance inferior to 500Ω and were characterized by CV, EIS and electrical recordings, in comparison to those obtained through the standard "2PaC" protocol. First, voltammetric traces recorded for intermediate steps of fabrication confirmed the occurrence of an electrochemical modification due to the SAM formation for 1PaC devices,

while the comparison between the voltammograms obtained for the final 1PaC and 2PaC devices highlighted a superimposable electrochemical behaviour, in both cases dominated by the capacitive character typical of PEDOT:PSS. Then, EIS experiments allowed for the evaluation of impedance spectra associated to the interface channel/electrolyte and the collected data were successfully modelled to the same equivalent circuit. Finally, 1PaC and 2PaC OECTs were electrically characterized by assessing their steady state behaviour. Meanwhile, PDMS microfluidic cells were fabricated by soft lithography to afford different sizes of microstructures, whose peculiarity was the presence of a bottleneck in the microchannel that allows for 3D cell cultures trapping at the desired location. The fully assembled platform was tested and calibrated by performing frequency-dependent measurements of transconductance with and without polystyrene microbeads, to simulate controlled blockage of the microchannel. The device validation experiments show that it is possible to record changes in the ionic flow due to the presence of the polystyrene bead inside the microfluidic trap. For instance, the presence of a 60 µm diameter PS bead trapped at a 50 µm width bottleneck produced a 141 Hz decrease in the cut off frequency of the OECT. The strength of this setup is that it allows for using an impedance-based approach in order to extract biologically relevant parameters about 3D cell cultures, such as TEER (trans-epithelial/endothelial electric resistance), by employing a simple equivalent circuit to model the system. Further calibrations have been planned to test different sizes of microbeads and microchannels, while additional characterizations are desirable to assess the influence of the PEDOT:PSS channel dimensions, thus improving the impedance sensor's sensitivity. The BEL group is currently working on the development of spheroids with a co-culture of MDCK II/stromal cells obtained through the hanging drop technology. The final aim is to perform short term and long term TEER monitoring of the spheroids, once trapped in the proposed microfluidic platform.

Appendix: theoretical principles of Electrochemical Techniques

In order to examine the theoretical principles that govern the mostly used electrochemical techniques in this work, the present dissertation will be referred to a generic reduction reaction (1), occurring in a solution where only species O is present at t = 0.

$$O + ne^- \Leftrightarrow R \quad (1)$$

1. Cyclic Voltammetry

In a CV experiment, the working electrode potential is ramped linearly versus time at a fixed scan rate, while the current flowing between WE and CE is recorded and plotted as a function of the applied potential to give the voltammetric trace, i.e. the voltammogram (figure 1b). The slope of the potential waveform, dE/dt, represents the scan rate, which generally ranges from a few tens of mV s^{-1} up to thousands V s^{-1}. At a certain time $t = \lambda$ and for $E = E_\lambda$ (switching potential), the direction of the scan in switched, thus the resulting potential waveform is triangle-shaped (Figure 1a).

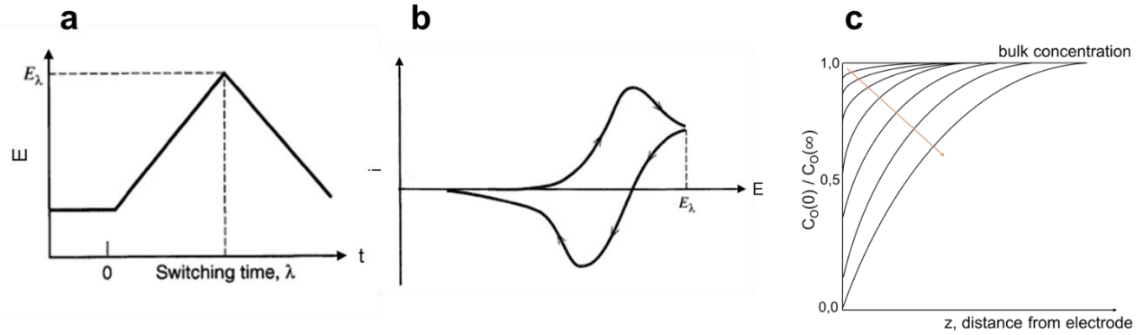

Fig. 1 **a**) potential waveform in CV experiments; **b**) resulting voltammetric trace; **c**) concentration profiles during WE polarization (red arrow direction). Adapted from[78].

The applied potential as a function of time can be expressed as follows:

$$E(t) = E_i \pm 2\,\nu\lambda \pm \nu t \quad (2)$$

where E_i [V] is the initial potential, ν [V s^{-1}] is the scan rate and λ [s] is the switching time. This kind of waveform implies that the working electrode assumes the same potential value twice, i.e. during the direct and the reverse scan.

The peculiarity of the acquired voltammogram is that, once reached a peak current, the curve i vs E decreases continuously. The occurrence of a mass transport, which is responsible for the generation of concentration profiles at the electrodic surface, should be considered in order to interpret this typical trend. Concentration profiles of species O for increasing time (red arrow), i.e. during the potential scan, from $C_O(0)/C_O(\infty) = 1{,}0$ (the applied potential does not allow for an electrochemical process to occur) to $C_O(0)/C_O(\infty) = 0{,}0$, are shown in figure 1c.

Following the red arrow in the graph, the stronger the electrode polarization becomes, the lower the profiles appear, progressively expanding at greater distances from the electrode surface. Indeed, while the potential is linearly ramped, not only the consumption rate at which O undergoes reduction at the electrode surface increases, but also the diffusion layer grows. Thus, the concentration gradients reach a maximum peak at the electrode surface.

Moreover, being the diffusion flux of species O at an electrode surface

$$q_O(0,t) = D_O \frac{\delta C_O(0,t)}{\delta z} \tag{3}$$

where q_O [mol m^{-2} s^{-1}] is the diffusion flux, D_O [m^2 s^{-1}] is the diffusion coefficient, C_O [mol m^{-3}] is the concentration and z [m] is the distance from the electrodic surface, and the measured current

$$i(t) = nFA \cdot q_O(0,t) \tag{4}$$

where i [A] is the current, n is the number of electrons, F [96 485.3329 s A mol^{-1}] is the Faraday constant and A [m^2] is the surface area, the measured current shows a maximum behaviour as well.

For a reversible process and in case of a semi-infinite linear diffusion, the resulting peak current i_p is

$$i_p = 268600 \cdot 10^8 \, n^{3/2} \, A \, {D_O}^{1/2} \, C_O^* \, \nu^{1/2} \quad (\textit{Randles–Sevcik eqn.}) \tag{5}$$

where i_p is expressed in A, A in cm^2, D_O in $cm^2\ s^{-1}$, C_O^* (bulk concentration of O) in mol cm^{-3} and ν (scan rate) in V s^{-1}. Otherwise, in case of diffusion occurring at a thin layer electrode, the peak current should be expressed as follows[78]:

$$i_p = \frac{n^2\ F^2\ \nu\ A\ C_O^*}{4\ R\ T} \tag{6}$$

However, once O has undergone reduction, the reduced species R will be present in the electrode proximity. If the electrochemical process is reversible, also R is susceptible to the redox phenomenon and its oxidation will generate, in turns, an anodic peak during the reverse scan. In electrochemistry, the term reversible does not have an absolute meaning; rather, it is more appropriate to refer to a system's particular degree of reversibility, which is directly responsible for the shape of the resulting voltammetric trace. For an ideal, reversible process, $i_{pA}/i_{pC} = 1$ and $\Delta E_p = 59/n$ mV. For redox systems with a lower degree of reversibility, ΔE_p value is higher and the peaks appear less sharp. If the process is totally irreversible, no peak is observed during the reverse scan.

2. Differential Pulse Voltammetry

Differential pulse voltammetry is similar to normal pulse voltammetry, since the potential is scanned with a series of pulses. However, differently from NPV, in DPV each potential pulse has a fixed amplitude (from 10 to 100 mV) and the pulses are superimposed on base potential stair steps (Fig. 2a). Current is measured twice for each pulse, the first one (at $t = \tau$) just before the pulse and the second one at the end of the pulse (at $t = \tau'$). This sampling approach allows for the decay of the nonfaradaic (capacitive) current, and the difference between current measurements at these points for each pulse, i.e. $\delta i = i(\tau') - i(\tau)$, is plotted against the base potential (Fig. 2b). Consequently, the measurement of the faradic current associated to the analyte reaction is more accurate than in a CV experiment and an higher sensitivity can be obtained.

The output signal, $\delta i/\delta E$, represents the derivative of the standard sigmoidal voltammetric trace. As a consequence, E_p value in DPV traces correspond to the inflection point potential value in the standard voltammograms.

For an ideal, reversible system, the "peak current" can be expressed as follows:

$$(\delta i)_{MAX} = \frac{nFAD_O^{1/2}C_O^*}{\pi^{1/2}(\tau'-\tau)^{1/2}} \cdot \frac{1-\vartheta}{1+\vartheta} \tag{7}$$

where ϑ is an exponential parameter

$$\vartheta = e^{\frac{nF\Delta E}{2RT}} \quad (8)$$

The fraction $\frac{1-\vartheta}{1+\vartheta}$ decreases if ΔE (pulse amplitude) is reduced, while it is equal to 1 for high pulse amplitudes, which are always avoided as the peak resolution would be lowered.

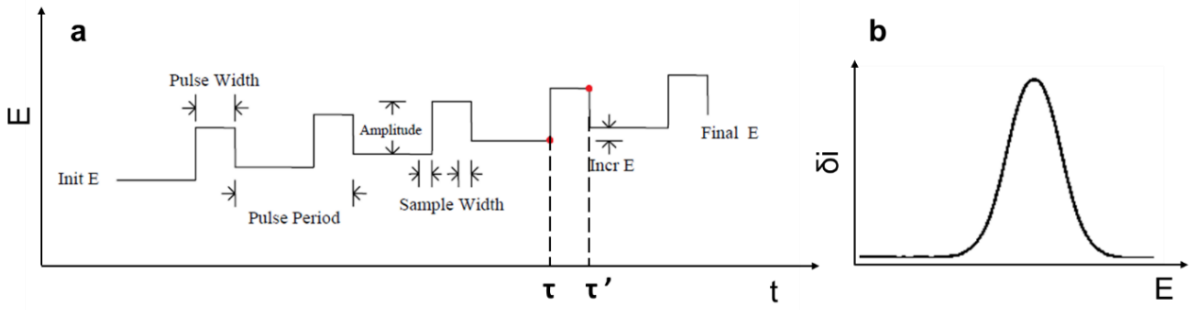

Fig. 2 **a**) potential waveform in DPV experiments; **b**) resulting voltammetric trace. Adapted from Chi user's manual.

The experimental parameters that must be set in order to carry out a DPV experiment are illustrated in figure 2a and include: Init E [V], the initial potential; Final E [V], the final potential; Incr E [V], the increment potential of each point; Amplitude [V], the potential pulse amplitude; Pulse Width [s], the potential pulse width; Sampling Width [s], data sampling width; Pulse Period [s], the potential pulse period.

3. Electrochemical Impedance Spectroscopy

EIS is a powerful AC technique that allows for the effective detection of interfaces' electric and electrochemical features. By applying a sinusoidal potential excitation

$$E(t) = E_m \, sen(\omega t) \quad (9)$$

(where where E_m is the amplitude of the signal and ω is the radial frequency [rad s^{-1}]) with a frequency ν = ω/2π, an AC signal is generated and can be analyzed as a sum of sinusoidal functions (a Fourier series). The output current will be a sinusoid shifted in phase (θ), with respect to the applied potential function, and can be expressed as

$$I(t) = I_m \, sen(\omega t+\theta) \quad (10)$$

Therefore, the impedance of the electrochemical cell is

$$Z(\omega) = E(t)/I(t) \tag{11}$$

and its modulus is

$$|Z(\omega)| = E_m(\omega)/I_m(\omega) \tag{12}$$

All the aforementioned quantities can be expressed as complex functions and, applying Euler's relationship

$$e^{j\theta} = \cos(\theta) + j\text{sen}(\theta) \tag{13}$$

new expressions are obtained for E(t) and I(t), while the resulting equation for impedance is:

$$Z(\omega) = |Z|\cos(-\theta) + j|Z|\text{sen}(-\theta) = |Z|\cos(\theta) - j|Z|\text{sen}(\theta) \tag{14}$$

The expression for Z(ω) consists of a real and an imaginary part. Consequently, impedance can be represented in the complex plane in the form Z = a + jb, where a = Z' = Re(Z) = |Z|cos(θ) and b = −Im(Z) = Z''= |Z|senθ, with a modulus $|Z| = [(Z')^2 + (Z'')^2]^{1/2}$ (Figure 3b).

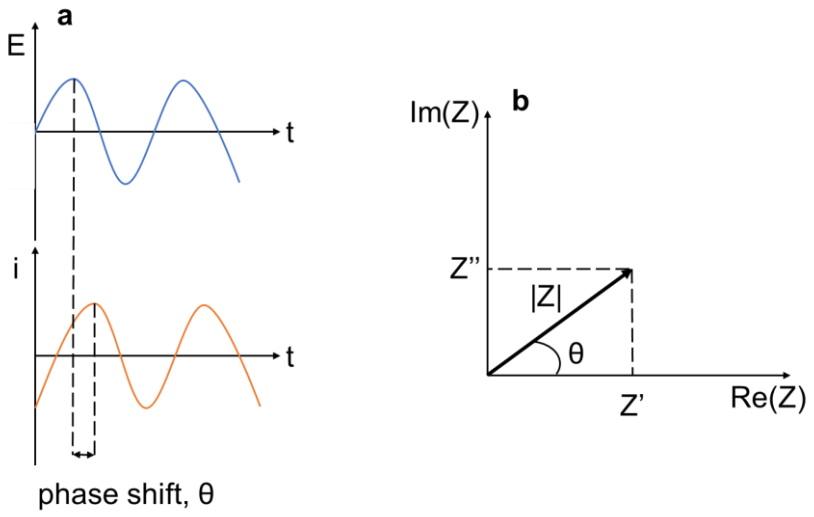

Fig. 3 **a**) schematic representations of the sinusoidal applied potential and the resulting current shifted in phase; **b**) impedance in the complex plane.

Graphically, the most popular formats are the Bode and the Nyquist plots. In the Bode plots, log |*Z*| and φ are represented as a function of log *f*, while in the Nyquist plot data are represented as the real component of impedance (Re(Z)) on the *x*-axis and imaginary component (Im(Z)) on the *y*-axis.

Impedance data can be exploited in order to extract relevant information about the electrical features of the cell by fitting the real system to an equivalent circuit model. Indeed, chemical and physical processes occurring in the cell and at the electrode can be represented as simple circuital elements. For instance, the conduction phenomenon is associated to a resistance, while charge accumulation at an electrical double layer is described as a capacitor.

Bibliography

1. Shirakawa, H., Louis, E. J., MacDiarmid, A. G., Chiang, C. K. & Heeger, A. J. Synthesis of electrically conducting organic polymers: halogen derivatives of polyacetylene, (CH). *J. Chem. Soc. Chem. Commun.* 578–580 (1977).

2. Shirakawa, H. The Discovery of Polyacetylene Film: The Dawning of an Era of Conducting Polymers (Nobel Lecture). *Angew. Chem. Int. Ed. Engl.* **40,** 2574–2580 (2001).

3. Zhang, X., Bäuerle, P., Aida, T., Skabara, P. & Kagan, C. Organic Electronics for a Better Tomorrow : Innovation , Accessibility , Sustainability. *A White Pap. from Chem. Sci. Soc. Summit* 34 (2012).

4. Rivnay, J., Owens, R. M. & Malliaras, G. G. The rise of organic bioelectronics. *Chem. Mater.* **26,** 679–685 (2014).

5. Owens, R. M. & Malliaras, G. G. Organic Electronics at the Interface with Biology. *MRS Bull.* **35,** 449–456 (2010).

6. K. Reuter, S. Kirchmeyer, U. Merker, P. W. L. and T. M.-F. *PEDOT: Principles and Applications of an Intrinsically Conductive Polymer*. (2011).

7. Yassar, A., Roncali, J. & Garnier, F. Conductivity and conjugation length in poly(3-methylthiophene) thin films. *Macromolecules* **22,** 804–809 (1989).

8. Sheina, E. E., Khersonsky, S. M., Jones, E. G. & McCullough, R. D. Highly conductive, regioregular alkoxy-functionalized polythiophenes: A new class of stable, low band gap materials. *Chem. Mater.* **17,** 3317–3318 (2005).

9. Kroon, R. *et al.* Thermoelectric plastics: from design to synthesis, processing and structure–property relationships. *Chem. Soc. Rev.* (2016).

10. Zanardi, C., Terzi, F. & Seeber, R. Polythiophenes and polythiophene-based composites in amperometric sensing. *Anal. Bioanal. Chem.* **405,** 509–531 (2013).

11. Brédas, J. L., Beljonne, D., Coropceanu, V. & Cornil, J. Charge-transfer and energy-transfer processes in π-conjugated oligomers and polymers: A molecular picture. *Chem. Rev.* **104,** 4971–5003 (2004).

12. Sengodu, P. & Deshmukh, A. Conducting Polymers and their Inorganic Composites for Advanced Li-ion Batteries: a Review. *RSC Adv.* **5,** 42109–42130 (2015).

13. Ziadan, K. M. Conducting Polymers Application. *New Polym. Spec. Appl.* **Chapter 1,** 3–24 (2012).

14. Guimard, N. K., Gomez, N. & Schmidt, C. E. Conducting polymers in biomedical engineering. *Prog. Polym. Sci.* **32,** 876–921 (2007).

15. Armour, M., Davies, A. G., Upadhyay, J. & Wassermann, A. Colored electrically conducting polymers from furan, pyrrole, and thiophene. *J. Polym. Sci. Part A-1 Polym. Chem.* **5,** 1527–1538 (1967).

16. Collier, J. H., Camp, J. P., Hudson, T. W. & Schmidt, C. E. Synthesis and characterization of polypyrrole-hyaluronic acid composite biomaterials for tissue engineering applications. *J. Biomed. Mater. Res.* **50,** 574–84 (2000).

17. Pepitone, M. F., Hardaker, S. S. & Gregory, R. V. Synthesis and characterization of photoluminescent 3,4-ethylenedioxythiophene derivatives. *Chem. Mater.* **15,** 557–563 (2003).

18. Larmat, F., Reynolds, J. R., Reinhardt, B. a, Brott, L. L. & Clarson, S. J. Comparative Reactivity of Thiophene and 3,4-(Ethylenedioxy)thiophene as Terminal Electropolymerizable Units in Bis-Heterocycle Arylenes. *J. Polym. Sci. Part A-Polymer Chem.* **35,** 3627–3636 (1997).

19. Levermore, P. A. *et al.* High efficiency organic light-emitting diodes with PEDOT-based conducting polymer anodes. *J. Mater. Chem.* **18,** 4414–4420 (2008).

20. Lee, S. J., Pil Kim, H., Mohd Yusoff, A. R. Bin & Jang, J. Organic photovoltaic with PEDOT:PSS and V2O5 mixture as hole transport layer. *Sol. Energy Mater. Sol. Cells* **120,** 238–243 (2014).

21. Dietrich, M., Heinze, J., Heywang, G. & Jonas, F. Electrochemical and spectroscopic characterization of polyalkylenedioxythiophenes. *J. Electroanal. Chem.* **369,** 87–92 (1994).

22. R, P. R. A., Thomas, M. S. & Varughese, S. Multi-region to single region shear thinning transitions in drying PEDOT:PSS dispersions: contributions from charge density fluctuations. *Soft Matter* (2015).

23. Louwet, F. 10 years of click chemistry: Synthesis and applications of ferrocene-derived triazoles. *J. Solid State Electrochem.* **6,** 1–9 (2003).

24. RAO, M. C. & SHEKHAWAT, M. S. A Brief Survey on Basic Properties of Thin Films for Device Application. *Int. J. Mod. Phys. Conf. Ser.* **22,** 576–582 (2013).

25. Nardes, A. M. *et al.* Conductivity , work function , and environmental stability of PEDOT : PSS thin films treated with sorbitol. *Org. Electron.* **9,** 727–734 (2008).

26. Saghaei, J., Fallahzadeh, A. & Yousefi, M. H. Improvement of electrical conductivity of PEDOT:PSS films by 2-Methylimidazole post treatment. *Org. Electron. physics, Mater. Appl.* **19,** 70–75 (2015).

27. Worfolk, B. J. *et al.* Ultrahigh electrical conductivity in solution-sheared polymeric transparent films. *Proc. Natl. Acad. Sci.* **112,** 14138–14143 (2015).

28. Cao, Z., Chen, Z. & Escoubas, L. Optical , structural , and electrical properties of PEDOT : PSS thin films doped with silver nanoprisms. *Opt. Mater. Express* **4,** 3375–3384 (2014).

29. Deguchi, T., Tomeoku, H. & Takashiri, M. Preparation and characterization of electropolymerized poly (3 , 4-ethylenedioxythiophene) thin films with different dopant anions materials poly (3 , 4-ethylenedioxythiophene) thin fi lms with different dopant anions. *Jpn. J. Appl. Phys.* **55,** (2016).

30. Zhang, S. *et al.* Solvent-induced changes in PEDOT:PSS films for organic electrochemical transistors. *APL Mater.* **3,** (2015).

31. Kim, J. Y., Jung, J. H., Lee, D. E. & Joo, J. Enhancement of electrical conductivity of poly(3,4-ethylenedioxythiophene)/poly(4-styrenesulfonate) by a change of solvents. *Synth. Met.* **126,** 311–316 (2002).

32. Zhang, F., Nyberg, T. & Inganäs, O. Conducting Polymer Nanowires and Nanodots Made with Soft Lithography. *Nano Lett.* **2,** 1373–1377 (2002).

33. Ouyang, J., Chu, C. W., Chen, F. C., Xu, Q. & Yang, Y. High-conductivity poly(3,4-ethylenedioxythiophene):poly(styrene sulfonate) film and its application in polymer optoelectronic devices. *Adv. Funct. Mater.* **15,** 203–208 (2005).

34. Kim, Y. H. *et al.* Highly conductive PEDOT:PSS electrode with optimized solvent and thermal post-treatment for ITO-free organic solar cells. *Adv. Funct. Mater.* **21,** 1076–1081 (2011).

35. Krebs, F. C. Fabrication and processing of polymer solar cells : A review of printing and coating techniques. *Sol. Energy Mater. Sol. Cells* **93,** 394–412 (2009).

36. Patra, S., Barai, K. & Munichandraiah, N. Scanning electron microscopy studies of PEDOT prepared by various electrochemical routes. *Synth. Met.* **158,** 430–435 (2008).

37. Scavetta, E. *et al.* Dopamine amperometric detection at a ferrocene clicked PEDOT:PSS coated electrode. *J. Mater. Chem. B* **2,** 2861 (2014).

38. Tait, J. G. *et al.* Spray coated high-conductivity PEDOT : PSS transparent electrodes for stretchable and mechanically-robust organic solar cells. *Sol. Energy Mater. Sol. Cells* **110,** 98–106 (2013).

39. Defranco, J. A., Schmidt, B. S., Lipson, M. & Malliaras, G. G. Photolithographic patterning of organic electronic materials. *Org. Electron.* **7,** 22–28 (2006).

40. White, H. S., Kittlesen, G. P. & Wrighton, M. S. Chemical Derivatization of an Array of Three Gold Microelectrodes with Polypyrrole: Fabrication of a Molecule-Based Transistor. *J. Am. Chem. Soc.* **106,** 5375–5377 (1984).

41. Bernards, D. A. & Malliaras, G. G. Steady-state and transient behavior of organic electrochemical transistors. *Adv. Funct. Mater.* **17,** 3538–3544 (2007).

42. Strakosas, X., Bongo, M. & Owens, R. M. The organic electrochemical transistor for biological applications. *J. Appl. Polym. Sci.* **132,** (2015).

43. Khodagholy, D. *et al.* High transconductance organic electrochemical transistors. *Nat. Commun.* **4,** 2133 (2013).

44. Murray, R. W. Chemically Modified Electrodes. *Acc. Chem. Res.* **117,** 135–141 (1980).

45. Seeber, R. & Terzi, F. The evolution of amperometric sensing from the bare to the modified electrode systems. *J. Solid State Electrochem.* **15,** 1523–1534 (2011).

46. Murray, R. W. Chemically modified electrodes for electrocatalysis. *Phil. Trans. R. Soc. Lond.* **A,** 253–265 (1981).

47. Seeber, R., Pigani, L., Terzi, F. & Zanardi, C. Amperometric sensing. A melting pot for material, electrochemical, and analytical sciences. *Electrochim. Acta* **179,** 350–363 (2015).

48. Damier, P., Hirsch, E. C., Agid, Y. & Graybiel, A. M. The substantia nigra of the human brain: I. Nigrosomes and the nigral matrix, a compartmental organization based on calbindin D(28K) immunohistochemistry. *Brain* **122,** 1421–1436 (1999).

49. Kamyabi, M. & Shafiee, M. Electrocatalytic oxidation of dopamine, ascorbic acid and uric acid at poly2, 6 diaminopyridine on the surface of carbon nanotubes/GC electrodes. *J. Braz. Chem. Soc.* **23,** 593–601 (2012).

50. Safavi, A., Maleki, N., Moradlou, O. & Tajabadi, F. Simultaneous determination of dopamine, ascorbic acid, and uric acid using carbon ionic liquid electrode. *Anal. Biochem.* **359,** 224–229 (2006).

51. Basavanna, S., Chethan, B. K. & Naik, Y. A. Research Article Simultaneous electrochemical determination of ascorbic acid , dopamine and uric acid using hollow gold nanospheres modified electrode. *J. Chem. Pharm. Res.* **6,** 823–831 (2014).

52. Belaidi, F. S. *et al.* PEDOT-modified integrated microelectrodes for the detection of ascorbic acid, dopamine and uric acid. *Sensors Actuators, B Chem.* **214,** 1–9 (2015).

53. Fabregat, G., Casanovas, J., Redondo, E., Armelin, E. & Alemán, C. A rational design for the selective detection of dopamine using conducting polymers. *Phys. Chem. Chem. Phys.* **16,** 7850–61 (2014).

54. Gualandi, I. *et al.* A simple all-PEDOT:PSS electrochemical transistor for ascorbic acid sensing. *J. Mater. Chem. B* **3,** 6753–6762 (2015).

55. Tang, H., Lin, P., Chan, H. L. W. & Yan, F. Highly sensitive dopamine biosensors based on organic electrochemical transistors. *Biosens. Bioelectron.* **26,** 4559–4563 (2011).

56. Liao, C., Zhang, M., Niu, L., Zheng, Z. & Yan, F. Organic electrochemical transistors with graphene-modified gate electrodes for highly sensitive and selective dopamine sensors. *J. Mater. Chem. B* **2,** 191–200 (2014).

57. Tybrandt, K., Kollipara, S. B. & Berggren, M. Organic electrochemical transistors for signal amplification in fast scan cyclic voltammetry. *Sensors Actuators, B Chem.* **195,** 651–656 (2014).

58. Malliaras, G. G. Organic bioelectronics: A new era for organic electronics. *Biochim. Biophys. Acta - Gen. Subj.* **1830,** 4286–4287 (2013).

59. Berggren, M. & Richter-Dahlfors, A. Organic bioelectronics. *Adv. Mater.* **19,** 3201–3213 (2007).

60. Pampaloni, F., Reynaud, E. G. & Stelzer, E. H. K. The third dimension bridges the gap between cell culture and live tissue. *Nat. Rev. Mol. Cell Biol.* **8,** 839–845 (2007).

61. Fennema, E., Rivron, N., Rouwkema, J., van Blitterswijk, C. & De Boer, J. Spheroid culture as a tool for creating 3D complex tissues. *Trends Biotechnol.* **31,** 108–115 (2013).

62. Srinivasan, B., Kolli, A. R., Shuler, L. & Hickman, J. J. TEER measurement techniques for in vitro barrier model systems. *J Lab Autom* **20,** 107–126 (2015).

63. Benson, K., Cramer, S. & Galla, H.-J. Impedance-based cell monitoring: barrier properties and beyond. *Fluids Barriers CNS* **10,** 5 (2013).

64. Rivnay, J. *et al.* Organic electrochemical transistors for cell-based impedance sensing. *Appl. Phys. Lett.* **106,** (2015).

65. Jimison, L. H. *et al.* Measurement of barrier tissue integrity with an organic electrochemical transistor. *Adv. Mater.* **24,** 5919–5923 (2012).

66. Huerta, M., Rivnay, J., Ramuz, M., Hama, A. & Owens, R. M. Research Update: Electrical monitoring of cysts using organic electrochemical transistors. *APL Mater.* **3,** (2015).

67. Ruppen, J. *et al.* A microfluidic platform for chemoresistive testing of multicellular pleural cancer spheroids. *Lab on a Chip* 1198–1205 (2014).

68. Tan, Q., Ferrier, G. A., Chen, B. K., Wang, C. & Sun, Y. Quantification of the specific membrane capacitance of single cells using a microfluidic device and impedance spectroscopy measurement. *Biomicrofluidics* **6,** (2012).

69. Dayton, M. a., Ewing, A. G. & Wightman, R. M. Response of microvoltammetric electrodes to homogeneous catalytic and slow heterogeneous charge-transfer reactions. *Anal. Chem.* **52,** 2392–2396 (1980).

70. Martell, A. E. & Smith, R. M. *Critical Stability Constants, vol. 3: Other Organic Ligands*. (1977).

71. Bello, A. *et al.* Optimization of the DPV potential waveform for determination of ascorbic acid on PEDOT-modified electrodes. *Sensors Actuators, B Chem.* **121,** 430–435 (2007).

72. Saraceno, R. A., Pack, J. G. & Ewing, A. G. Catalysis of slow charge transfer reactions at polypyrrole-coated glassy carbon electrodes. *J. Electroanal. Chem.* **197,** 265–278 (1986).

73. Schmidt, E. M., McIntosh, J. S. & Bak, M. J. Long-term implants of Parylene-C coated microelectrodes. *Med. Biol. Eng. Comput.* **26,** 96–101 (1988).

74. Shen, Y., Wu, T., Zhang, Y. & Li, J. Comparison of two-typed (3-mercaptopropyl)trimethoxysilane-based networks on Au substrates. *Talanta* **65,** 481–488 (2005).

75. Zhong, X. *et al.* Glucose biosensor based on self-assembled gold nanoparticles and double-layer 2d-network (3-mercaptopropyl)-trimethoxysilane polymer onto gold substrate. *Sensors Actuators, B Chem.* **104,** 191–198 (2005).

76. Vericat, C., Vela, M. E., Benitez, G., Carro, P. & Salvarezza, R. C. Self-assembled monolayers of thiols and dithiols on gold: new challenges for a well-known system. *Chem. Soc. Rev.* **39,** 1805 (2010).

77. Rivnay, J. *et al.* High-performance transistors for bioelectronics through tuning of channel thickness. *Sci. Adv.* **1,** e1400251–e1400251 (2015).

78. Bard, A. J., Faulkner, L. R., Swain, E. & Robey, C. *Electrochemical Methods*. (1980).

Acknowledgements

First of all, I would like to express my sincerest gratitude to Prof. Erika Scavetta, for being my inspiring mentor and supervisor, and for her trust in me all these years.

A special appreciation and thanks to Prof. Róisín Owens and Prof. George Malliaras, for kindly hosting me in Gardanne during my Erasmus traineeship at École des Mines de Saint-Étienne and for letting me taste the world of Bioelectronics. I would also like to thank Prof. Rita Mazzoni, who patiently takes care of my synthetic efforts in the Organometallics lab, Department of Industrial Chemistry (Bologna).

I wish to acknowledge Prof. Domenica Tonelli and the entire Electrochemistry group of the Department of Industrial Chemistry (Bologna), for their great contribution to my academic growth. I am particularly grateful to Isacco for his valuable advice. I would also like to extend my thanks to Prof. Beatrice Fraboni and all the people joining the Material Physics group of the Department of Physics and Astronomy (Bologna), for the fruitful collaboration.

I would especially like to thank all the extraordinary colleagues of the BEL crew for both friendship and helpful support for my thesis. Thanks to Vincenzo, for enthusiastically teaching me his clean room tips and all that I know about Microfluidics.

I am heartily thankful to all my closest friends, whose presence incessantly boosts my days. Thank you Giulia, Massimo, Maria, Lorenzo, Silvia and Cristina for your authentic friendship and the special way each of you contributes to my life. You do it inestimably.

Thank you Francesco, for your love and for being always by my side, no matter what. Thanks for being just the way you are.

Finally, I would like to thank my family for being my home and support: my brother Maurizio, my grandma Vera and especially my parents, Daniela and Roberto, to whom this work is dedicated. Thank you not only for unconditionally encouraging me, but mostly for reminding me who I am when I get a bit lost.